PHOTOPHYSICS AND ELECTROCHEMISTRY OF d^4 METAL CLUSTERS

Thesis by

Thomas Christopher Zietlow

In Partial Fulfillment of the Requirements

for the Degree of

Doctor of Philosophy

California Institute of Technology

Pasadena, California

1985

(Submitted March 25, 1985)

ACKNOWLEDGEMENTS

I would like to thank my advisor, Harry Gray, for putting up with me for the past years and for making my research enjoyable. I hope some of his way of thinking about chemical problems has rubbed off on me. Thanks also go to my collaborators in my research: Mike Hopkins, both for the projects we worked on together, and for always being willing to be a sounding board for my wilder ideas; Dan Nocera for his work on the clusters; special thanks to Bill Schaefer and his co-workers Behzad Sadeghi and Nhi Hua for their crystal structure determinations. Bill deserves a special thanks for allowing me to learn how to determine a structure when just solving it himself would have been easier. I appreciate Professor Anson and his group for allowing me the use of some of their electrochemical equipment and their expertise. Thanks also to John Bercaw for use (abuse) of his tube furnace. I appreciate the time Mike and Miriam took to proof this manuscript.

My time at Caltech has been enjoyable in large part to my friends and coworkers in the Gray group: Terrance P., the Mav, Steve, Winkie, Les, Jon, Wally-Bob and all the Bio people, Janet, Al, Catherine, and, of course, Precious. I appreciate Tad and Miriam for brightening up my declining years (so to speak) with their enthusiasm and good cheer. I've come to enjoy both Van Halen and Tarheel basketball; it's time to leave.

Most importantly, I would like to thank my family for all the love, support and encouragement they have given me throughout my life.

Finally, I would like to acknowledge the Sun Oil Company for a fellowship from 1983-85.

to my parents

Abstract.

The metal-ligand and metal-metal interactions in d^4 metal cluster systems have been examined using emission spectroscopy and electrochemical techniques. A detailed picture of the electronic structure of the hexanuclear molybdenum and tungsten clusters has not yet been achieved, but significant insight has been obtained through studying the effects of ligand, temperature, and molecular structure on the properties of the emissive excited state. Through these studies, and through analogy to the $(d^4)_2$ quadruply bonded molybdenum and tungsten dimers, the dynamics of the excited state, and its relevance to the chemistry out of that state, can be better understood.

The work done on the excited state properties of the $Mo_6X_{14}^{2-}$ (X = Cl, Br, I) clusters is outlined in Chapter 2. The energy of the emissive excited state is independent of halide ligand and is best described as a metal-localized state with very little ligand character. Energy transfer quenching data have determined that the emissive excited states are spin triplets.

The unusual emissive behavior of the tungsten series $W_6X_8Y_6^{2-}$ (X,Y = Cl, Br, I) is discussed in Chapters 3 and 4. The energy of the emissive states order: $W_6Cl_{14}^{2-}$ (1.83 eV) < $W_6Br_{14}^{2-}$ (1.85 eV) < $W_6I_{14}^{2-}$ (2.05 eV), the opposite trend from that expected by including charge transfer character into the transition. Variation of axial and facial halides leads to the conclusion that the μ^3-bridging halides dominate the electronic structure of the cluster, but that the axial halides have a strong influence on the non-radiative rate. The structural studies show that the W-W bonds are longer in the $W_6I_{14}^{2-}$

cluster than in the $W_6Cl_{14}^{2-}$ structure, indicating that the metal-metal bond overlap is not the sole determining factor in the energy of the emitting excited states.

Chapters 5, 6, and 7 describe the chemistry and properties of derivatives of these hexanuclear clusters. The $W_6Br_{14}^{-}$ anion has been synthesized and its crystal structure determined. The effect of alkylphosphine ligands on the electrochemistry and photophysics of the Mo_6Cl_{12} cluster has been found to be very small. Although the $Mo_5X_{13}^{n-}$ (n = 1, 2, 3) clusters do not appear to have any interesting photochemical properties, the observation of the splitting between spin-orbit states in a high nuclearity cluster has implications in the photochemistry of the hexanuclear clusters.

Finally, the last two chapters describe work done on the electrochemistry of $Mo_2X_4(PR_3)_4$ dimers. An unexpected ordering of the redox potentials is ascribed to π-backbonding from the metal center to the halide ligand. Efficient electrogenerated chemiluminescence has been observed for several of these dimers.

Table of Contents

List of Figures

Chapter 5

Chapter 6

Chapter 7

CHAPTER 1

Introduction

Inorganic chemistry has progressed greatly in the last two decades, and no area has progressed more than the study of complexes containing metal-metal interactions[1]. These interactions can be weak, as in the $d^8 - d^8$ dimer systems where there is only a small configuration interaction and no formal bond in the ground state[2], or the metals can be intimately connected as in the quadruply bonded $d^4 - d^4$ metal dimers[3]. The size of the clusters also varies from dimeric species to discrete clusters of tens of metal atoms[4]. Unfortunately, a detailed electronic picture of the metal-metal interactions in these systems has lagged far behind the synthesis of new clusters. Studies of the bonding in these discrete molecular clusters have largely relied on crystallographic measurements to correlate metal-metal bond length with bond order[5], while computational methods have been used to estimate the electronic properties of the clusters. These calculational methods have often failed to produce results which accorded at all well with experimental data. A good example is the inability of a variety of calculational models to correctly predict the energies of the $^1(\delta\delta^*)$ and $^3(\delta\delta^*)$ excited states of quadruply bonded systems[6]. Only through careful experimentation using absorption and emission spectroscopies has a clear understanding of the dynamics of the excited states of these $(d^4)_2$ complexes been realized[7]. As for the larger clusters, there have been very little spectroscopic data which could lead the way to the same level of understanding as has been achieved in the dimers. For the low-valent, high-nuclearity clusters with π-acid ligands there have been some successful electron counting schemes and molecular

structure correlation[4].

This laboratory has taken the approach that the development of a detailed picture of the metal-metal interactions in large molecular clusters will depend on a thorough understanding of the electronic similarities of these clusters with smaller, better-understood dimer systems. Recently our attention has been focussed on clusters which are derived from square planar d^4-transition-metal monomers:

	Example
$(d^4)_2$	$Mo_2Cl_4(PR_3)_4$
$(d^4)_3$	$Re_3Cl_{12}^{3-}$
$(d^4)_4$	$Mo_4Cl_8(PR_3)_4$
$(d^4)_5$	$Mo_5Cl_{13}^{3-}$
$(d^4)_6$	$Mo_6Cl_{14}^{2-}$, $W_6Cl_{14}^{2-}$

While obviously these systems have different stoichiometries and geometries, they have significant localized structural, and therefore electronic, features in common (Figure 1.) such as the symmetry of the ligands about the metals, and the type of metal-metal interactions. For example, the symmetry of metal-ligand bonding around the molybdenum atoms in $Mo_2Cl_8^{4-}$ $[(d^4)_2]$ and $Mo_6Cl_{14}^{2-}$ $[(d^4)_6]$ is very much the same, and each molybdenum atom has four metal-metal bonds. The metal-ligand environment dictates that the molecular orbitals which make up the HOMO and LUMO are derived from the same atomic orbitals on the metals. However, these MOs have

Figure 1. Comparison of the generalized molecular structures of M_2X_8 and $(M_6X_8)X_6$ systems.

M_2X_8

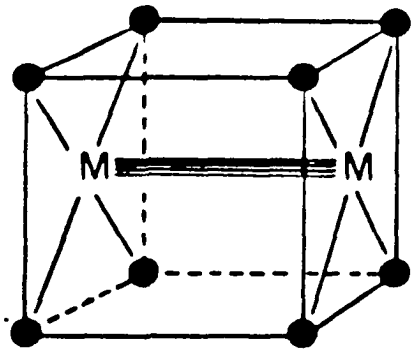

$\underset{\sim}{D}_{4h}$

M = Cr(II), Mo(II), W(II)
Tc(III), Re(III)

$(M_6X_8)X_6$

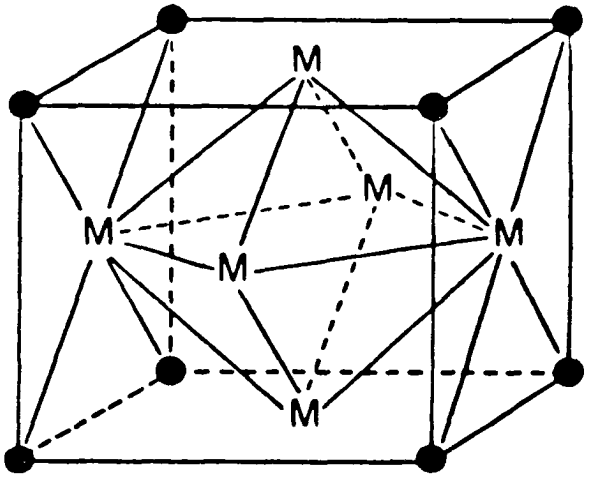

$\underset{\sim}{O}_h$

M = Mo(II), W(II)

different properties due to the geometry of the cluster involved. In the dimers, the photophysically important interaction is the δ bond formed by the weak overlap of the d_{xy} orbitals on the metals (Figure 2.)[7]. These same d_{xy} orbitals combine to form the highest energy filled MOs in the hexanuclear clusters[8], but the trans-cube interaction to form a δ bond with the opposite metal atom is negligible due to the very long distance (3.6 Å)(Chapter 4). However, in the cluster these d_{xy} functions can combine and form σ overlaps with neighboring metals. This difference in geometry, and therefore orbital symmetry, between the dimers and clusters is responsible for major differences in their electronic structures.

The general approach we have taken has been to probe the properties of the ground and low-lying excited states of these metal-metal bonded clusters by investigating their spectroscopic, photophysical, and photochemical behavior. A great deal of experimental and theoretical work has been done on the quadruply bonded dimers, resulting in a clear picture of the ground and lowest lying excited states[7]. The hexanuclear[9] and pentanuclear[10] clusters have also been studied, but the problem is much more complex. By use of the electronic analogy to the well-understood dimer systems, the electronic properties of the emitting excited state of the $Mo_6Cl_{14}^{2-}$ and $W_6Cl_{14}^{2-}$ clusters have been better understood. By utilizing this approach to understanding and developing the photochemistry of the emissive excited states of the $(d^4)_2$ and $(d^4)_6$ systems, the importance of factors such as the spin state of the excited molecule (the $(d^4)_2$ emissive state is a spin singlet, while the

Figure 2. Diagram of d_{xy} orbital overlaps in the (a) $(d^4)_2$ and (b) $(d^4)_6$ clusters.

M_2X_8

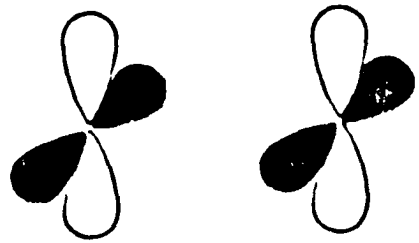

δ orbital

$Mo_6X_8(X_6)^{2-}$

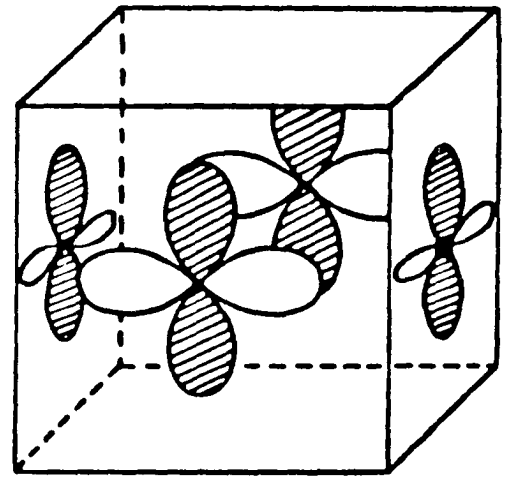

e_g orbital ("δ")

$(d^4)_6$ emissive state is a triplet), and the geometric requirements, such as the accessibility of the substrate to the metal, which are central to inorganic photochemistry, may be conveniently studied.

REFERENCES

1. Cotton, F.A.; Walton, R.A. *Multiple Bonds Between Metal Atoms*; Wiley:New York, 1982.
2. (a.) Rice, S.F.; Gray, H.B. *J. Am. Chem. Soc.*, **1981**, *101*, 1593. (b.) Rice, S.F.; Gray, H.B. *J. Am. Chem. Soc.*, **1983**, *105*, 4571.
3. Trogler, W.C.; Gray, H.B. *Accts. Chem. Res.*, **1978**, *11*, 232.
4. Johnson, B.F.G. (ed.) *Transition Metal Clusters*; Wiley:New York, 1980.
5. Cotton, F.A.; Powell, G.L. *Inorg. Chem.*, **1983**, *22*, 1507.
6. Hay, P.J. *J. Am. Chem. Soc*, **1978**, *100*, 2897; **1982**, *104*, 7007.
7. (a.) Hopkins, M.D.; Gray, H.B. *J. Am. Chem. Soc.*, **1984**, *106*, 2468. (b.) Hopkins, M.D.; Zietlow, T.C.; Miskowski, V.M.; Gray, H.B. *J. Am. Chem. Soc.*, **1985**, *107*, 510. (c.) Miskowski, V.M.; Goldbeck, R.A.; Kliger, D.S.; Gray, H.B. *Inorg. Chem.*, **1979**, *18*, 86.
8. Hoffmann, R.; Hughbanks, T., personal communication.
9. Maverick, A.W.; Nadjdzionek, J.S.; MacKenzie, D.; Nocera, D.G.; Gray. H.B. *J. Am. Chem. Soc.*, **1983**, *105*, 1878.
10. Meissner, H.; Korol'kov, D.V. *Z. Anorg. Allg. Chem.*, **1983**, *496*, 175.

CHAPTER 2

Photophysics of $Mo_6X_{14}^{2-}$ Clusters

For the past dozen years this laboratory has been investigating the electronic structures of metal-metal bonded systems with the goal of using such systems in photochemical reaction sequences. The complexes have ranged from d^8-d^8 dimers, which have a very weak metal-metal interaction in the ground state[1], to d^4-d^4 dimers, which feature a quadruple bond between the metals[2]. From these investigations a clear picture of the overall dynamics of their emissive excited states has emerged. Photochemical reactions have been devised which take advantage of the electronic and structural features of the two excited states[3,4]. In contrast to these two systems, the molybdenum and tungsten hexanuclear clusters are not well understood as to the nature of the ground state, much less the emissive excited state. Due to the complexity of the spectroscopic problem, the approach taken in the study of the Mo_6 clusters has been to determine the properties of the long-lived excited state: the halide dependence[5], the temperature dependence[6], and its photochemical reactions. Using these observations, a basic insight into the properties of this excited state can be achieved.

The $Mo_6Cl_{14}^{2-}$ ion consists of an octahedron of metal atoms, with eight μ_3-chlorides (one above each face of the octahedron) and six axial chlorides (one terminal chloride per metal) (Figure 1)[7]. The idealized symmetry of these clusters is O_h, making spectroscopic techniques such as polarized electronic spectroscopy less informative in these clusters than in other M-M bonded systems. Synthetic attempts to lower the symmetry by replacement of a molybdenum atom with a heterometal (i.e., tungsten) have been on the

Figure 1. Idealized molecular structure of $Mo_6Cl_{14}^{2-}$.

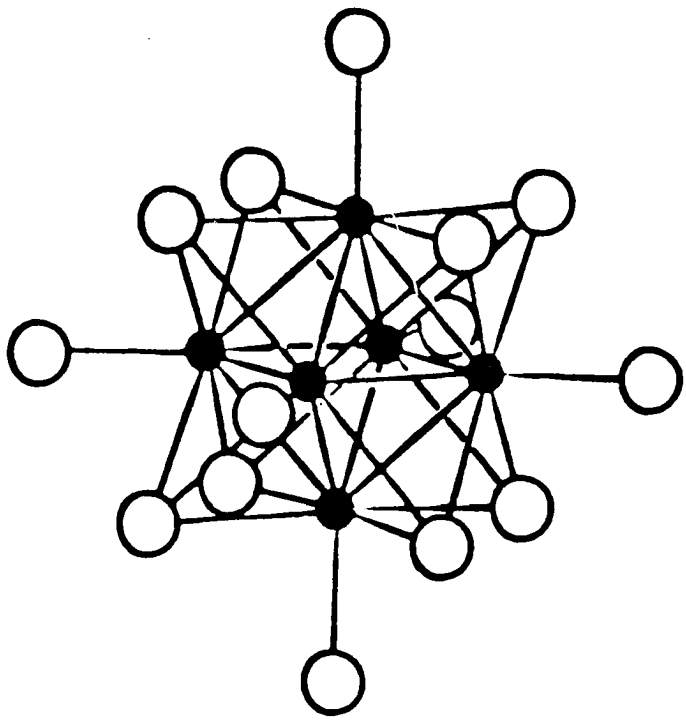

whole unsuccessful primarily due to the inability to separate the product mixtures. Also, characterization of these species would have been difficult since disorder in the crystals would almost certainly occur in this highly symmetric system.

The terminal halides are very easily replaced at room temperature in aqueous solution by other halides[8], but the triply bridging ligands are not replaced under these conditions. Fused alkali halide melts at high (300-500°C) temperatures are required for exchange of the bridging halides[9]. The relative lability of the terminal halides can be exploited to make derivatives of the molybdenum and tungsten clusters which are discussed later (Chapter 6).

The original observation which spurred interest in the photochemical properties of these hexanuclear clusters was that the $Mo_6Cl_{14}^{2-}$ anion possesses a very long-lived luminescent excited state. Both the very long emission lifetime (180 μsec in acetonitrile solution at room temperature) and the high emission quantum yield (0.19) are unusual for inorganic complexes[5,10]. Work on the $Mo_6Br_{14}^{2-}$ and $Mo_6I_{14}^{2-}$ clusters showed that they also possess long-lived, highly emissive excited states[5]. The emissive states of the $Mo_6Cl_{14}^{2-}$, $Mo_6Br_{14}^{2-}$, and $Mo_6I_{14}^{2-}$ ions are isoenergetic. From these data, the halide character in the emissive excited state is concluded to be minimal; the excited state is highly metal-localized, with little or no ligand-to-metal charge transfer character[5]. This metal-centered excited state could account for the very low rate of non-radiative decay of the excited state. With most

of the dynamics (bond length distortions, electron redistribution) shielded from the surrounding medium by the halide ligands, very little solvent interaction would be expected. Also, the cluster anion has no high-frequency vibrational modes[11] to act as acceptors in the weak coupling model for non-radiative decay, leading to a low k_{nr} [12].

EXPERIMENTAL SECTION

The amorphous Mo_6Cl_{12} starting material was purchased from Cerac Company and purified as described elsewhere[13]. The other $Mo_6X_{14}^{2-}$ complexes were synthesized by exchanging the halides of Mo_6Cl_{12} in a LiX/KX melt at temperatures > 400°C and then extracting the product into ethanol[9], followed by addition of TBAX to precipitate the $(TBA)_2Mo_6X_{14}$ cluster. Recrystallization from methylene chloride/petroleum ether resulted in large crystals. The solvents used in photophysical measurements were reagent grade and dried and vacuum distilled before use.

RESULTS

The radiative rate of the emissive excited state is relatively small, indicating that the transition between this state and the ground state is highly forbidden. While determining the orbital symmetries involved in the transition is impossible at this time, the role of the spin quantum number could

be conveniently probed by energy transfer quenching studies. Using organic acceptors with well-defined triplet excited state energies, the excited states of the Mo_6 clusters are found to be spin triplets [6]. Efficient quenching by the organic acceptors is observed for all $Mo_6X_{14}^{2-}$ clusters (Table 1). As a control $(n\text{-}Bu_4N)_2Re_2Cl_8$ was also examined due to its singlet excited state[2]; as expected, $k_q(\text{azulene}) < 10^5\ M^{-1}s^{-1}$. Delayed fluorescence of the organic quencher was observed for anthracene, confirming that the quenching of the cluster luminescence occurs via an energy transfer mechanism[14].

One very peculiar aspect of the energy transfer data is the very low quenching rate constant for $(TBA)_2Mo_6Cl_{14}$ by azulene. The azulene triplet excited state energy is much lower than that of the $Mo_6Cl_{14}^{2-*}$ energy[15], which should result in efficient quenching ($k_q \approx 10^9\ M^{-1}s^{-1}$) like that observed for $(TBA)_2Mo_6I_{14}$. The mechanism of energy transfer may involve the coupling of ligand orbitals with the orbitals directly involved in the excited state. The $Mo_6Cl_8Br_6^{2-}$ and $Mo_6Cl_8I_6^{2-}$ ions were synthesized and their quenching rate constants with azulene determined. For $(TBA)_2Mo_6Cl_8Br_6$, $k_q = 1.9 \times 10^8 M^{-1}s^{-1}$, and for $(TBA)_2Mo_6Cl_8I_6$, $k_q = 2.5 \times 10^7 M^{-1}s^{-1}$. So, although the rate constant is terminal halide dependent, the exact relationship is not clear due to the lack of a consistent trend. Further work on the energy transfer properties of the molybdenum clusters is required in order to determine what the ligand effects on the quenching rate constant imply about the excited state.

The temperature dependence of the lifetime of the emissive state of

Table 1.

Energy Transfer Quenching of Molybdenum Clusters
in Acetonitrile Solution at 295 K

Cluster (E_t)	azulene[a]	DCA[b]	anthracene	t-stilbene
	E_t=1.3eV	1.7	1.8	2.2
$Mo_6Cl_{14}^{2-}$ (1.9 eV)	$6.7x10^7$ [c]	$1.7x10^8$	$3.8x10^7$	$1.1x10^5$
$Mo_6Br_{14}^{2-}$ (1.9 eV)	$1.5x10^8$	$3.4x10^8$	$9.4x10^7$	
$Mo_6I_{14}^{2-}$ (1.9 eV)	$2.0x10^9$	$1.8x10^9$	$1.7x10^7$	

[a]Quencher triplet energies are from Murov, S.L. *Handbook of Photochemistry*;Marcel Dekker: New York, 1973. [b]DCA = 9,10-dichloroanthrancene. [c]Rate constants are all $M^{-1}s^{-1}$.

crystalline $(TBA)_2Mo_6Cl_{14}$ was determined over the range 77-300 K (Figure 2). The general shape of the curves can be described using an Arrhenius-type expression

$$k_{obs} = k_0 + k_1 exp(-E_a/kT)$$

where $k_{obs} = 1/\tau$, k_0 is the temperature independent term of the rate constant, k_1 is the pre-exponential (or frequency factor) and E_a is the activation energy for this non-radiative pathway. From work done on a $Mo_6Cl_{12}(PR_3)_2$ derivative which has been shown to display emissive behavior similar to the $Mo_6Cl_{14}^{2-}$ emissive excited state, the change in the emission lifetime as a function of temperature in this range is due to the change of the non-radiative rate of the excited state as the radiative rate stays constant (Chapter 6). When the curves are evaluated, the activation energy of the thermally accessible non-radiative pathway is found to be about 2000 cm^{-1} above the excited state. The activation energies for the three clusters ($Mo_6Cl_{14}^{2-}$, $Mo_6Br_{14}^{2-}$, and $Mo_6I_{14}^{2-}$) are similar, with the major distinction between their photophysical behavior being the temperature independent term, k_0, in the Arrenhius expression. A discussion of the similar temperature dependence of the lifetime of the emissive excited states of the tungsten series is in Chapter 3. Although the mechanism of this deactivation is not clear, the presence of this temperature dependence may have implications for the efficiency of the electrogenerated chemiluminescence of the molybdenum chloride cluster (Chapter 9).

Figure 2. Temperature dependence of k_{obs}^{em} in crystalline $(TBA)_2Mo_6X_{14}$.

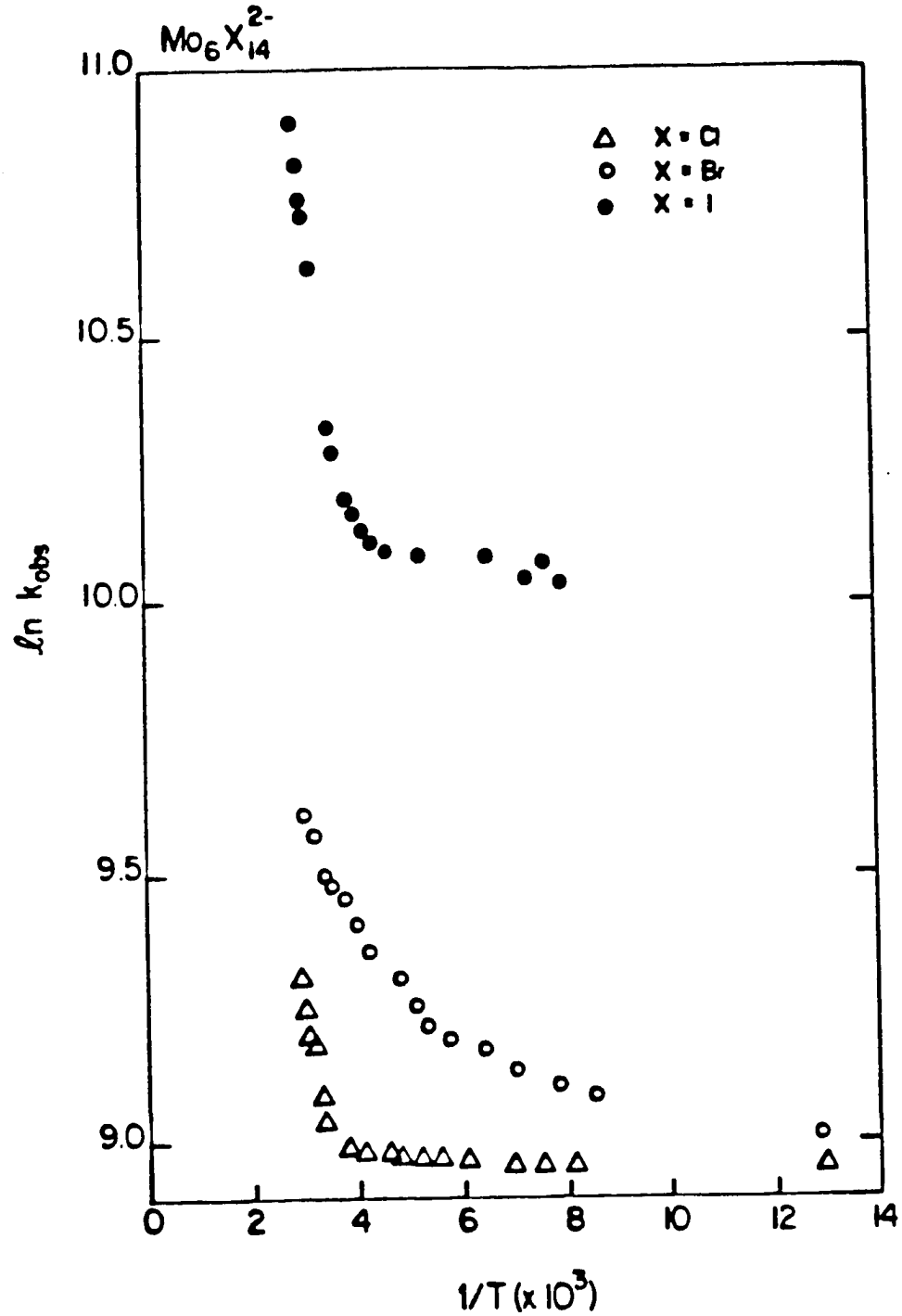
$Mo_6X_{14}^{2-}$
11.0
10.5
10.0
9.5
9.0
ln k_{obs}
X = Cl
X = Br
X = I
0
2
4
6
8
10
12
14
1/T (x 10^3)

REFERENCES

1. a.) Rice, S.F.; Gray, H.B. *J. Am. Chem. Soc.*, **1981**, *103*, 1593. b.) Rice, S.F.; Gray, H.B. *J. Am. Chem. Soc.*, **1983**, *105*, 4571.
2. Trogler, W.C.; Gray, H.B. *Acc. Chem. Res.*, **1978**, *11*, 232.
3. a.) Mann, K.R.; Gray, H.B. *Adv. Chem. Ser.*, **1979**, *No.173*, 225. b.) Caspar, J.V.; Gray, H.B. *J. Am. Chem. Soc.*, **1984**, *106*, 3029.
4. Nocera, D.G.; Gray, H.B. *Inorg. Chem.*, **1984**, *23*, 3686.
5. Maverick, A.W.; Nadjdzionek, J.S.; MacKenzie, D.; Nocera, D.G.; Gray, H.B. *J. Am. Chem. Soc.*, **1983**, *105*, 1878.
6. Zietlow, T.C.; Hopkins, M.D.; Gray, H.B. *J. Solid State Chem.*, in press.
7. Vaughn, P.A. *Proc. Nat. Acad. Sci.*, **1950**, *36*, 461.
8. Hogue, R.D.; McCarley, R.E. *Inorg. Chem.*, **1970**, *9*, 1354.
9. Sheldon, J.C. *J. Chem. Soc.*, **1962**, 410.
10. Maverick, A.W.; Gray, H.B. *J. Am. Chem. Soc.*, **1981**, *103*, 1298.
11. Woodruff, W., personal communication.
12. Englman, R.; Jortner, J. *Molecular Physics*, **1970**, *18*, 145.
13. Maverick, A.W. Ph.D. Dissertation, California Institute of Technology, **1982**.
14. Turro, N. *Modern Molecular Photochemistry*, Benjamin/Cummings Publishing:Menlo Park, CA, 1978.
15. Murov, S.L. *Handbook of Photochemistry*, Marcel Dekker:New York, 1973.

CHAPTER 3

Hexanuclear Tungsten Halide Clusters. Unusual Halide Dependence of the Emissive State

Hexanuclear Tungsten Halide Clusters. Unusual Halide Dependence of the Emissive State

Thomas C. Zietlow, Daniel G. Nocera, and Harry B. Gray*

Contribution No. ____ from the Arthur Amos Noyes Laboratory of Chemical Physics, California Institute of Technology, Pasadena, California, 91125.

Abstract. A variety of techniques have been used to study the emissive behavior and electrochemistry of hexanuclear tungsten halide clusters. The three $W_6X_{14}^{2-}$ (X = Cl, Br, I) clusters possess emissive excited states characterized by microsecond lifetimes and large emission quantum yields (up to 0.39). The energy of the emitting excited state increases: $W_6Cl_{14}^{2-}$ (1.83 eV) < $W_6Br_{14}^{2-}$ (1.85 eV) < $W_6I_{14}^{2-}$ (2.05 eV), the opposite trend from that expected when charge transfer character is mixed into a primarily metal-localized transition. Room temperature and variable temperature emission data have been collected for the $(TBA)_2W_6X_8Y_6$ (X,Y = Cl, Br, I) clusters. This work indicates that the μ^3-bridging halides primarily determine the energy of the emitting excited state. As the μ^3-halide is exchanged from Cl to Br to I, the influence of the axial halides on the energy of the emissive state diminishes. The axial halides do have a profound effect on the non-radiative rate, with k_{nr} decreasing as the outer halide is exchanged Cl to Br to I. The variable temperature data can be fit to an Arrhenius expression, resulting in the same activation energy for all the various halides, but with different pre-exponential terms. The one-electron oxidation potentials for several of the clusters are reported; these potentials imply that the μ^3-halides dominate the electrochemistry of the clusters as well as the photophysical properties.

One of the primary goals of this laboratory is to investigate possible reaction pathways involving multi-electron transfer steps out of long-lived excited states of inorganic complexes. Our work has become focussed on polynuclear systems, with the idea that these types of clusters may undergo multiple changes in oxidation state without losing their structural integrity. Work in this lab has shown that the hexanuclear d^4 clusters $M_6X_{14}^{2-}$ (M = Mo, W; X = Cl, Br, I) possess the desirable characteristics of having long-lived excited states and several accessible oxidation states[1].

Earlier work on the luminescence of $Mo_6Cl_{14}^{2-}$, $Mo_6Br_{14}^{2-}$, and $W_6Cl_{14}^{2-}$ cluster anions suggested that the electronic transition from the emissive excited state to the ground state is primarily localized on the metal core[2]. Further work has confirmed this as a good description for the $Mo_6X_{14}^{2-}$ (X = Cl, Br, I) series[3], but the emissive behavior of the analogous tungsten halide cluster series is more complex. In order to shed some light on the emissive excited state of the clusters, the mixed halide cluster $W_6X_8Y_6^{2-}$ (X, Y = Cl, Br, I) have been prepared and their photophysical and electrochemical behavior studied. In this way, the influence of the outer halides on the chemistry of these systems may be better understood; in particular, their effect on the radiative and non-radiative processes out of the emissive excited state can be discerned.

EXPERIMENTAL SECTION

Cluster compounds. The $[(n\text{-}C_4H_9)_4N]_2Mo_6Cl_{14}$, $[(n\text{-}C_4H_9)_4N]_2Mo_6Br_{14}$, and $[(n\text{-}C_4H_9)_4N]_2W_6Cl_{14}$ clusters were prepared as described previously[2]. The other $[(n\text{-}C_4H_9)_4N]_2M_6X_{14}$ clusters were prepared by alkali melt reactions as described by Sheldon[4]. The mixed halide clusters $[(n\text{-}C_4H_9)_4N]_2M_6X_8Y_6$ were prepared by reflux and repeated recrystallization of the hydronium salt in aqueous HY solution as described by McCarley and coworkers[5], followed by treatment of the aqueous HY solution with $(n\text{-}C_4H_9)_4NY$. All carbon, hydrogen and nitrogen analyses were satisfactory.

Solvents. The acetonitrile and propylene carbonate solvents used in the photophysical measurements were Burdick and Jackson reagent grade. The acetonitrile was dried over CaH_2, then vacuum-transferred onto activated alumina. All samples were degassed by repeated freeze-pump-thaw cycles. All other solvents were of reagent grade and used without further purification.

Instrumentation. Absorption spectra were measured on a Cary 17 spectrophotometer. The emission spectra were recorded on an apparatus built at Caltech and described elsewhere[6]. All emission spectra were corrected for monochromator and photomultiplier response. Electrochemical measurements were performed on PAR Models 175, 173, and 179 electronics. Working and counter electrodes were platinum. Emission lifetime experiments were done using the 355 nm line of a Nd:YAG laser (fwhm = 8 ns). Emission lifetimes were calculated using a least squares fit to signal-averaged

data on a PDP11 computer interfaced to the laser system.

RESULTS

The cluster anions $W_6X_{14}^{2-}$ are lemon-yellow to deep orange in color in both the solid and in solution. The absorption spectra are dominated by charge transfer bands in the near ultraviolet region (Figure 1). These bands progressively red shift upon exchange of the halides from chloride through iodide, confirming their ligand-to-metal charge transfer character. There are a number of very weak features at low energy which are resolved at low temperature in the $[(n\text{-}C_4H_9)_4N]_2W_6Cl_{14}$ crystal absorption spectrum. No clear assignment of these bands can be made at this time, although it is likely that one or more of these bands correspond to the absorption into the emissive excited state. Emission spectroscopy has proved to be a much better technique to examine the properties of the lowest electronic excited state of these clusters.

The hexanuclear cluster systems $W_6X_8Y_6^{2-}$ are all luminescent in solution as well as in the solid. Emission spectra for the homologous complexes $W_6X_{14}^{2-}$ (X = Cl, Br, I) are displayed in Figure 2. Numerical data from the spectra of all nine $W_6X_8Y_6^{2-}$ clusters in acetonitrile are given in Table 1. In contrast to the molybdenum series, where the emissive excited state energies were the same for $Mo_6Cl_{14}^{2-}$, $Mo_6Br_{14}^{2-}$ [3], and $Mo_6I_{14}^{2-}$, the tungsten cluster emission spectra are halide dependent. The energy of the emitting excited state increases in the $W_6X_{14}^{2-}$ spectra according to Cl(1.83 eV) < Br(1.85

Figure 1. Optical absorption spectra in acetonitrile solution for (a.) $(TBA)_2W_6Cl_{14}$; (b.) $(TBA)_2W_6Cl_8Br_6$; (c.) $(TBA)_2W_6Cl_8I_6$; (d.) $(TBA)_2W_6Br_6Cl_6$; (e.) $(TBA)_2W_6Br_{14}$; (f.) $(TBA)_2W_6Br_8I_6$; (g.) $(TBA)_2W_6I_8Cl_6$; (h.) $(TBA)_2W_6I_8Br_6$; (i.) $(TBA)_2W_6I_{14}$.

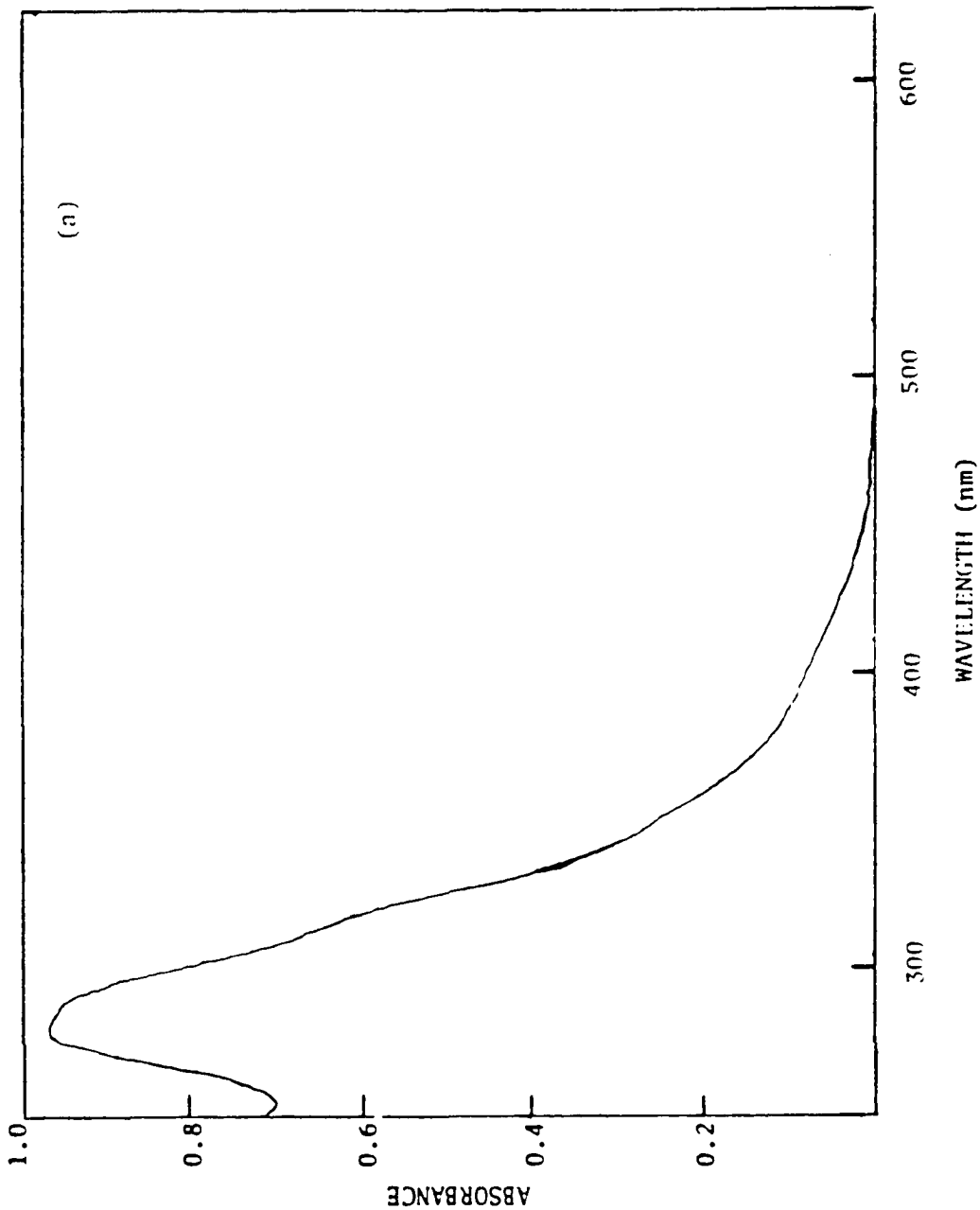
(a)
1.0
0.8
0.6
0.4
0.2
ABSORBANCE
300
400
500
600
WAVELENGTH (nm)

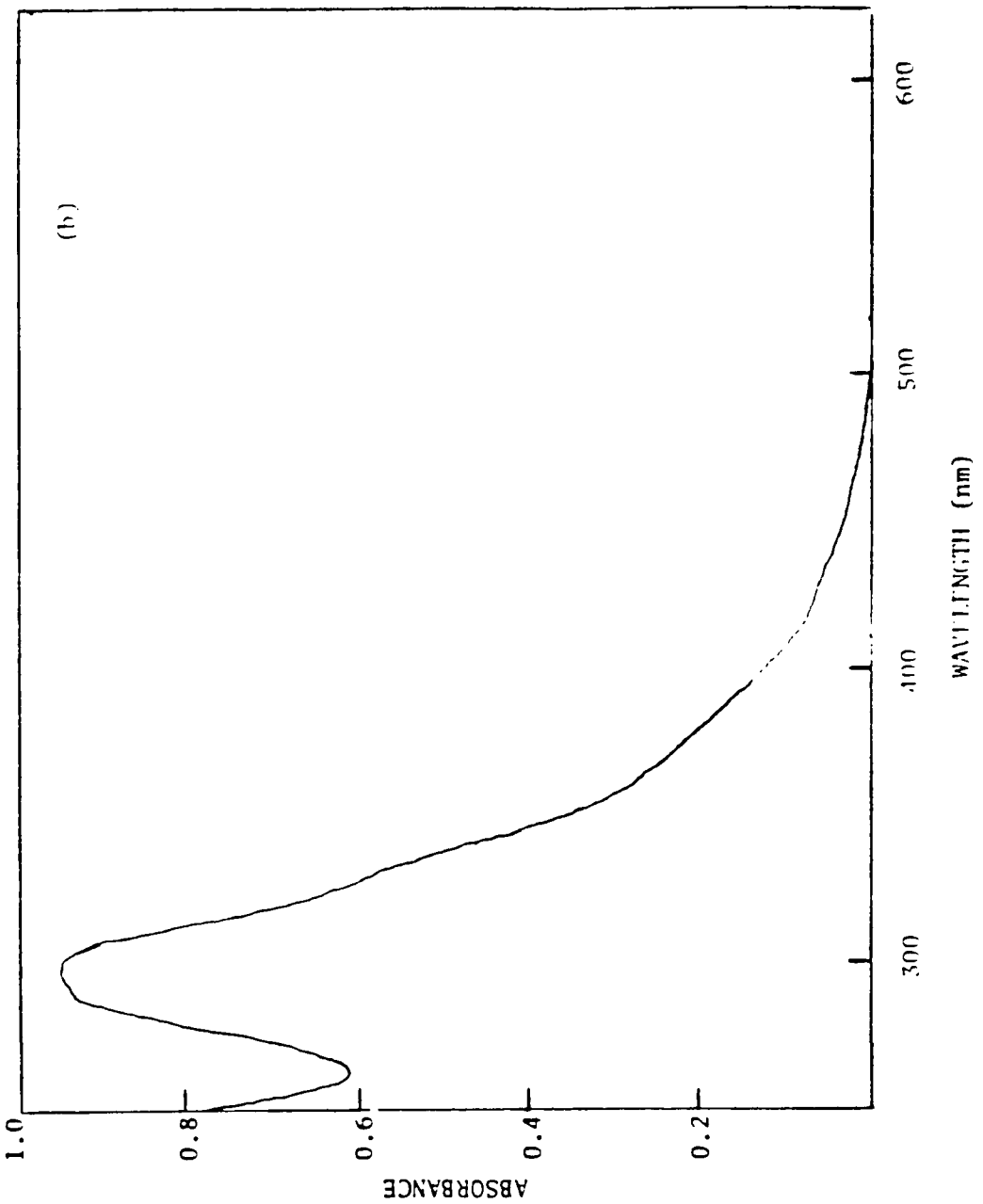
(b)
1.0
0.8
0.6
0.4
0.2
ABSORBANCE
300
400
500
600
WAVELENGTH (nm)

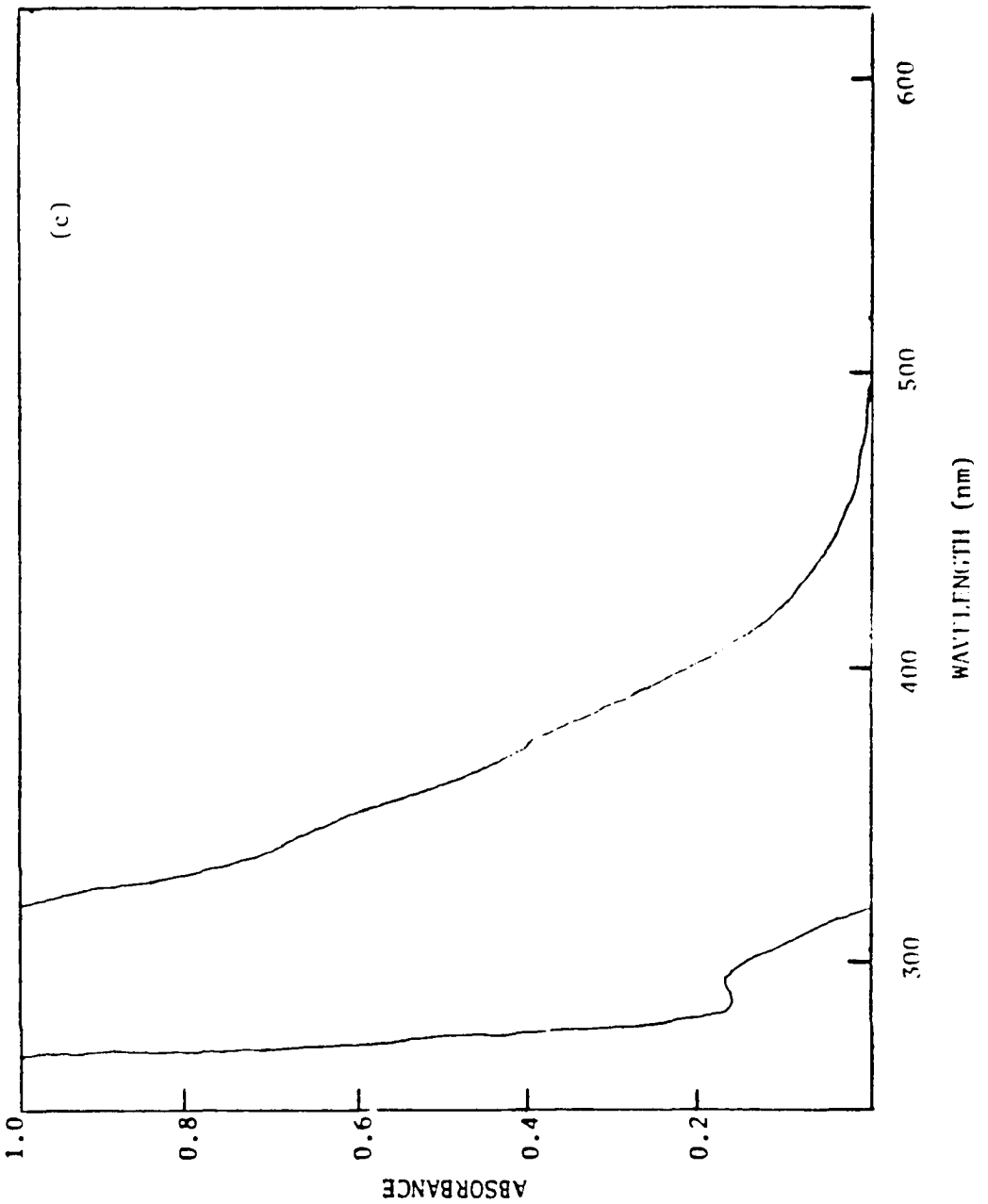
(c)
1.0
0.8
0.6
0.4
0.2
ABSORBANCE
300
400
500
600
WAVELENGTH (nm)

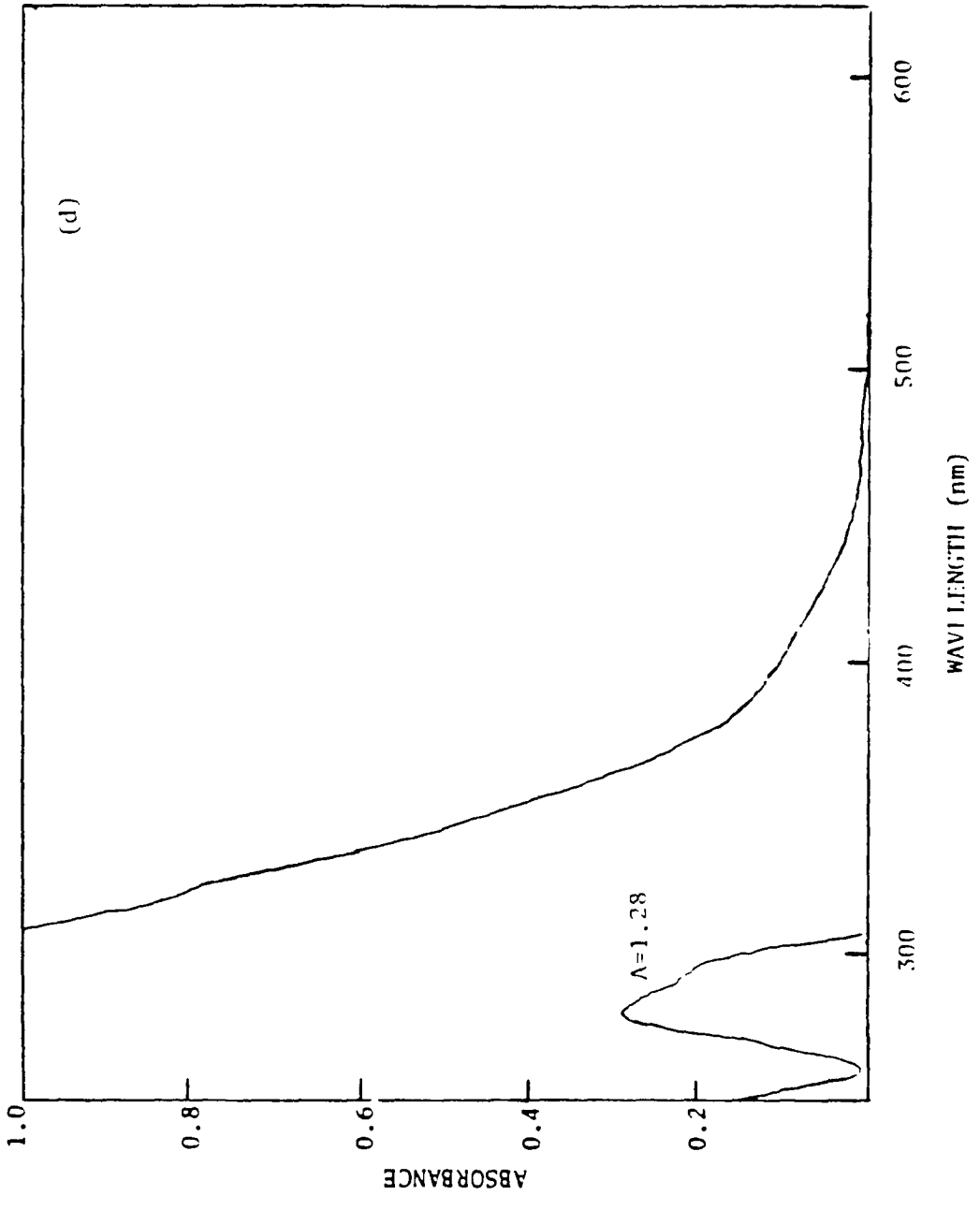
(d)
A=1.28
ABSORBANCE
1.0
0.8
0.6
0.4
0.2
300
400
500
600
WAVELENGTH (nm)

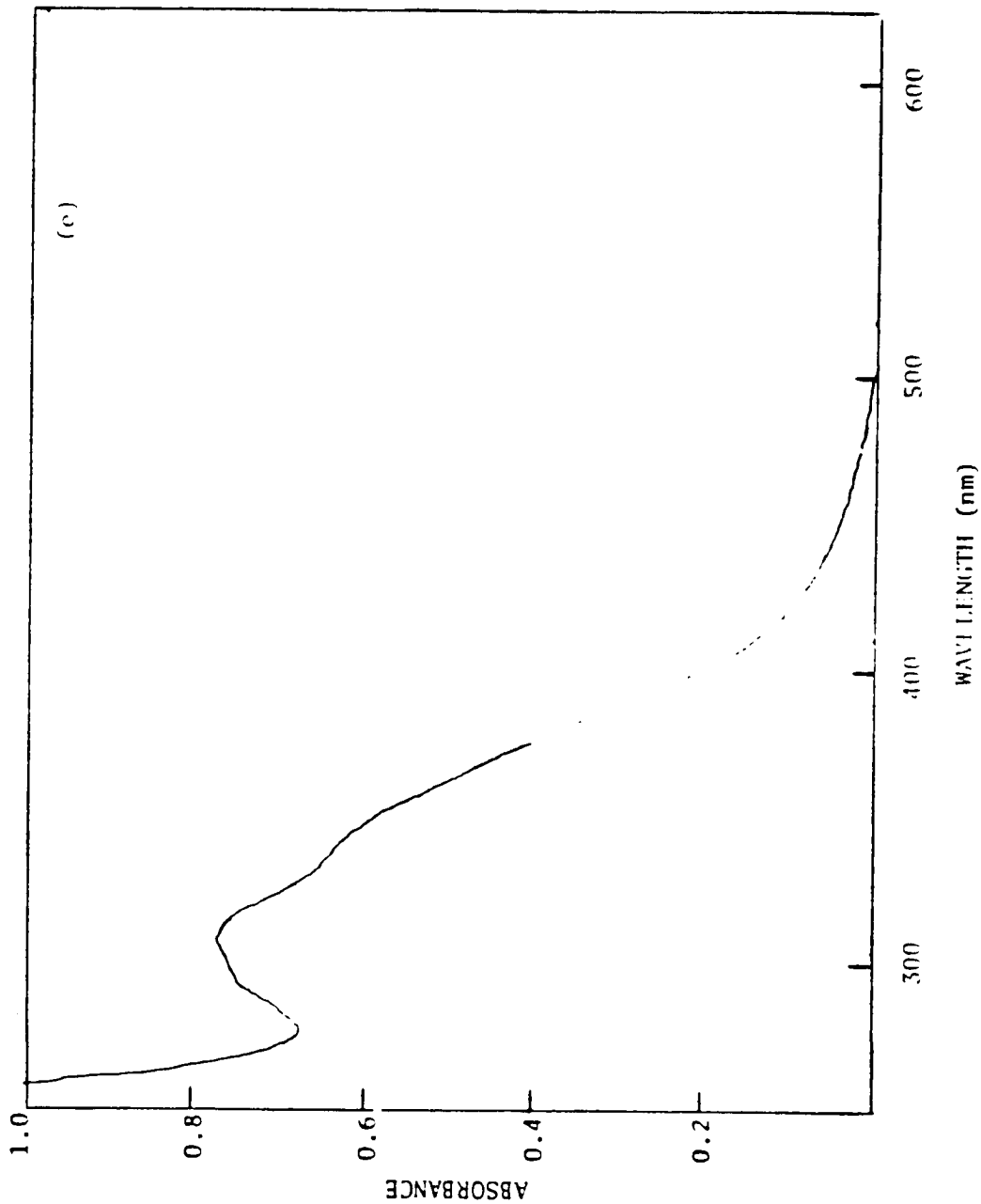
(c)
1.0
0.8
0.6
0.4
0.2
ABSORBANCE
300
400
500
600
WAVELENGTH (nm)

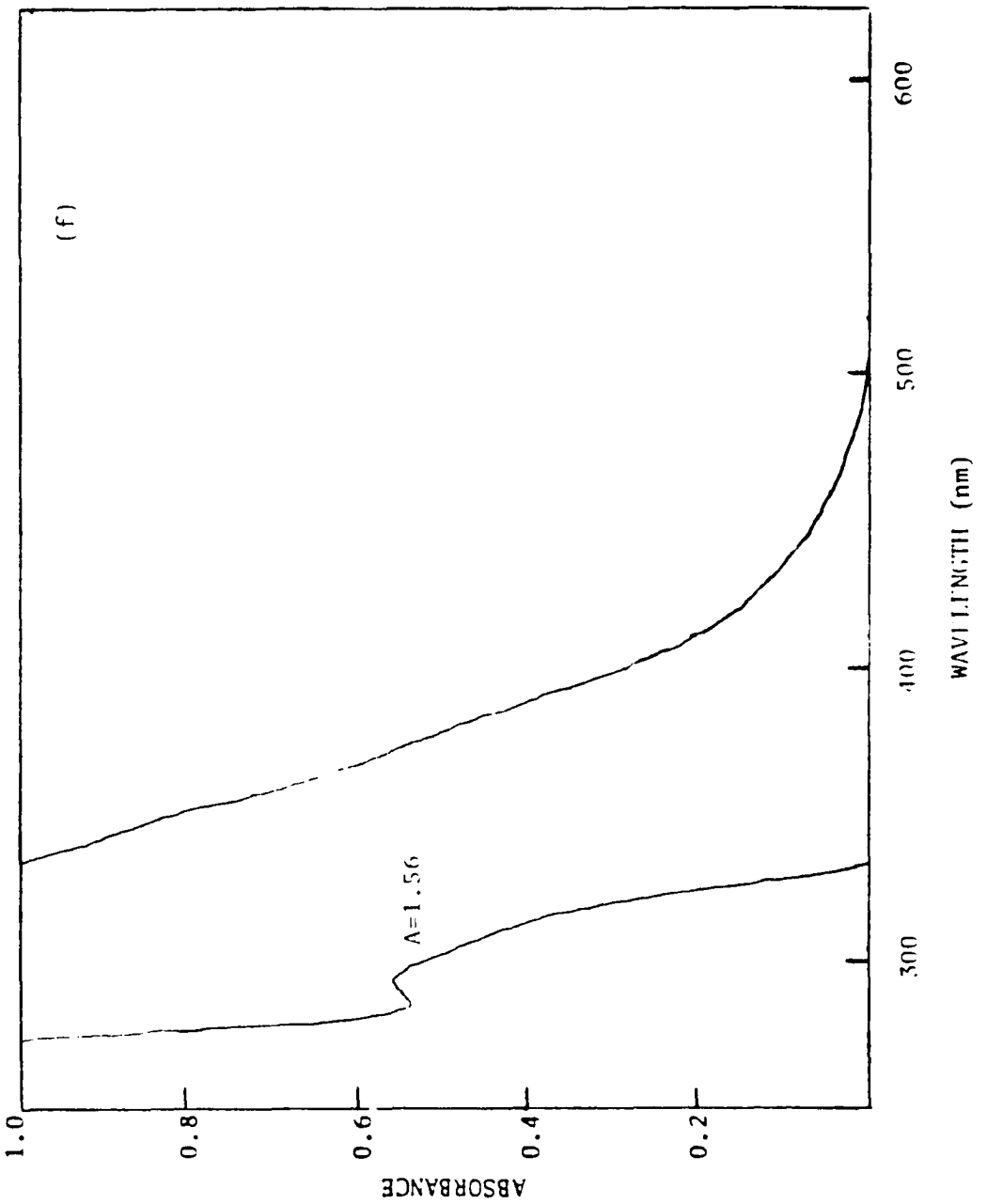
(f)
A=1.56
ABSORBANCE
1.0
0.8
0.6
0.4
0.2
300
400
500
600
WAVELENGTH (nm)

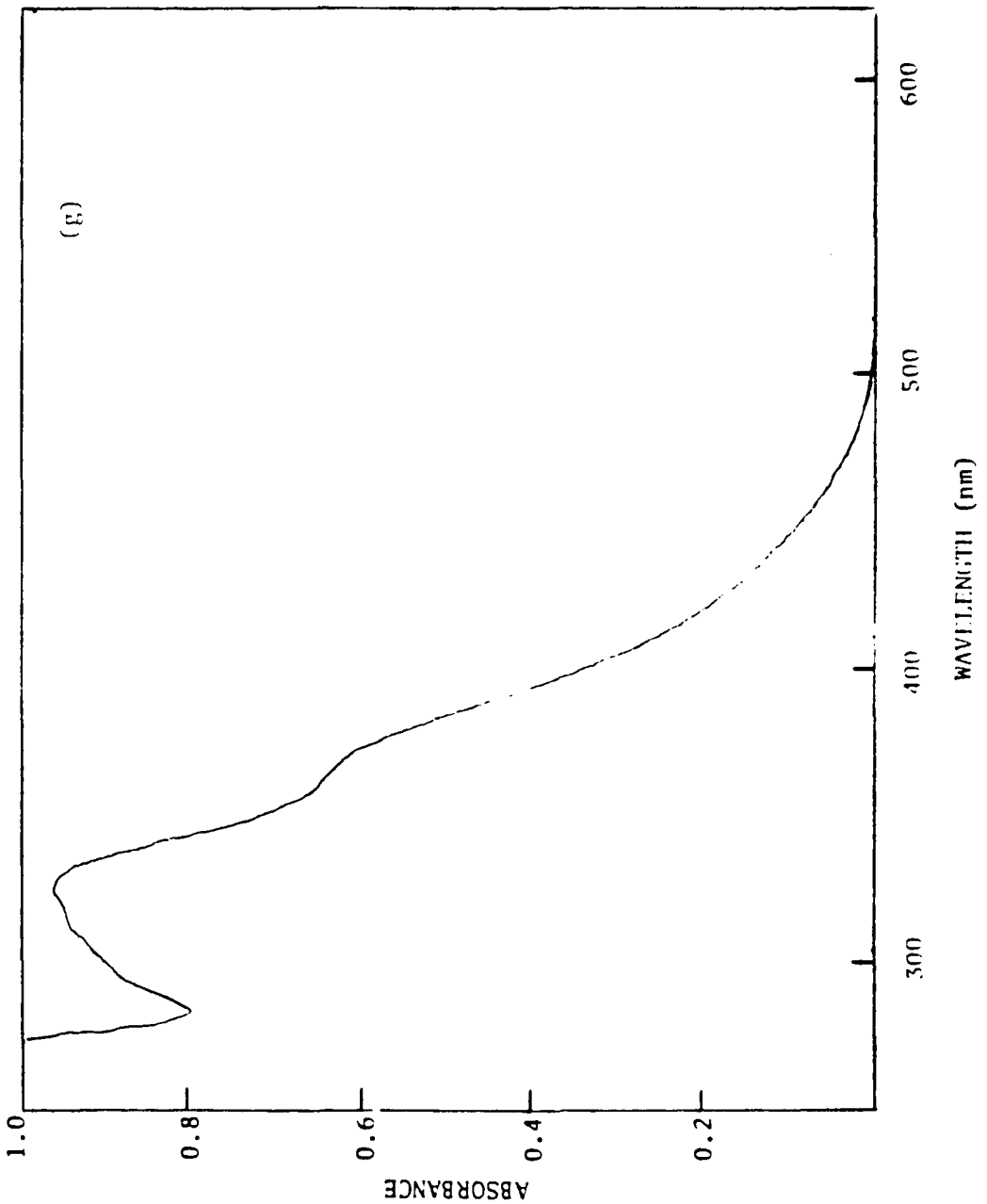
(g)
1.0
0.8
0.6
0.4
0.2
ABSORBANCE
300
400
500
600
WAVELENGTH (nm)

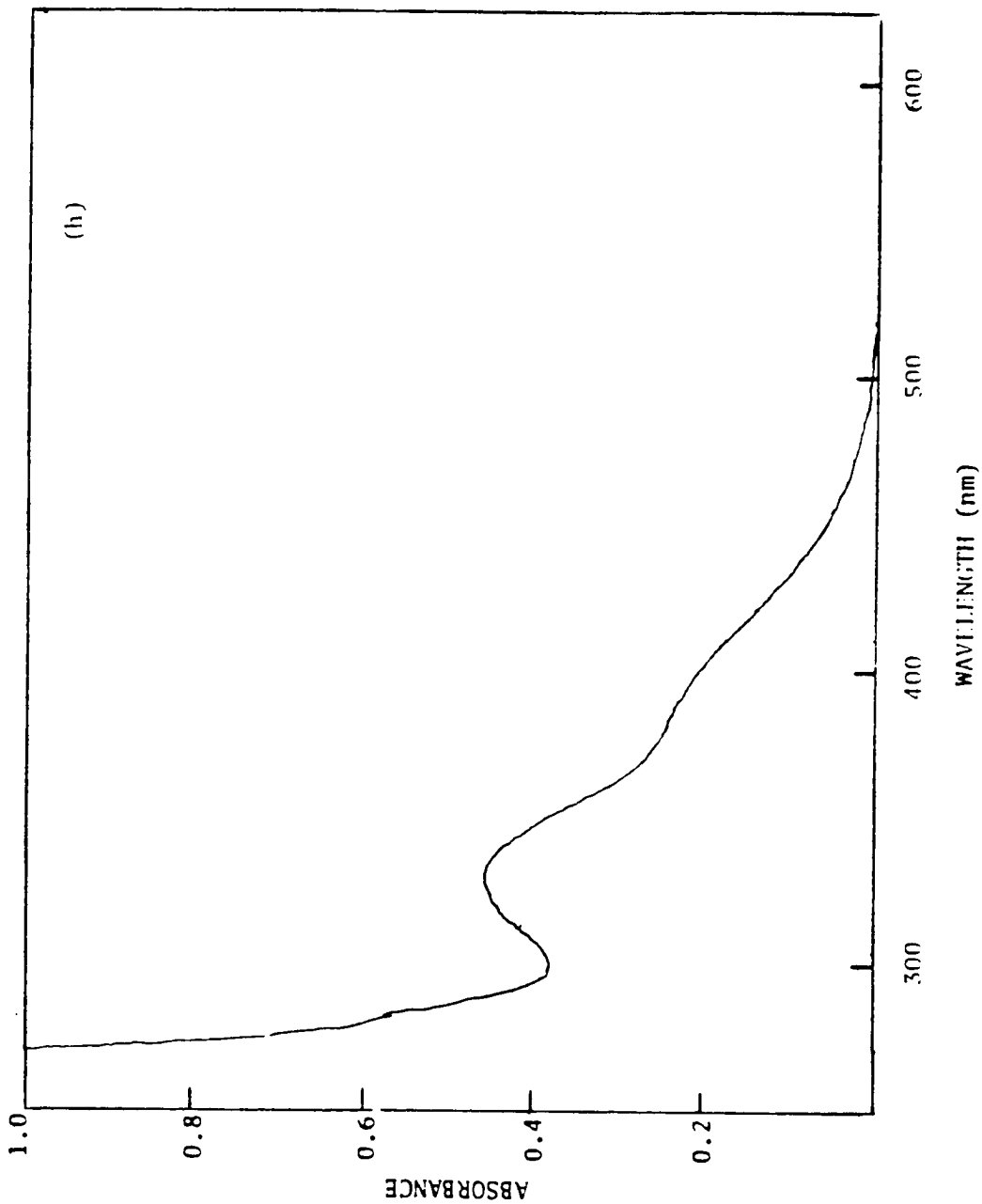
(h)
1.0
0.8
0.6
0.4
0.2
ABSORBANCE
300
400
500
600
WAVELENGTH (nm)

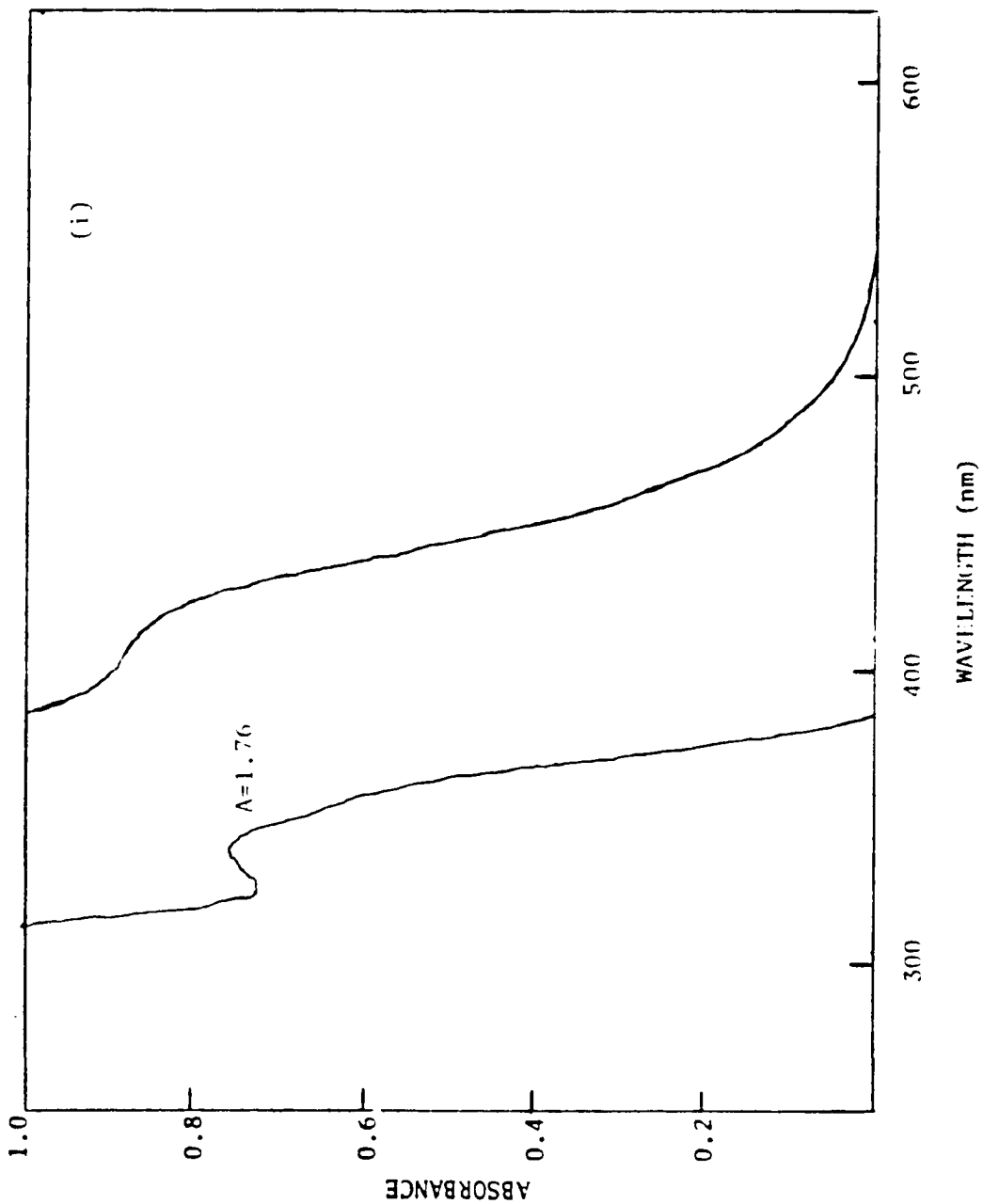
(i)
A=1.76
1.0
0.8
0.6
0.4
0.2
ABSORBANCE
300
400
500
600
WAVELENGTH (nm)

Figure 2. Corrected emission spectra in acetonitrile solution for (a.) $(TBA)_2W_6Cl_{14}$; (b.) $(TBA)_2W_6Br_{14}$; (c.) $(TBA)_2W_6I_{14}$. Emission intensity is arbitrary.

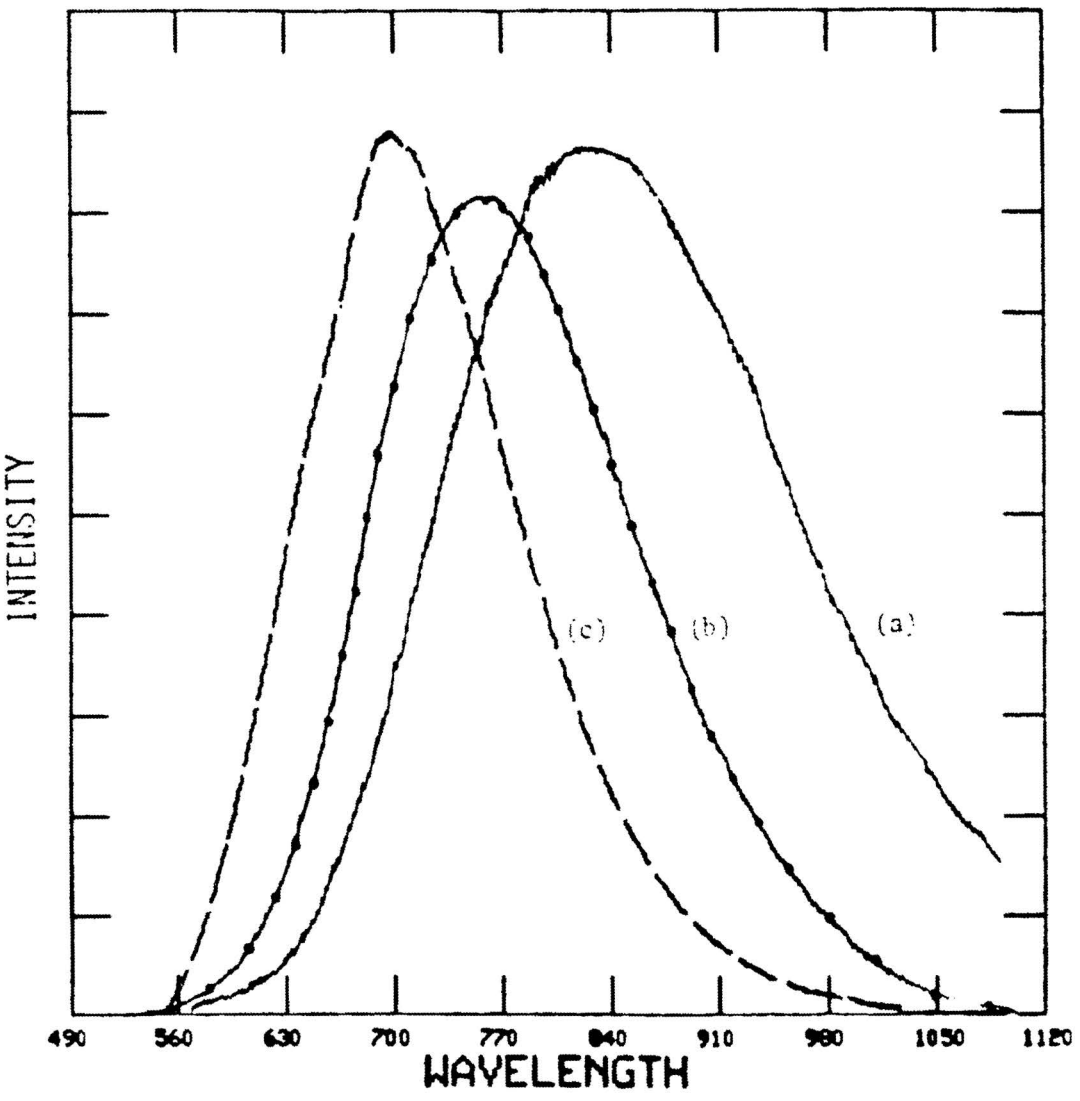
INTENSITY
(c)
(b)
(a)
490
560
630
700
770
840
910
980
1050
1120
WAVELENGTH

Table 1.

Emission Spectral Data

Complex	Emission Energy		fwhm*
	λ_{max} (nm)	$\bar{\nu}$ (cm^{-1})	$\bar{\nu}$ (cm^{-1})
$(TBA)_2W_6Cl_{14}$	833	12004	3689
$(TBA)_2W_6Cl_8Br_6$	814	12285	3671
$(TBA)_2W_6Cl_8I_6$	802	12469	3776
$(TBA)_2W_6Br_8Cl_6$	766	13055	3481
$(TBA)_2W_6Br_{14}$	758	13192	3387
$(TBA)_2W_6Br_8I_6$	752	13298	3360
$(TBA)_2W_6I_8Cl_6$	701	14265	3445
$(TBA)_2W_6I_8Br_6$	698	14327	3451
$(TBA)_2W_6I_{14}$	698	14327	3291

All data recorded in acetonitrile solution at 21±2°C. TBA = $(n\text{-}C_4H_9)_4N^+$. fwhm = full width at half-maximum.

eV) < I(2.05 eV)[7]. This is the opposite trend from that expected when ligand-to-metal charge transfer character is mixed into what is viewed as a primarily metal centered transition (by analogy to the Mo_6 clusters). No vibrational structure has been observed at low temperature in the emission spectra of any of these tungsten clusters.

Room temperature emission lifetime and quantum yield measurements were determined for all nine cluster systems $W_6X_8Y_6^{2-}$ (X,Y = Cl, Br, I) in acetonitrile solution at 21 ± 2°C (Table 2). All emission decay traces displayed first-order kinetics over at least three lifetimes. The resulting calculated radiative and non-radiative rates for the emissive excited states are also displayed in Table 2. The lifetime of the excited state increases in the order Y(terminal halide) = Cl < Br < I for a given bridging halide X. The quantum yield for emission follows the same trend, implying that the radiative rate for a particular cluster excited state is independent of the terminal halide, but the non-radiative rate out of the emissive excited state does depend on the terminal ligand.

Earlier work reported on these cluster systems involved the temperature dependence of the lifetime of the excited state of $[(n\text{-}C_4H_9)_4N]_2M_6X_8Y_6$ (M = Mo, W; X = Cl, Br, I) in crystalline form[8]. This work indicated that there is a non-radiative pathway available to the excited state ≈ 2000 cm^{-1} above the emitting excited state in the tungsten systems. In trying to understand the nature of this decay pathway, the temperature dependences of the lifetime of all nine $[(n\text{-}C_4H_9)_4N]_2W_6X_8Y_6$ molecules were determined in propy-

Table 2.

Room Temperature Emission Data

Complex	$\tau(\mu sec)$	ϕ_{em}	$k_r(s^{-1})$	$k_{nr}(s^{-1})$
$(TBA)_2W_6Cl_{14}$	1.5	0.02	$1.3x10^4$	$6.5x10^5$
$(TBA)_2W_6Cl_8Br_6$	2.3	0.04	$1.7x10^4$	$4.2x10^5$
$(TBA)_2W_6Cl_8I_6$	3.0	0.07	$2.3x10^4$	$3.1x10^5$
$(TBA)_2W_6Br_8Cl_6$	9.7	0.10	$1.0x10^4$	$9.3x10^4$
$(TBA)_2W_6Br_{14}$	15	0.15	$1.0x10^4$	$5.7x10^4$
$(TBA)_2W_6Br_8I_6$	15	0.25	$1.7x10^4$	$5.0x10^4$
$(TBA)_2W_6I_8Cl_6$	10	0.11	$1.1x10^4$	$8.9x10^4$
$(TBA)_2W_6I_8Br_6$	22	0.25	$1.1x10^4$	$3.4x10^4$
$(TBA)_2W_6I_{14}$	30	0.39	$1.3x10^4$	$2.0x10^4$

Data recorded in acetonitrile solution at 21 ± 2^oC.

lene carbonate solution. Propylene carbonate was chosen for its favorable solvent properties, its high boiling point (enabling a large temperature range for the experiment), and the similarity of the photophysics of the clusters in propylene carbonate solution and acetonitrile solution at room temperature. A sample plot of the data for the $[(n\text{-}C_4H_9)_4N]_2W_6Cl_8X_6$ clusters is shown in Figure 3. The results of the variable temperature lifetime experiments for all the clusters are given in Table 3. Using an Arrhenius-type expression

$$k_{obs} = k_0 + k_1 exp[-E_a/kT]$$

where k_0 is the non-thermally activated rate constant, k_1 is the pre-exponential term (or frequency factor) and E_a is the Arrhenius activation energy, the data show that all the clusters have the same activation barrier. The pre-exponential term is responsible for the variation in the room temperature photophysics. The pre-exponential term is consistently in the order $k_1(I) < k_1(Br) < k_1(Cl)$ for k_1 (terminal halide Y) for all the W_6X_8 cores. All of the cluster lifetimes became temperature independent at low temperature as the k_0 term of the Arrhenius expression becomes dominant.

Energy transfer experiments using organic acceptors with well-established triplet excited state energies show that the emissive excited states of the clusters are spin triplets. Efficient quenching by the triplet organic acceptors is observed for all three clusters (Table 4). As a control, $[(n\text{-}C_4H_9)_4N]_2Re_2Cl_8$ was also examined, since the long-lived emissive excited state for this dimer has been shown to be a singlet[9], as expected, $k_q(\text{azulene}) < 10^5\ M^{-1}s^{-1}$. Delayed fluorescence was observed from the

Figure 3. Temperature dependence of k_{obs}^{em} in $(TBA)_2W_6Cl_8X_6$ (propylene carbonate solution).

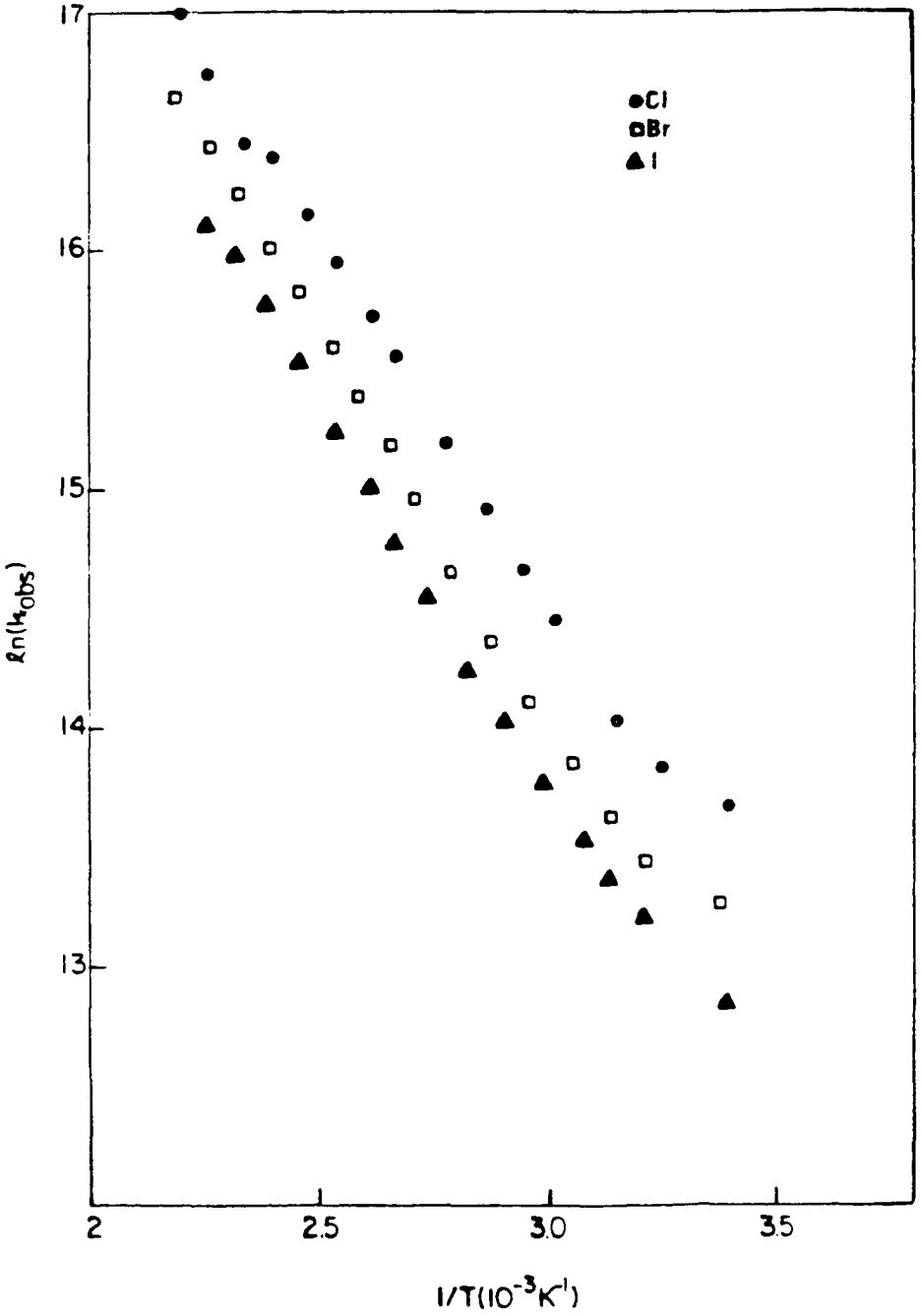
17
16
15
14
13
2
2.5
3.0
3.5
ln(k_obs)
1/T(10^-3 K^-1)
●Cl
□Br
▲I

Table 3.

Arrhenius Activation Parameters

$$k_{obs} = k_0 + k_1 \exp[-E_a/kT]$$

Complex	E_a (cm^{-1})	k_1 (s^{-1})
$(TBA)_2W_6Cl_{14}$	2189	2.5×10^{10}
$(TBA)_2W_6Cl_8Br_6$	2241	2.1×10^{10}
$(TBA)_2W_6Cl_8I_6$	2291	1.8×10^{10}
$(TBA)_2W_6Br_8Cl_6$	2337	4.2×10^{9}
$(TBA)_2W_6Br_{14}$	2340	2.9×10^{9}
$(TBA)_2W_6Br_8I_6$	2357	2.4×10^{9}
$(TBA)_2W_6I_8Cl_6$	2084	1.2×10^{9}
$(TBA)_2W_6I_8Br_6$	2173	8.2×10^{8}
$(TBA)_2W_6I_{14}$	2224	8.2×10^{8}

Table 4.

Energy Transfer Quenching of Tungsten Clusters

in Acetonitrile Solution at 295 K

Cluster (E_t)	azulene[a]	DCA[b]	anthracene	t-stilbene
	E_t=1.3eV	1.7	1.8	2.2
$W_6Cl_{14}^{2-}$ (1.83 eV)	$1.1x10^9$ [c]	$8.7x10^8$	$1.0x10^7$	$< 10^5$
$W_6Br_{14}^{2-}$ (1.85 eV)	$1.2x10^9$	$8.1x10^8$	$1.1x10^8$	$< 10^5$
$W_6I_{14}^{2-}$ (2.05 eV)	$1.9x10^9$	$5.9x10^9$	$1.9x10^9$	$2.7x10^7$

[a]Quencher triplet energies are from Murov, S.L. *Handbook of Photochemistry*; Marcel Dekker: New York, 1973. [b]DCA = 9,10-dichloroanthracene. [c]Rate constants are all $M^{-1}s^{-1}$.

organic quencher, confirming the energy transfer mechanism[10]. The anthracene quenching data clearly shows the same energy ordering for the emissive states of $W_6X_{14}^{2-}$ as the emission data, $W_6Cl_{14}^{2-} < W_6Br_{14}^{2-} < W_6I_{14}^{2-}$.

The one-electron oxidation potentials for the $Mo_6Cl_{14}^{2-}$, $Mo_6Br_{14}^{2-}$, and $W_6Cl_{14}^{2-}$ clusters were reported earlier[2]. The cyclic voltammograms of some of the mixed halide tungsten clusters have also been recorded in acetonitrile solution. Not all of the cluster oxidation waves were fully reversible, and with some of the clusters there was a problem with adsorption onto the platinum electrode. The half-wave potentials of the tungsten clusters are given in Table 5. The cyclic voltammogram of $[(n\text{-}C_4H_9)_4N]_2W_6Br_{14}$ at several scan rates is shown in Figure 4 as an example. All of the oxidation potentials listed as reversible fulfill the criteria that the $i_{p,c} = i_{p,a}$, and a plot of $\nu^{\frac{1}{2}}$ versus i_p is linear. The peak separations were typically greater than 60 mV without compensation for solution resistance. There is further oxidative current as the potential is made more positive, but the couple is not at all reversible. Whether this denotes a structural change in the cluster (perhaps resulting in the formation of the M_6X_{18} structure with μ^2-bridging halides[11]) is being investigated. The reductive electrochemistry of the tungsten clusters does not appear to be reversible in any of the systems studied.

DISCUSSION

From the results described above, the role of the ligands in determining the properties of the emissive excited state in the tungsten system can

Table 5.

Oxidation Potentials in Acetonitrile

Complex	$E_{\frac{1}{2}}(ox)$
$(TBA)_2W_6Cl_{14}$	+1.12 V
$(TBA)_2W_6Cl_8Br_6$	+1.16 V
$(TBA)_2W_6Br_8Cl_6$	+0.93 V
$(TBA)_2W_6Br_{14}$	+0.97 V
$(TBA)_2W_6I_{14}$	+0.71 V

All potentials are versus the SCE reference electrode (0.1 M $TBAPF_6$ in acetonitrile, 22°C.)

Figure 4. Cyclic voltammogram of $(TBA)_2W_6Br_{14}$ in acetonitrile (0.1 M $TBAClO_4$, 25°C).

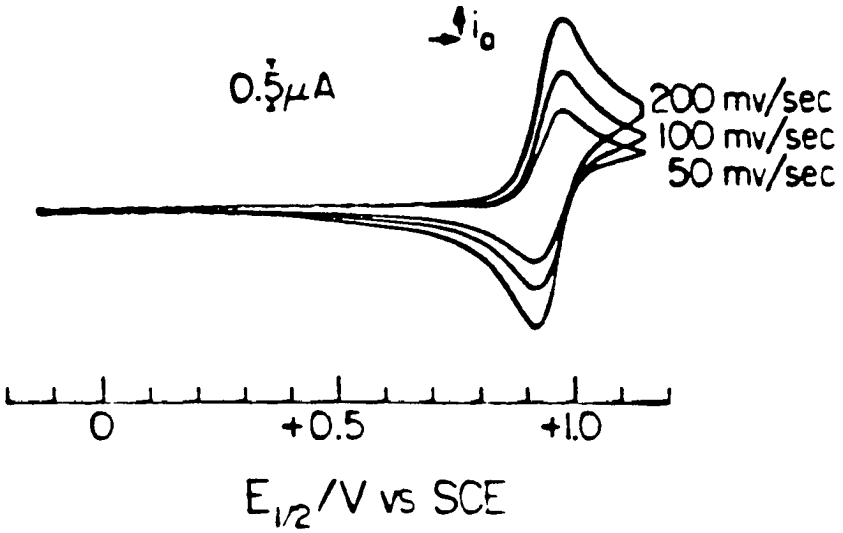
i_a
0.5 μA
200 mv/sec
100 mv/sec
50 mv/sec
0
+0.5
+1.0
$E_{1/2}$/V vs SCE

be discerned. The six halides in the terminal positions affect the emission energy only slightly; this effect diminishes as the inner core halides become larger. For example, the electronic interaction of the six tungsten atoms with the terminal halides is much smaller in the $W_6I_8^{4+}$ core. This diminished interaction is also observed in the kinetic data where the radiative rate out of the $W_6I_8X_6^{2-}$ excited state is completely independent of X. In all of the tungsten clusters, the terminal halides have a strong effect upon the non-radiative decay rates out of the excited state. The non-radiative path that is thermally activated in the temperature range 300-450 K is apparently not due to dissociation of a terminal halide, as a large difference in the activation energy for the different halides would be expected. In fact, the difference is in the pre-exponential term, with the iodide k_1 term being consistently less than the bromide which is less than the chloride.

The pre-exponential terms also seem to depend upon the bridging halide, with a difference of about an order of magnitude between the clusters with bridging chlorides and the clusters with bridging iodide ligands. Since the activation energies are all about the same for this non-radiative pathway, this order of magnitude difference in the pre-exponential term of the Arrhenius expression is responsible for the big difference in the quantum yield and emission lifetimes of the various tungsten clusters with the same bridging halide at room temperature.

Despite a compilation of activation parameters, very little insight has been developed into the meaning of the pre-exponential term in this type

of analysis for inorganic systems. Organic photochemists have been able to group reaction types to typical values of k_1. In general, bimolecular reactions have $k_1 = 10^8\ s^{-1}$ and unimolecular reactions have $k_1 = 10^{15} - 10^{12}\ s^{-1}$ [10]. Work done on an electronically similar system, the quadruply bonded $Mo_2X_4(PR_3)_4$ dimers, where the excited state dynamics are better understood, resulted in k_1 terms on the order of $10^{13}\ s^{-1}$ [12], which puts these dimers in the region of unimolecular reactions. The clusters have k_1 values which are considerably less, indicating perhaps that the entropy of the deactivation process is unfavorable in the clusters. However, an associative mechanism is hard to envision for the clusters, and solvation of an outer halide appears unlikely, due to the very small differences in activation energies upon exchange of the terminal halides. The fact that the highest k_1 term occurs for the smallest halide may imply that the non-radiative pathway may involve structural reorganization in the cluster. The emission spectra of these clusters indicate a large distortion in the excited state, and a further thermally activated structural deformation may allow the excited state to quickly decay to ground.

The energy transfer data raise two very interesting points. First of all, these experiments indicate clearly that a spin designation for these excited states is very reasonable as there is a substantial difference in reactivity between a singlet state ($Re_2Cl_8^{2-*}$) and a triplet state ($W_6Cl_{14}^{2-*}$) with organic triplet acceptors. This is despite the fact that these have been shown to be metal-centered transitions involving 5d metals. Previous work with

the lowest energy excited state of diplatinum (II) pyrophosphite showed a very small spin-orbit splitting of the components of the $^3A_{2u}$ excited state (40 cm^{-1})[13]. Very low temperature emission spectroscopy has not yet been done on the tungsten clusters to determine the magnitude of the spin-orbit interaction in the triplet excited state, but work on the ground state of another high nuclearity cluster, $Mo_5Cl_{13}^{3-}$, has shown that spin-orbit splittings are on the order of 10 cm^{-1} in these cluster molecules (Chapter 7). Apparently, for transitions involved with metal-metal bonds, spin-orbit coupling is minimized and spin remains a chemically relevant parameter. Secondly, since spin is important in the description of these states, the reactivity of the excited state may depend on the spin associated with that state. Under the time constraints involved in excited state chemistry, triplet states may be confined to "diradical" type chemistry, while singlet states which approach "zwitterionic" character could be able to do acid-base type chemistry. The photoreactivities of the $W_6X_{14}^{2-}$ clusters and the $W_2X_4(PR_3)_4$ dimers, where the spin of the emissive excited states are triplet and singlet, respectively, will be interesting to contrast in light of the spin restrictions on each state.

The energy gap law relates the non-radiative rate out of excited states based on the same chromophore and the energy of the excited state above the ground state[14]. Under conditions where the law is applicable, a plot of $ln\ k_{nr}$ versus emission energy should be linear. The law is based on the extent of vibrational coupling between the ν_0 vibrational level of the excited state and the highly vibrationally excited isoenergetic levels of the

ground state[15]. At 77 K, the tungsten clusters are clearly near the weak coupling limit. A plot of $ln\ k_{nr}$ (77 K) versus the corrected peak maxima (Figure 5) shows the data to correlate rougly to this: the higher the energy of the emissive excited state, the lower the non-radiative rate of that state. Unfortunately, a detailed analysis of the type done on simpler systems is not possible due to the lack of understanding of the important vibrational promoting and accepting modes in the clusters. However, the data do imply that the emitting states of all the tungsten clusters are similar; the increase in the emission energy upon exchange of halide is probably not due to different emitting states, but rather to a greater splitting of the relevant molecular orbitals.

The redox potentials are also primarily a function of the metal and inner core halides. The data (presented in Table 5) show that a tungsten cluster is consistently more easily oxidized than the corresponding molybdenum cluster. Also, the shift in oxidation potential upon exchange of the inner halides corresponds to that expected, based on electron donating ability of the respective halides. The outer halides appear to have little to do with the electron density on the metal core; indeed the shift in potential upon variation of the terminal halides is in the opposite direction from that expected from electron donation, and that seen for the bridging halides. This shift is probably due to strong solvent effects in the potential of the electron transfer. The clusters with the softer, more polarizable ligands in the terminal positions are much better solvated, stabilizing the dianion relative to

Figure 5. A plot of the $ln\ k_{nr}$ (low temperature limit) versus the emission energy (corrected peak maxima).

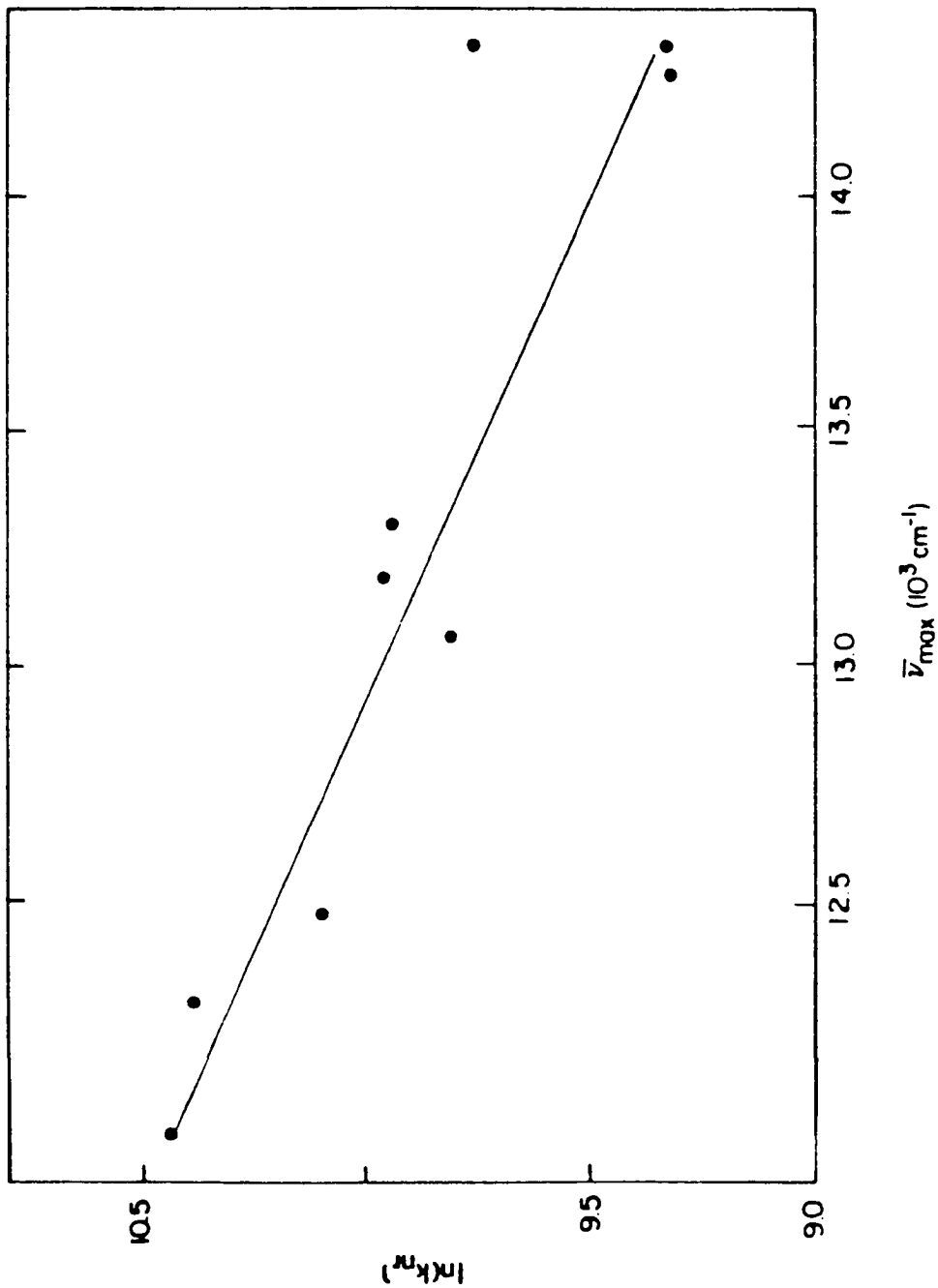
10.5
9.5
9.0
ln(k_nr)
12.5
13.0
13.5
14.0
ν̄max (10³cm⁻¹)

that of the monoanion. The data on the homologous metal cluster systems with different solvents show that these effects can be rather large for dianions in non-polar media. The same oxidation couple $W_6X_{14}^{2-/-}$ is about 200 mV more positive in the more polar acetonitrile than in dichloromethane. With the large variety of redox potentials and excited state energies available in this $W_6X_8Y_6$ cluster series, the one-electron potential for reducing a substrate is tunable in the whole range from -0.5 V to -1.4 V.

The results reported here do not shed a great deal of light on the most interesting observation in the tungsten cluster photophysics, the increase in emission energy upon exchange of bridging halides from Cl to Br to I. This is in direct contrast to the picture developed for the molybdenum series, with the metal-centered nature of the emitting excited state unperturbed by the halides. Clearly, the exchange of the outer halides is not the major factor, since the bands shift little upon their exchange. Rather, the important factor is in the inner shell of halide ligands, which allow for a larger splitting of the orbitals involved in the state. Initial structural data imply that the cube of triply bridging halides become more strongly bound to the metal atoms progressing from Cl to Br to I. Further structural and vibrational data are needed before a clear, complete picture of this phenomenon can be elucidated.

REFERENCES AND NOTES

1. Maverick, A.W.; Gray, H.B. *J. Am. Chem. Soc.*, **1981**, *103*, 1298.
2. Maverick, A.W.; Nadjdzionek, J.S.; MacKenzie, D.; Nocera, D.G.; Gray, H.B. *J. Am. Chem. Soc.*, **1983**, *105*, 1878.
3. Zietlow, T.C.; Nocera, D.G.; Gray, H.B., unpublished observations.
4. Sheldon, J.C. *J. Chem. Soc.*, **1962**, 410.
5. Hogue, R.D.; McCarley, R.E. *Inorg. Chem.*, **1970**, *9*, 1355.
6. Rice, S.F., Doctoral Thesis, California Institute of Technology, **1982**.
7. Emissive excited state energies are estimated ν_{0-0} transitions from low temperature emission spectra.
8. Zietlow, T.C.; Hopkins, M.D.; Gray, H.B. *J. Solid State Chem.*, in press.
9. Trogler, W.C.; Gray, H.B. *Acc. Chem. Res.*, **1978**, *11*, 232.
10. Turro, N.J. *Modern Molecular Photochemistry*, Benjamin/Cummings Publishing:Menlo Park, CA, **1978**.
11. Kepert, D.L.; Marshall, R.E.; Taylor, D. *J. Chem. Soc., Dalton*, **1974**, 506.
12. Hopkins, M.D.; Gray, H.B., manuscript in preparation.
13. Fordyce, W.A.; Brummer, J.G.; Crosby, G.A. *J. Am. Chem. Soc.*, **1981**, *103*, 7061. Rice, S.F.; Gray, H.B. *J. Am. Chem. Soc.*, **1983**, *105*, 4571.
14. Englman, R.; Jortner, J. *Molecular Physics*, **1970**, *18*, 145.
15. Caspar, J.V.; Kober, E.M.; Sullivan, B.P.; Meyer, T.J. *J. Am. Chem. Soc.*, **1982**, *104*, 630.

CHAPTER 4

The Structures of the $W_6Cl_{14}^{2-}$, $W_6Br_{14}^{2-}$, and $W_6I_{14}^{2-}$ Anions. Relevance to Unusual Emissive Behavior

The Structures of the $W_6Cl_{14}^{2-}$, $W_6Br_{14}^{2-}$, and $W_6I_{14}^{2-}$ Anions. Relevance to Unusual Emissive Behavior

Thomas C. Zietlow, William P. Schaefer, Behzad Sadeghi, Nhi Hua and Harry B. Gray*

Contribution No. from the Arthur Amos Noyes Laboratory of Chemical Physics, California Institute of Technology, Pasadena, California, 91125.

Abstract. The compound $[(n\text{-}C_4H_9)_4N]_2W_6Cl_{14}$ crystallizes in space group $P2_1/n$. The unit cell dimensions are a = 18.512(3), b = 11.661(1), and c = 12.789(1) Å; $\beta = 90.17(1)^o$ and z = 2. The compound $[(n\text{-}C_4H_9)_4N]_2W_6Br_{14}$ crystallizes in the monoclinic space group $P2_1/n$ with a = 18.968(8), b = 11.913(6), and c = 13.263(6) Å; $\beta = 90.87(4)^o$ and z = 2. The compound $[(n\text{-}C_4H_9)_4N]_2W_6I_{14}$ crystallizes in the monoclinic space group $P2_1/n$. The unit cell dimensions are a = 11.553(7), b = 11.468(3), and c = 24.554(13) Å; $\beta = 96.77(4)^o$ and z = 2. The structural studies confirm the trend established by the emission data, that the μ^3-bridging halogens interact with the tungsten atoms more in the $W_6I_{14}^{2-}$ cluster than in the $W_6Cl_{14}^{2-}$ cluster. The tungsten-tungsten bonds are longer in the $W_6I_{14}^{2-}$ structure than in the $W_6Cl_{14}^{2-}$ cluster. This implies that the overlap of the tungsten orbitals is not the sole determining factor in the ordering of the excited state energies. Ligand backbonding to the metal is suggested as an explanation of the emission energy trends in the $W_6X_{14}^{2-}$ clusters.

The study of the photophysical behavior of the hexanuclear clusters $M_6X_{14}^{2-}$ (M = Mo, W; X = Cl, Br, I) has resulted in a description of the emissive excited state of the $Mo_6X_{14}^{2-}$ clusters as a highly distorted, metal-centered excited state[1,2]. Both the energy of the emissive excited state and the radiative decay rate are invariant upon exchange of halide. The temperature dependence of the lifetime of the excited state shows that the three molybdenum clusters, $Mo_6Cl_{14}^{2-}$, $Mo_6Br_{14}^{2-}$, and $Mo_6I_{14}^{2-}$, differ only in their non-radiative decay rates, with the largest k_{nr} associated with the iodide ligand, the most polarizable and interactive with the solvent[3]. The tungsten series, $W_6X_{14}^{2-}$, presents a different picture of the emissive excited state. The energy of the excited state is halide dependent; the energies of the states' order: $W_6Cl_{14}^{2-}$ (1.83 eV) < $W_6Br_{14}^{2-}$ (1.85 eV) < $W_6I_{14}^{2-}$ (2.05 eV), the *opposite* trend from that expected by incorporation of some ligand-to-metal charge transfer character into the transition[4]. From previous work done on the tungsten clusters, the inner core of triply bridging halides dominates the determination of the energy of the emissive state, with the terminal halides playing only a small part. This terminal halide effect diminishes as the triply bridging halide is changed from chloride to bromide to iodide. The outer halides do exert a great influence on the non-radiative decay rate, but very little on the radiative rate[5]. Clearly, one way to examine the effect of the halide ligands in these tungsten clusters is to measure their ground state molecular structures and thereby infer the relative levels of metal-metal and metal-halide interaction as the halide is varied. The results of the x-ray

structural studies of $(TBA)_2W_6Cl_{14}$, $(TBA)_2W_6Br_{14}$, and $(TBA)_2W_6I_{14}$ are reported herein along with their relevance to our study of their emission properties.

EXPERIMENTAL SECTION

The complexes were synthesized as described previously[6], and were crystallized by layering petroleum ether on a methylene chloride solution of the cluster.

X – ray Structures

$[(n-C_4H_9)_4N]_2W_6Cl_{14}$: A crystal with dimensions 0.24 x 0.24 x 0.17 mm was mounted on a glass fiber. The crystal was then centered on a CAD4 diffractometer equipped with graphite-monochromated MoKα radiation for intensity data collection. Unit cell dimensions were obtained from the setting angles of 15 reflections with $25^o < 2\theta < 31^o$. Space group $P2_1/n$, a special setting of #14, was chosen based on the systematic absences h0l, h+l=2n+1, and 0k0, k=2n+1 in the intensity data. This space group has four equivalent positions $\pm$(x,y,z; $\frac{1}{2}$-x, $\frac{1}{2}$+y, $\frac{1}{2}$-z). Two sets of data were collected with a total of 10,766 reflections in the quadrants $\pm$ h,k,l and $\pm$ h,-k,l. Crystal data are collected in Table 1. After every 10,000 seconds of x-ray exposure, 3 check reflections were monitored to check crystal decay: they showed no variations greater than those expected statistically. The data were corrected for absorption by Gaussian integration over an 8 x 8 x 8 grid; transmission factors varied from 0.081 to 0.172. After correcting for background, the two data sets were merged to give 4858 independent reflections, which were all

Table 1.

Crystal Data for $[(n\text{-}C_4H_9)_4]_2\ [W_6Cl_{14}]$

$W_6Cl_{14}N_2C_{32}H_{72}$	formula weight 2096.55
a = 18.512(3) Å	
b = 11.661(1) Å	Space Group $P2_1/n$ (# 14)
c = 12.789(1) Å	
β = 90.17(4)°	T = 21°C
V = 2760(1) Å^3	λ MoKα 0.71073 Å
μ = 134.39 cm^{-1}	d_x = 2.52 g cm^{-3}
F(000) = 960 e	

used in the structure solution and refinement. Variances were assigned to individual reflections based on counting statistics plus an additional term, $(0.014I)^2$, to account for intensity-dependent errors. Final variances were assigned by standard propagation of error plus an additional term, $(0.014\bar{I})^2$.

The centrosymmetric anions are located at a center of symmetry in the unit cell. Interpretation of Patterson maps gave the positions of the three tungsten atoms. From structure factor-Fourier calculations the seven chlorine atoms and the non-hydrogen atoms in the cation were located. The positions of the hydrogen atoms were calculated from known geometry and assumed staggered conformations. The tungsten and chlorine atoms were given anisotropic thermal parameters while the atoms in the cation were given isotropic thermal parameters. Several cycles of least-squares refinement led to convergence with R of 0.062 for 4157 data. For the strong data with $F_o^2 > 3\sigma F_o^2$, R = 0.053 for 3519 reflections. The goodness of fit $(=[\Sigma W(F_o^2-F_c^2)^2/(n-p)]^{\frac{1}{2}})$ is 2.72 for n = 4858 reflections and p = 160 parameters (6 strong, low angle reflections were given zero weight in this refinement). Final parameters are in Table 2[7] and bond lengths are in Table 3.

$\underline{[(n-C_4H_9)_4N]_2W_6Br_{14}}$: Preliminary photographs showed a monoclinic cell with systematic absences indicating space group $P2_1/n$ (the same as the $W_6Cl_{14}^{2-}$ space group). An irregularly shaped crystal with dimensions 0.17 x 0.13 x 0.15 mm was carefully centered on a Nicolet $P2_1$ diffractome-

Table 2.

Final Parameters for $[(C_4H_9)_4N]_2\ W_6Cl_{14}$

Atom	x	y	z	U_{eq} or B
W(1)	1950(3)	5404(5)	86765(4)	382(1)
W(2)	8474(3)	6377(5)	4864(4)	366(1)
W(3)	95159(3)	13395(5)	3083(4)	375(1)
Cl(1)	19573(19)	14551(36)	11428(32)	611(10)
Cl(2)	5370(18)	24154(31)	94870(28)	493(8)
Cl(3)	89152(17)	12032(30)	85570(25)	431(8)
Cl(4)	85386(17)	1315(32)	10897(26)	462(8)
Cl(5)	1633(19)	13882(33)	20225(26)	503(9)
Cl(6)	38721(22)	19270(38)	57539(36)	711(12)
Cl(7)	4343(23)	11956(45)	69167(30)	768(13)
N(1)	2087(7)	-249(10)	4750(9)	4.15(0.25)
C(1)	1369(9)	-882(15)	4814(14)	5.50(0.38)
C(2)	1390(13)	-2114(20)	4745(18)	8.58(0.59)
C(3)	710(14)	-2675(25)	5214(21)	9.69(0.67)
C(4)	714(26)	-3773(47)	5345(36)	22.36(1.78)
C(5)	2391(9)	-409(14)	3643(13)	5.14(0.36)
C(6)	3087(10)	257(15)	3388(14)	5.61(0.38)
C(7)	3752(14)	-428(21)	3411(19)	9.32(0.64)
C(8)	4392(15)	210(24)	3000(20)	10.71(0.74)
C(9)	2623(9)	-702(14)	5514(13)	5.02(0.35)
C(10)	2382(12)	-664(19)	6618(17)	8.11(0.55)
C(11)	3112(18)	-984(31)	7458(26)	13.89(0.99)
C(12)	2841(18)	-2033(30)	7322(26)	13.90(1.02)
C(13)	1955(9)	1010(14)	4969(12)	4.87(0.34)
C(14)	1463(10)	1619(16)	4199(14)	5.80(0.40)
C(15)	1383(11)	2861(17)	4490(15)	6.76(0.46)
C(16)	2071(12)	3528(20)	4417(17)	8.37(0.56)

Tungsten and chlorine positional parameters have been multiplied by 10^5; other positional parameters and all U_{eq} by 10^4.

Table 3.

Bond Lengths in the $W_6Cl_{14}^{2-}$ Anion

Atom	Atom	Dist(Å)	Atom	Atom	Dist(Å)
W(1)	W(2)	2.610(1)	Cl(2)	W(1)	2.500(4)
	W(3)	2.611(1)		W(2)	2.501(4)
	W(2)'	2.602(1)		W(3)	2.502(4)
	W(3)'	2.603(1)			
			Cl(3)	W(1)	2.496(3)
W(2)	W(3)	2.607(1)		W(2)	2.509(3)
	W(3)'	2.607(1)		W(3)	2.503(3)
W(1)	W(1)'	3.686(1)	Cl(4)	W(1)	2.489(3)
W(2)	W(2)'	3.685(1)		W(2)	2.484(3)
W(3)	W(3)'	3.688(1)		W(3)	2.503(3)
W(1)	Cl(7)	2.419(4)	Cl(5)	W(1)	2.509(4)
W(2)	Cl(1)	2.413(4)		W(2)	2.498(4)
W(3)	Cl(6)	2.416(4)		W(3)	2.496(4)

ter. Unit cell dimensions were obtained by least-squares fit to the setting angles of 15 reflections with $20^o < 2\theta < 26^o$. Crystal data are given in Table 4. A total of 11386 reflections with $2\theta < 55^o$ in the quadrants h,±k,±l was measured with $\theta - 2\theta$ scans of 2^o plus dispersion at a scan speed in 2θ of 2^o or 4^o/minute. Three check reflections were monitored every 97 reflections and showed no changes greater than those expected from counting statistics. The data were corrected for absorption by Gaussian integration, and Lorentz and polarization corrections were applied. The data were merged to give 5572 independent reflections, of which 4410 had $F_o^2 > 0$ but only 1763 had $F_o^2 > 3\sigma F_o^2$. Variances were assigned in the same manner as above. The coordinates of the three independent tungsten atoms were obtained from a Patterson map. Subsequent structure factor-Fourier cycles gave the coordinates of the remaining non-hydrogen atoms. Several cycles of least-squares refinement with anisotropic thermal parameters for the tungsten and bromine atoms, isotropic thermal parameters for the nitrogen and carbon atoms in the cation, including a secondary extinction parameter, converged with R = 0.158 for all data with $F_o^2 > 0$ and 0.065 for the data with $F_o^2 > 3\sigma F_o^2$. The goodness of fit is 1.31 for n = 5572 reflections and p = 160 parameters. The maximum shift of any parameter in the final cycle was less than 25% of its standard deviation; the secondary extinction parameter was zero within its standard deviation. Final parameters are given in Table 5[7]; bond lengths and angles are in Table 6.

$\underline{[(n-C_4H_9)_4)N]_2W_6I_{14}}$: A crystal with dimensions 0.33 x 0.24 x 0.29 mm

Table 4.

Crystal Data for $[(n\text{-}C_4H_9)_4]_2\ [W_6Br_{14}]$

$W_6Br_{14}N_2C_{32}H_{72}$	formula weight 2692.76
a = 18.968(8) Å	
b = 11.913(6) Å	Space Group $P2_1/n$ (# 14)
c = 13.263(6) Å	
β = 90.87(4)°	T = 21°C
V = 2997(1) Å^3	λ MoKα 0.71073 Å
μ = 220.35 cm^{-1}	d_x = 2.98 g cm^{-3}
F(000) = 1205 e	

Table 5.

Final Parameters for $[(C_4H_9)_4N]_2\ W_6Br_{14}$

Atom	x	y	z	U_{eq} or B
W(1)	1812(7)	-5729(14)	-12780(10)	455(4)
W(2)	8434(7)	-6099(14)	4897(10)	444(4)
W(3)	4680(8)	13167(13)	3395(11)	454(4)
Br(1)	11246(18)	12946(36)	14263(26)	568(10)
Br(2)	-5518(20)	15011(32)	4591(30)	632(10)
Br(3)	14856(17)	1090(34)	-11145(25)	613(10)
Br(4)	-1950(20)	13499(37)	-20946(26)	648(11)
Br(5)	-20186(18)	14269(36)	-11785(31)	735(12)
Br(6)	-4184(22)	13220(41)	30729(27)	828(13)
Br(7)	11098(21)	31419(36)	-8505(32)	826(13)
N(1)	2058(14)	244(23)	4783(18)	4.36(0.59)
C(1)	2347(18)	422(30)	3766(24)	4.96(0.75)
C(2)	3055(29)	-127(46)	3513(36)	10.34(1.46)
C(3)	3647(41)	429(61)	3174(48)	15.67(2.19)
C(4)	4253(31)	-231(50)	2840(39)	11.79(1.63)
C(5)	2582(19)	772(31)	5554(26)	5.76(0.86)
C(6)	2344(29)	735(46)	6604(39)	11.48(1.58)
C(7)	2909(23)	1517(39)	7172(32)	8.23(1.21)
C(8)	3327(62)	759(99)	7671(32)	33.78(0.74)
C(9)	1366(24)	856(39)	4923(30)	8.27(1.19)
C(10)	1364(26)	2168(43)	4780(32)	9.29(1.31)
C(11)	648(30)	2547(51)	5315(37)	11.38(1.59)
C(12)	688(39)	3739(72)	5280(52)	18.19(2.56)
C(13)	1912(20)	-995(34)	5052(27)	6.45(0.97)
C(14)	1465(18)	-1612(31)	4296(24)	5.23(0.82)
C(15)	1325(24)	-2822(40)	4585(30)	8.12(1.17)
C(16)	1992(26)	-3499(41)	4472(33)	9.34(1.32)

Tungsten and chlorine positional parameters have been multiplied by 10^5; other positional parameters and all U_{eq} by 10^4.

Table 6.

Bond Lengths in the $W_6Br_{14}^{2-}$ Anion

Atom	Atom	Dist(Å)	Atom	Atom	Dist(Å)
W(1)	W(2)	2.643(2)	Br(1)	W(1)	2.626(4)
	W(3)	2.625(2)		W(2)	2.637(4)
	W(2)'	2.630(2)		W(3)	2.638(4)
	W(3)'	2.643(2)			
			Br(2)	W(1)	2.633(4)
W(2)	W(3)	2.631(2)		W(2)	2.636(4)
				W(3)	2.631(4)
W(1)	W(1)'	3.728(2)	Br(3)	W(1)	2.610(4)
W(2)	W(2)'	3.729(2)		W(2)	2.612(4)
W(3)	W(3)'	3.722(2)		W(3)	2.629(4)
W(1)	Br(6)	2.588(4)	Br(4)	W(1)	2.628(4)
W(2)	Br(5)	2.586(4)		W(2)	2.627(4)
W(3)	Br(7)	2.587(4)		W(3)	2.629(4)

was mounted on a glass fiber. Oscillation photographs of the crystal showed only one axis of symmetry which characterizes monoclinic cells. The crystal was then centered on a Nicolet $P2_1$ diffractometer equipped with graphite-monochromated MoKα radiation for intensity data collection. Unit cell dimensions were obtained from the setting angles of 15 reflections with $25^o < 2\theta < 28^o$. Space group $P2_1/n$ (the same space group as in the $(TBA)_2W_6Cl_{14}$ and $(TBA)_2W_6Br_{14}$ crystals) was chosen based on the systematic absences h0l, h+l=2n+1, and 0k0, k=2n+1 in the intensity data. Two sets of data were collected with a total of 9860 reflections in the quadrants h,k,±l, and h,-k,±l. Crystal data are collected in Table 7.

At every 97 reflections, 3 check reflections were monitored to check crystal decay; they showed no variations greater than those expected statistically. The data were corrected for absorption by Gaussian integration over an 8 x 8 x 8 grid; transmission factors varied from 0.107 to 0.212. After correcting for background, the two data sets were merged to give 4269 independent reflections, which were all used in the structure solution and refinement. Variances were assigned to the individual reflections in the same manner as described above.

The centrosymmetric anions are located at a center of symmetry in the unit cell. Interpretation of Patterson maps gave the positions of the three tungsten atoms. From structure factor-Fourier calculations the seven iodine atoms and the non-hydrogen atoms in the cation were located. The positions of the hydrogen atoms were calculated from known geometry and as-

Table 7.

Crystal Data for $[(n\text{-}C_4H_9)_4]_2\,[W_6I_{14}]$

$W_6I_{14}N_2C_{32}H_{72}$	formula weight 3364.71
a = 11.553(7) Å	
b = 11.486(3) Å	Space Group $P2_1/n$ (# 14)
c = 24.554(13) Å	
β = 96.77(4)°	T = 21°C
V = 3235(3) Å^3	λ MoKα 0.71073 Å
μ = 179.96 cm^{-1}	d_x = 3.45 g cm^{-3}
F(000) = 2518 e	

sumed staggered conformations. The tungsten and iodine atoms were given anisotropic thermal parameters while the atoms in the cation were given isotropic thermal parameters. Several cycles of least-squares refinement led to convergence with R of 0.090 for 3463 data with $F_o^2 > 3\sigma F_o^2$. The goodness of fit (defined above) is 2.23 for n = 4260 reflections and p = 167 parameters (9 strong, low-angle reflections were given zero weight in the refinement). Final parameters are given in Table 8[7] and bond lengths are listed in Table 9.

RESULTS AND DISCUSSION

Although not imposed crystallographically, all three clusters have near perfect octahedra of tungsten atoms. An ORTEP drawing of the unit cell of $(TBA)_2W_6Br_{14}$ is shown in Figure 1. The octahedra expand in the order: (W-W bond length) $W_6Cl_{14}^{2-} < W_6Br_{14}^{2-} < W_6I_{14}^{2-}$ (Table 10). If the emissive excited state in the tungsten clusters were completely metal-centered, as appears to be the case in the molybdenum series[2], the energy of the emissive states should correspond to the metal-metal bond length. The shorter the metal-metal bond, the greater the overlap of the metal *d* orbitals, and therefore, the higher the energy of the emissive state[4]. Obviously, from the crystal structure data and the data on the emissive excited states of these tungsten clusters, the tungsten-tungsten bond distances are not the sole determining factor in the ordering of the excited state energies. The tungsten halide bond distances, also displayed in Table 10, show an interesting trend. In the tungsten chloride cluster, the tungsten-chloride (axial) bond is shorter

Table 8.

Final Parameters for $[(C_4H_9)_4N]_2\ W_6I_{14}$

Atom	x	y	z	U_{eq} or B
W(1)	4454(1)	4328(1)	5624(1)	597(4)
W(2)	6475(1)	4300(1)	5191(1)	602(4)
W(3)	4497(1)	3673(1)	4587(1)	622(4)
I(1)	3634(2)	3344(2)	6568(1)	967(8)
I(2)	8693(2)	3233(2)	5464(1)	1011(8)
I(3)	3794(3)	1692(2)	3950(1)	1135(9)
I(4)	3502(2)	5039(2)	3714(1)	778(6)
I(5)	5443(2)	2188(2)	5424(1)	800(6)
I(6)	6586(2)	3584(2)	4112(1)	839(7)
I(7)	2361(2)	3661(2)	5022(1)	747(6)
N(1)	5154(25)	4758(23)	1675(9)	6.3(0.60)
C(1)	3815(37)	4479(32)	1600(14)	8.10(1.00)
C(2)	3201(36)	4665(31)	2148(13)	7.50(0.90)
C(3)	2080(47)	4058(44)	2126(16)	10.30(1.20)
C(4)	2036(50)	2911(46)	2176(18)	12.00(1.40)
C(5)	5577(35)	4546(29)	1094(13)	7.00(0.80)
C(6)	6822(41)	4875(37)	1079(15)	9.20(1.00)
C(7)	6979(*)	4604(87)	485(44)	9.70(2.70)
C(8)	7872(86)	5164(79)	299(33)	7.40(2.00)
C(9)	5813(33)	3962(31)	2160(12)	6.70(0.80)
C(10)	5584(33)	2690(29)	2092(12)	6.50(0.80)
C(11)	6087(37)	2208(32)	2613(14)	7.90(0.90)
C(12)	5890(46)	840(40)	2587(16)	10.90(1.20)
C(13)	5438(30)	6015(26)	1866(11)	5.60(0.70)
C(14)	4985(37)	6940(34)	1453(14)	8.20(1.00)
C(15)	5474(38)	8178(34)	1654(14)	8.10(0.90)
C(16)	5139(40)	9105(35)	1261(15)	9.10(1.10)

All positional parameters and U_{eq} have been multiplied by 10^4.

Table 9.

Bond Lengths in the $W_6I_{14}^{2-}$ Anion

Atom	Atom	Dist(Å)	Atom	Atom	Dist(Å)
W(1)	W(2)	2.676(2)	I(4)	W(1)	2.800(2)
	W(3)	2.661(2)		W(2)	2.790(2)
	W(2)'	2.671(2)		W(3)	2.792(2)
	W(3)'	2.674(2)			
			I(5)	W(1)	2.778(3)
W(2)	W(3)	2.673(2)		W(2)	2.792(3)
	W(3)'	2.668(2)		W(3)	2.792(3)
W(1)	W(1)'	3.777(2)	I(6)	W(1)	2.792(3)
W(2)	W(2)'	3.785(2)		W(2)	2.792(3)
W(3)	W(3)'	3.768(2)		W(3)	2.803(3)
W(1)	I(1)	2.842(3)	I(7)	W(1)	2.788(2)
W(2)	I(2)	2.849(3)		W(2)	2.785(2)
W(3)	I(3)	2.826(3)		W(3)	2.802(2)

Figure 1. An ORTEP drawing of the unit cell of $(TBA)_2W_6Br_{14}$.

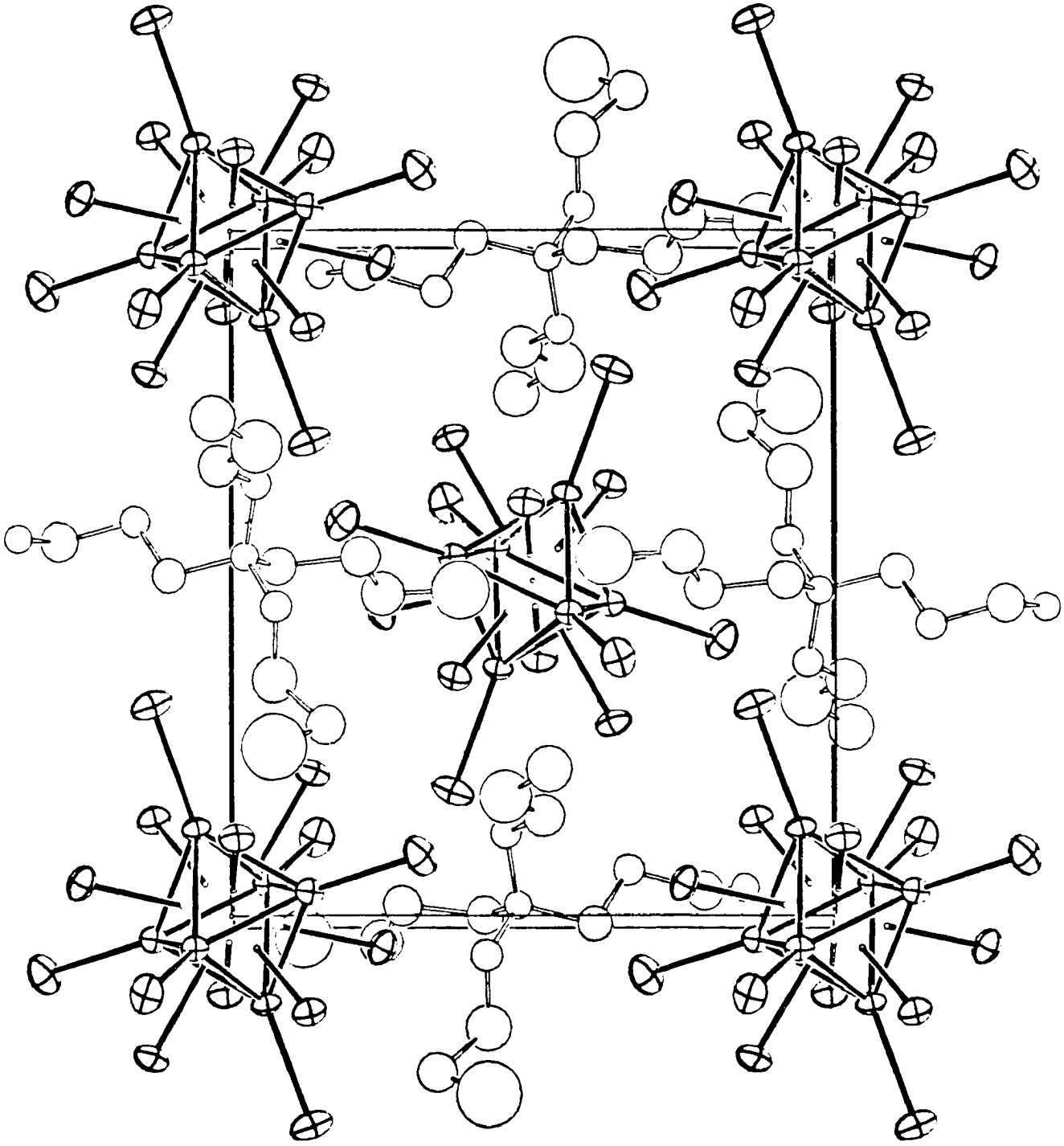

Table 10.

Bond Distances* $W_6X_{14}^{2-}$ Anions

Bond	$W_6Cl_{14}^{2-}$	$W_6Br_{14}^{2-}$	$W_6I_{14}^{2-}$
W-W(*cis*)	2.607(4)Å	2.635(9)	2.670(8)
W-W(*trans*)	3.686(1)	3.725(5)	3.777(8)
W-X(facial)	2.499(7)	2.628(10)	2.792(7)
W-X(axial)	2.416(2)	2.588(1)	2.839(12)

*Average bond distances.

than the tungsten-chloride (facial) bond. In the tungsten bromide cluster the bond lengths are on the same order, but there is a significantly smaller difference relative to the analogous tungsten chloride bonds. The tungsten iodide structure shows the tungsten-iodide (axial) bond is *longer* than the tungsten-iodide (facial) bond. There appears to be a greater interaction of the tungsten atom with the μ^3-iodide ligand than with the μ^3-chloride in the $W_6Cl_{14}^{2-}$ cluster.

This systematic change is manifested in the changes in the emission spectra as a function of axial halide. In the $W_6Cl_8^{4+}$ core, the emission bands shift over 400 cm^{-1} upon exchange of the terminal halides from chloride to iodide. With the $W_6I_8^{4+}$ core, this shift is only about 60 cm^{-1} [5]. Clearly, the axial halides have much more interaction with the metal framework in the $W_6Cl_8^{4+}$ core than in the $W_6I_8^{4+}$ core, in accord with these crystallographic findings.

While the exact nature of the emitting excited states in these clusters is not yet clear, a variety of molecular orbital calculations[8] and experimental data[5] indicate that the important orbitals making up the emissive excited state are derived from the d_{xy} atomic orbitals, which form the delta bond in the quadruply bonded dimers (Figure 2). These orbitals in the hexanuclear clusters are affected by the bridging ligands in a π interaction. Based on the expected ordering of π-donation, the more diffuse iodide ligands would be expected to decrease the energy gap between the HOMO and LUMO, which would be reflected in a lower energy emissive excited state. Since this is not

Figure 2. Diagram of orbitals involved in lowest electronic excited states in the (a) $(d^4)_2$ and (b) $(d^4)_6$ clusters.

M_2X_8

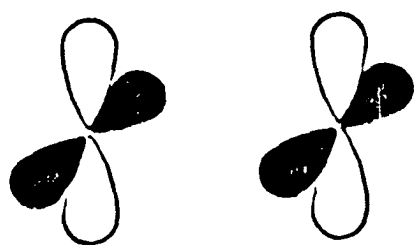

δ orbital

(a)

$Mo_6X_8(X_6)^{2-}$

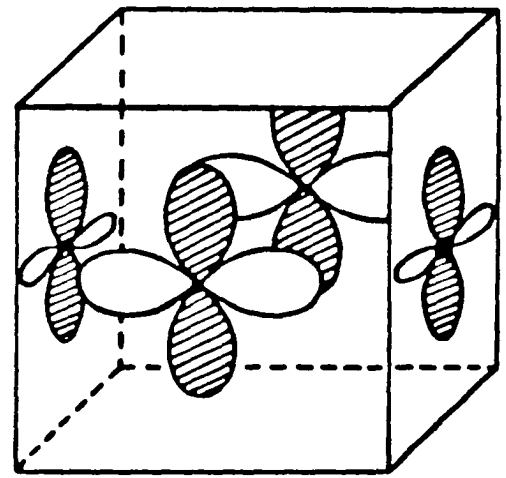

e_g orbital ("δ")

(b)

what is observed experimentally, the π-donation of the ligands must not be the important interaction in determining the energy of the emitting excited state.

The greater interaction of the facial iodides with the tungsten atoms may be a manifestation of ligand backbonding to the metal cluster, using the empty, available d orbitals on the iodide to accept electron density from the metal centers in a π-accepting fashion. The tungsten (II) atoms are electron-rich, with no good π-accepting ligands such as carbonyls to which electron density can be donated. The ordering of the emission bands can thus be explained, since the iodide ligands would certainly backbond better than the chloride ligands. This $d-d$ π-bonding would tend to lower the energy of the HOMO, resulting in a larger band gap for the tungsten iodide cluster, which is observed experimentally. The disturbing aspect of invoking π-backbonding to the iodide ligands in these clusters is that more electron density is being placed on an already anionic ligand. This type of bonding may also be useful in rationalizing trends in the electrochemistry of quadruply bonded dimer systems[9].

REFERENCES AND NOTES

1. Maverick, A.W.; Gray, H.B. *J. Am. Chem. Soc.*, **1981**, *103*, 1298.
2. Maverick, A.W.; Nadjdzionek, J.S.; MacKenzie, D.; Nocera, D.G.; Gray, H.B. *J. Am. Chem. Soc.*, **1983**, *105*, 1878.
3. See Chapter 2.
4. Zietlow, T.C.; Hopkins, M.D; Gray, H.B. *J. Solid State Chem.*, in press.
5. Zietlow, T.C.; Nocera, D.G.; Gray, H.B., manuscript in preparation.
6. Hogue, R.D.; McCarley, R.E. *Inorg. Chem.*, **1970**, *9*, 1355.
7. Definition:

$$U_{eq} = \frac{1}{3}[\Sigma_i \Sigma_j U_{ij}(a_i^* a_j^*)(\vec{a}_i \vec{a}_j)]$$

$$\sigma U_{eq} = \frac{1}{\sqrt{6}} \langle \frac{\sigma U_{ii}}{U_{ii}} \rangle U_{eq}$$

8. Hoffmann, R.; Hughbanks, T., personal communication on an extended Hückel molecular orbital calculation.
9. Zietlow, T.C.; Hopkins, M.D.; Gray, H.B., manuscript in preparation.

CHAPTER 5

Hexanuclear Tungsten Halide Clusters. Crystal Structure, Spectral and Magnetic Properties of $[((C_6H_5)_3P)_2N]W_6Br_{14}$

Hexanuclear Tungsten Halide Clusters. Crystal Structure, Spectral and Magnetic Properties of $[((C_6H_5)_3P)_2N]W_6Br_{14}$

Thomas C. Zietlow, William P. Schaefer, Behzad Sadeghi and Harry B. Gray*

Contribution No. ____ from the Arthur Amos Noyes Laboratory of Chemical Physics, California Institute of Technology, Pasadena, California, 91125.

Abstract. The compound $[(n\text{-}C_4H_9)_4N]W_6Br_{14}$ has been synthesized and its crystal structure determined. The complex crystallizes in the monoclinic space group $P2_1/n$ with a = 9.577(2), b = 22.478(6), and c = 24.430(4) Å; β = 97.42(2)° and z = 4. The cluster $W_6Br_{14}^-$ is the product of a one-electron oxidation of the $W_6Br_{14}^{2-}$ complex which has been shown to possess interesting photophysical properties. The structure of the $W_6Br_{14}^-$ anion did not display an axial distortion, as anticipated from EPR measurements. The tungsten-tungsten bonds were longer in the $W_6Br_{14}^-$ cluster than in the $W_6Br_{14}^{2-}$ structure, consistent with the electron being removed from a metal-metal bonding orbital. The metal-bromide bonds are shorter in the monoanion relative to the dianion, probably due to the greater electrostatic attraction of the 1- halide to the oxidized metal cluster. The electronic absorption spectra of several isoelectronic clusters with various halides have been measured, with the conclusion that the lowest energy allowed transition in the $W_6X_{14}^-$ clusters is due to a ligand-to-metal charge transfer from an axial halide.

The general approach to photochemistry used in this laboratory involves first understanding the excited state dynamics of a particular emissive complex and then using that information about bond changes and electron density redistribution to design photochemical reactions. Usually electronic absorption spectroscopy provides the means by which the electronic structure of the complex can be understood. In the case of the large molybdenum and tungsten halide clusters ($Mo_6X_{14}^{2-}$ and $W_6X_{14}^{2-}$; X = Cl, Br, I), the high symmetry (idealized O_h symmetry) and the large number of metal atoms make the absorption spectroscopy too difficult to handle. Other, less direct, methods must be used to determine the nature of the ground and emissive excited state. The photophysics have provided some insight into the properties of the excited states of the hexanuclear clusters,[1] but these types of studies are focussed on radiative and non-radiative processes in the molecular excited state rather than on the molecular distortions in the excited state relative to the ground state. In order to get some structural information on the excited state, a crystal structure has been performed on the one-electron oxidized analogue of the $W_6Br_{14}^{2-}$ ion, a member of the class of highly emissive $M_6X_{14}^{2-}$ anions. This structure may suggest the bond changes that would occur in the cluster upon removal of an electron from the highest occupied molecular orbital. Viewing the excited state as the electronic state produced by one electron being excited from the HOMO to the LUMO, this structural determination is modeling "half" the excited state.

EXPERIMENTAL SECTION

Optical absorption spectra were recorded on a Cary 17 spectrometer. Electronic paramagnetic resonance spectra were measured on a Varian E-Line Century Series spectrometer equipped with an Air-Products Heli-Tran cooling system. Variable temperature susceptibility measurements were made at the University of Southern California on a SQUID-based (S.H.E. Corporation) Model 805 variable temperature susceptometer with a 2 K option.

$\underline{(PPN)_2W_6Br_{14}}$ was synthesized by heating W_6Cl_{12} (0.50 g) in an evacuated tube with a 20-fold excess of LiBr:KBr (40:60 mixture) (3.07 g: 2.86 g) and heating the sealed tube at 360°C for 30 minutes. After cooling, the tube was broken and the contents dissolved in 6M HBr. This solution was treated with PPNCl, causing a precipitate to form which was then filtered off, dried *in vacuo*, and recrystallized from methylene chloride/ petroleum ether.

$\underline{(PPN)W_6Br_{14}}$ was synthesized by oxidation of $(PPN)_2W_6Br_{14}$ with $NOPF_6$ in degassed methylene chloride solution. Crystallization of the product by layering with petroleum ether resulted in deep red crystals and a few yellow crystals. The yellow crystals were carefully dissolved off with acetonitrile. Anal. for $C_{36}H_{30}P_2NW_6Br_{14}$: Calcd. C, 15.55; H, 1.10; N, 0.51. Found. C, 16.14; H, 1.17; N, 0.51.

X-ray Structure Determination

A crystal 0.23 x 0.28 x 0.20 mm with faces $\{011\}$ and $(10\bar{1})$, $(\bar{1},0,1)$ was chosen. Preliminary photographs showed a monoclinic cell; the crystal was transferred to a Nicolet $P2_1$ diffractometer equipped with graphite-monochromated MoKα radiation, and unit cell dimensions were obtained from the setting angles of 15 reflections with $20^o < 2\theta < 30^o$. Crystal data are given in Table 1. Systematic absences in the diffractometer data of $h0l, h + l = 2n + 1$, and $0k0, k = 2n + 1$ indicate space group $P2_1/n$, a special setting of #14, with equivalent postions $\pm(x, y, z; 1/2 - x, 1/2 + y, 1/2 - z)$. A total of 11,670 reflections with $2\theta < 40^o$ in quadrants $h, k, \pm l$ and $h, -k, \pm l$ was measured with omega scans 1^o wide at 1^o per minute. Three check reflections were monitored every 97 reflections and showed no variations greater than those expected statistically. The data were corrected for absorption by Gaussian integration over an 8 x 8 x 8 grid (transmission factors ranged from 0.013 to 0.044) and Lorentz and polarization factors were applied. The data were merged to give 4875 independent reflections, all of which were used in the structure solution and refinement. Variances were assigned to the values of F_0^2 based on counting statistics plus an additional term $(0.02I)^2$, to account for errors proportional to intensity.

The structure was solved by MULTAN[2] after the Patterson map proved difficult to interpret. With $z = 4$ in the space group $P2_1/n$, no special symmetry was imposed on the molecule. The anions, however, are located at the two different centers of symmetry and thus are constrained to be centrosym-

Table 1.

Crystal Data for $[\phi_3P{=}N{=}P\phi_3]$ $[W_6Br_{14}]$

$W_6Br_{14}P_2NC_{36}H_{30}$	formula weight 2760.43
a = 9.587(5) Å	
b = 22.501(12) Å	Space Group $P2_1/n$ (# 14)
c = 24.456(8) Å	
β = 97.42(2)°	T = 21°C
V = 5275(6) Å^3	λ MoKα 0.71073 Å
μ = 253.5 cm^{-1}	d_x = 3.47 g cm^{-3}
F(000) = 4868 e	

metric. The MULTAN solution gave all six tungsten atoms; subsquent structure factor-Fourier calculations located the 14 bromine atoms and the 39 non-hydrogen atoms of the cation. Several cycles of least-squares refinement, with tungsten and bromine atoms given anisotropic thermal parameters, led to convergence with an R ($= \Sigma||F_0| - |F_c||/\Sigma F_0$) of 0.046 for the 4580 data with $F_0^2 > 3\sigma(F_0^2)$. The goodness of fit ($= [\Sigma w(F_0^2 - F_c^2)^2/(n-p)]^{1/2}$ is 1.40 for $n = 4869$ reflections and $p = 337$ parameters (6 strong, low-angle reflections were given zero weight in the refinement). Final parameters are given in Table 2; bond lengths in the anion are listed in Table 3.

Analytical Procedures: Carbon, hydrogen, and nitrogen analyses were performed at the Analytical Laboratory, California Institute of Technology.

RESULTS

An ORTEP drawing of the contents of the unit cell of $(PPN)W_6Br_{14}$ is shown in Figure 1. The two independent anions are equivalent within experimental error and the following discussion will use average bond distances for the two. The tungsten atoms form a nearly regular octahedron with W-W (*cis*) distances of 2.652(9) Å, with maximum deviations of 0.013 Å from this average. The *trans* W-W distances average 3.750(10) Å, with maximum deviation from this of 0.012 Å. These deviations from perfect regularity appear to be random and cannot be described in terms of any systematic distortions. The longest *trans* W-W distances are associated with the longest W-Br(axial) distances, but no other correlations are evident. The devia-

Table 2.

Final Parameters for $[\phi_3P{=}N{=}P\phi_3]$ $[W_6Br_{14}]$

Tungsten and Bromine positional parameters x 10^5;

other positional parameters and all Ueq x 10^4.

Atom	x	y	z	U_{eq}[1] or B
W(1)	58844(7)	6331(3)	46786(3)	259(2)
W(2)	50234(8)	4413(3)	56486(3)	272(2)
W(3)	32295(7)	3205(3)	47418(3)	272(2)
W(4)	43765(8)	48054(3)	56729(3)	316(2)
W(5)	48770(8)	41957(3)	47922(3)	313(2)
W(6)	68657(8)	48897(3)	53152(3)	307(2)
Br(1)	40952(20)	5099(9)	37853(7)	424(5)
Br(2)	76553(20)	7353(9)	55853(7)	432(5)
Br(3)	50069(25)	10650(10)	65156(8)	622(6)
Br(4)	41550(21)	13726(9)	50534(8)	463(5)
Br(5)	70707(23)	15049(9)	42608(8)	545(6)
Br(6)	75743(19)	-1265(9)	42917(7)	441(5)
Br(7)	8246(22)	7549(11)	44280(10)	645(7)
Br(8)	24230(21)	41291(9)	51501(8)	490(5)
Br(9)	61038(21)	39092(9)	57748(8)	497(5)
Br(10)	73412(21)	42885(9)	44477(8)	508(5)
Br(11)	35427(27)	45334(12)	65816(8)	760(7)
Br(12)	36652(24)	45105(10)	38177(8)	575(6)
Br(13)	46553(26)	31029(10)	45028(9)	652(7)
Br(14)	93904(22)	47631(11)	57522(9)	691(6)
P(1)	6080(5)	3035(2)	2395(2)	2.6(1)
P(2)	4156(5)	2014(2)	2323(2)	2.5(1)
N	5103(15)	2540(6)	2596(5)	3.0(3)
C(11)	6806(20)	2867(9)	1753(7)	4.0(4)
C(12)	7884(22)	2432(9)	1802(8)	4.9(5)
C(13)	8342(25)	2250(11)	1284(9)	6.1(6)
C(14)	7793(26)	2488(11)	797(9)	6.3(6)
C(15)	6672(22)	2901(9)	764(8)	4.8(5)
C(16)	6136(20)	3090(9)	1249(7)	4.0(4)
C(21)	7505(18)	3138(7)	2931(6)	2.6(4)
C(22)	7447(19)	2909(8)	3443(7)	3.3(4)
C(23)	8544(22)	3004(9)	3862(8)	4.4(5)
C(24)	9746(23)	3345(10)	3761(8)	5.0(5)
C(25)	9816(24)	3564(11)	3247(9)	6.0(6)
C(26)	8717(20)	3465(9)	2801(7)	4.1(4)
C(31)	5126(19)	3727(8)	2290(7)	3.5(4)
C(32)	3824(20)	3774(8)	2487(7)	3.7(4)
C(33)	3080(21)	4337(9)	2410(8)	4.7(5)
C(34)	3691(21)	4786(9)	2186(8)	4.6(5)
C(35)	4957(24)	4745(11)	1944(8)	5.8(5)

Table 2.

(cont.)

C(36)	5725(22)	4196(10)	2019(8)	5.0(5)
C(41)	5066(16)	1315(7)	2426(6)	2.0(3)
C(42)	6282(18)	1290(8)	2788(7)	2.9(4)
C(43)	6915(12)	737(9)	2912(7)	3.8(4)
C(44)	6352(21)	226(9)	2649(8)	4.41(4)
C(45)	5131(22)	242(9)	2257(8)	4.7(5)
C(46)	4465(10)	809(9)	2154(7)	3.8(4)
C(51)	2641(19)	1941(8)	2678(6)	3.1(4)
C(52)	2730(20)	2177(8)	3218(7)	3.7(4)
C(53)	1593(22)	2059(9)	3528(8)	4.7(5)
C(54)	430(22)	1738(9)	3278(8)	4.4(5)
C(55)	378(22)	1531(9)	2758(8)	4.7(5)
C(56)	1486(20)	1647(9)	2451(7)	3.9(4)
C(61)	3577(18)	2111(8)	1591(6)	2.6(4)
C(62)	2515(20)	2519(9)	1445(7)	3.9(4)
C(63)	2151(21)	2664(9)	871(8)	4.4(5)
C(64)	2835(22)	2399(9)	498(8)	4.6(5)
C(65)	3884(21)	1991(9)	630(7)	4.1(4)
C(66)	4316(18)	1836(8)	1212(7)	3.1(4)

[1] $$Ueq = 1/3 \left\{ \sum_i \sum_j U_{ij} (a^*_i a^*_j) (\vec{a}_i \vec{a}_j) \right\}$$

$$\sigma(Ueq) = \frac{1}{\sqrt{6}} \left\langle \frac{\sigma(U_{ii})}{U_{ii}} \right\rangle Ueq$$

Table 3.

Bond Lengths in the Anion

Anion I			Anion II		
Atom	Atom	Dist(Å)	Atom	Atom	Dist(Å)
W(1)	W(2)	2.646	W(4)	W(5)	2.649
	W(3)	2.664		W(6)	2.652
	W(2')	2.658		W(5')	2.659
	W(3')	2.650		W(6')	2.643
W(2)	W(3)	2.639	W(5)	W(6)	2.661
	W(3')	2.659		W(6')	2.642
W(1)	Br(5)	2.547	W(4)	Br(11)	2.532
W(2)	Br(3)	2.545	W(5)	Br(13)	2.560
W(3)	Br(7)	2.530	W(6)	Br(14)	2.533
Br(1)	W(1)	2.612	Br(8)	W(4)	2.615
	W(2')	2.629		W(5)	2.618
	W(3)	2.616		W(6')	2.614
Br(6)	W(1)	2.615	Br(9)	W(4)	2.601
	W(2)	2.611		W(5)	2.616
	W(3')	2.616		W(6)	2.623
Br(2)	W(1)	2.623	Br(10)	W(4')	2.614
	W(2)	2.632		W(5)	2.617
	W(3)	2.613		W(6)	2.605
Br(4)	W(1)	2.598	Br(12)	W(4')	2.616
	W(2')	2.625		W(5)	2.611
	W(3')	2.607		W(6')	2.618
W(1)	W(1')	3.762	W(4)	W(4')	3.748
W(2)	W(2')	3.738	W(5)	W(5')	3.759
W(3)	W(3')	3.754	W(6)	W(6')	3.741

	I	II	avg.
W-W(cis) avg:	2.653(9)	2.651(8)	2.652(9)
W-W(trans) avg:	3.751(12)	3.749(9)	3.750(12)
W-Br(axial) avg:	2.541(9)	2.542(16)	2.542(16)
W-Br(facial) avg:	2.616(10)	2.614(6)	2.615(10)

Figure 1. ORTEP of the unit cell of $[(C_6H_5)_3{=}N{=}(C_6H_5)_3]W_6Br_{14}$.

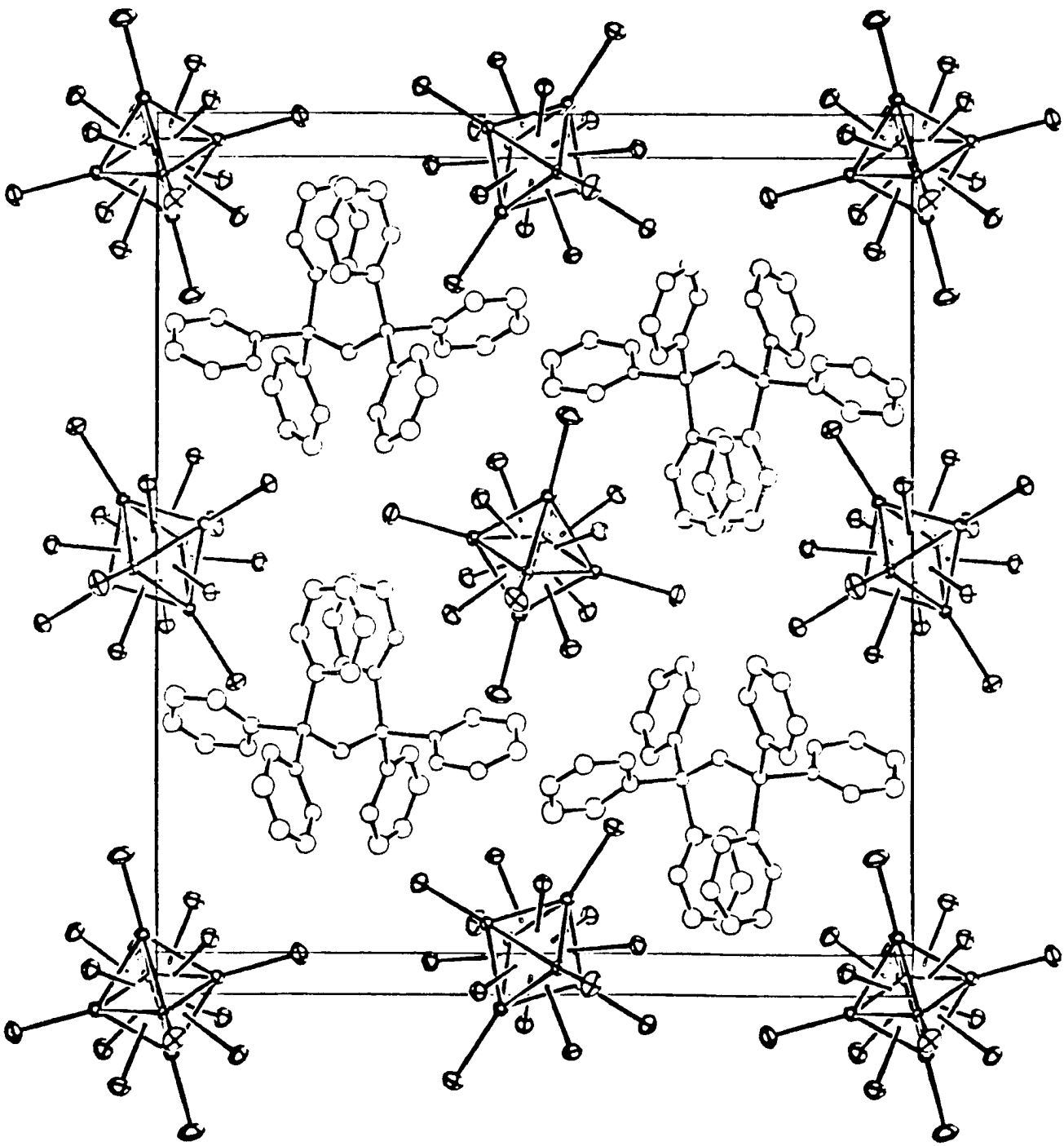

tions we see however, are much greater than the esd's in individual W-W distances, suggesting that, while they are real, they are not the result of a specific electronic structure in the anion. It is possible that there is a small molecular distortion that is not large enough to cause the distorted ions to be ordered in the crystal, and the x-ray structure then is some average over several orientations of the real structure. Such a disorder would be expected to show itself in abnormal thermal parameters of the tungsten or bromine atoms. These parameters, however, are not abnormal; thus we conclude that the small departures from regularity in this ion are random.

The $PPh_3{=}N{=}PPh_3^+$ cation in this structure shows normal bond distances and angles with moderately large standard deviations. The 2 N=P bonds average 1.580(14) Å and the 6 P-C bonds average 1.806(19) Å; both distances are normal. The C-C distances in the phenyl rings average 1.40(4) Å and the rings are all planar within 0.05 Å. The isotropic thermal parameters of the phosphorous nitrogen and inner carbon atoms average about 3 $Å^2$ while the carbon atoms farthest from the phosphorous atoms have values of about 5 $Å^2$. The closest Br-C approach is 3.4 Å and the closest non-bonded C-C approach is 3.2 Å; the Br-C distance is at the short end of a Van der Waals contact while the C-C distance is normal.

The electronic absorption spectrum of $(PPN)W_6Br_{14}$ in dichloromethane solution is displayed in Figure 2d. The most prominent feature of this spectrum is the broad band at 551 nm, which is responsible for the deep burgundy-red color of the solution. This band is probably due

Figure 2. Electronic absorption solution spectra of oxidized tungsten halide clusters in methylene chloride solution (1.26×10^{-4} M): (a.) $(TBA)W_6Cl_{14}$: (b.) $(TBA)W_6Cl_8Br_6$; (c.) $(TBA)W_6Br_8Cl_6$; (d.) $(PPN)W_6Br_{14}$: (e.) $(TBA)W_6I_8Br_6$.

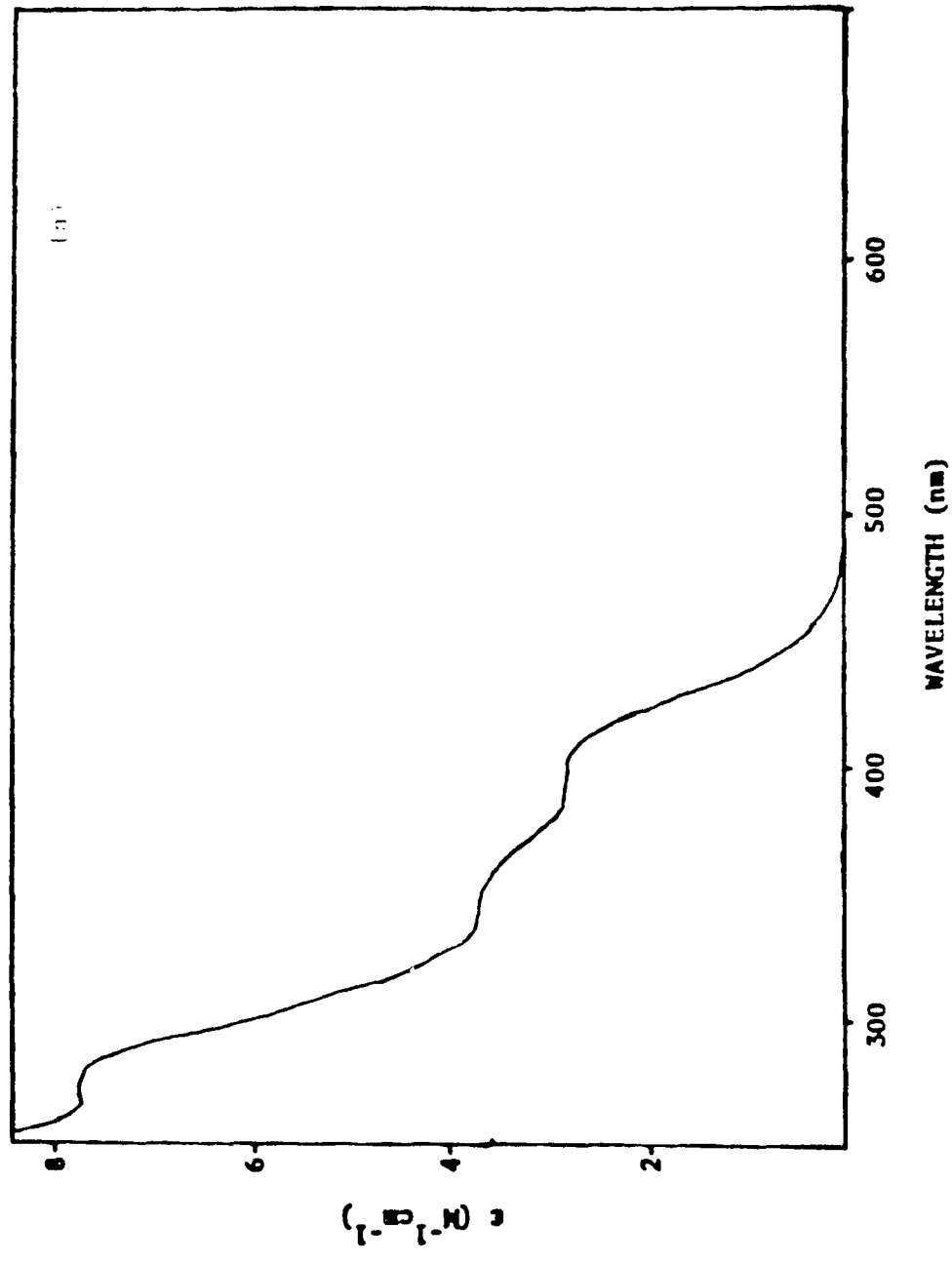
8
6
4
2
300
400
500
600
WAVELENGTH (nm)

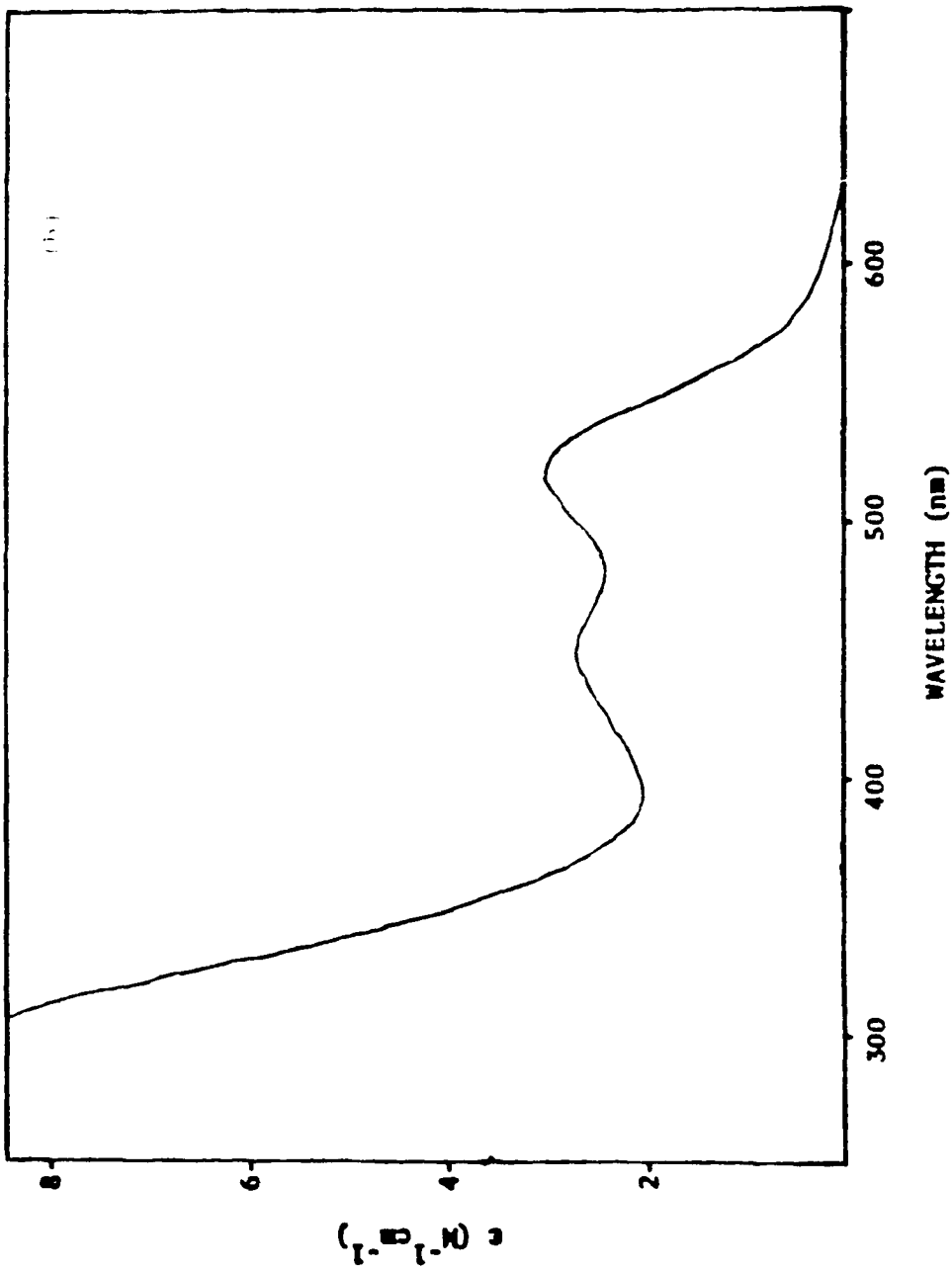
8
6
4
2
300
400
500
600
WAVELENGTH (nm)

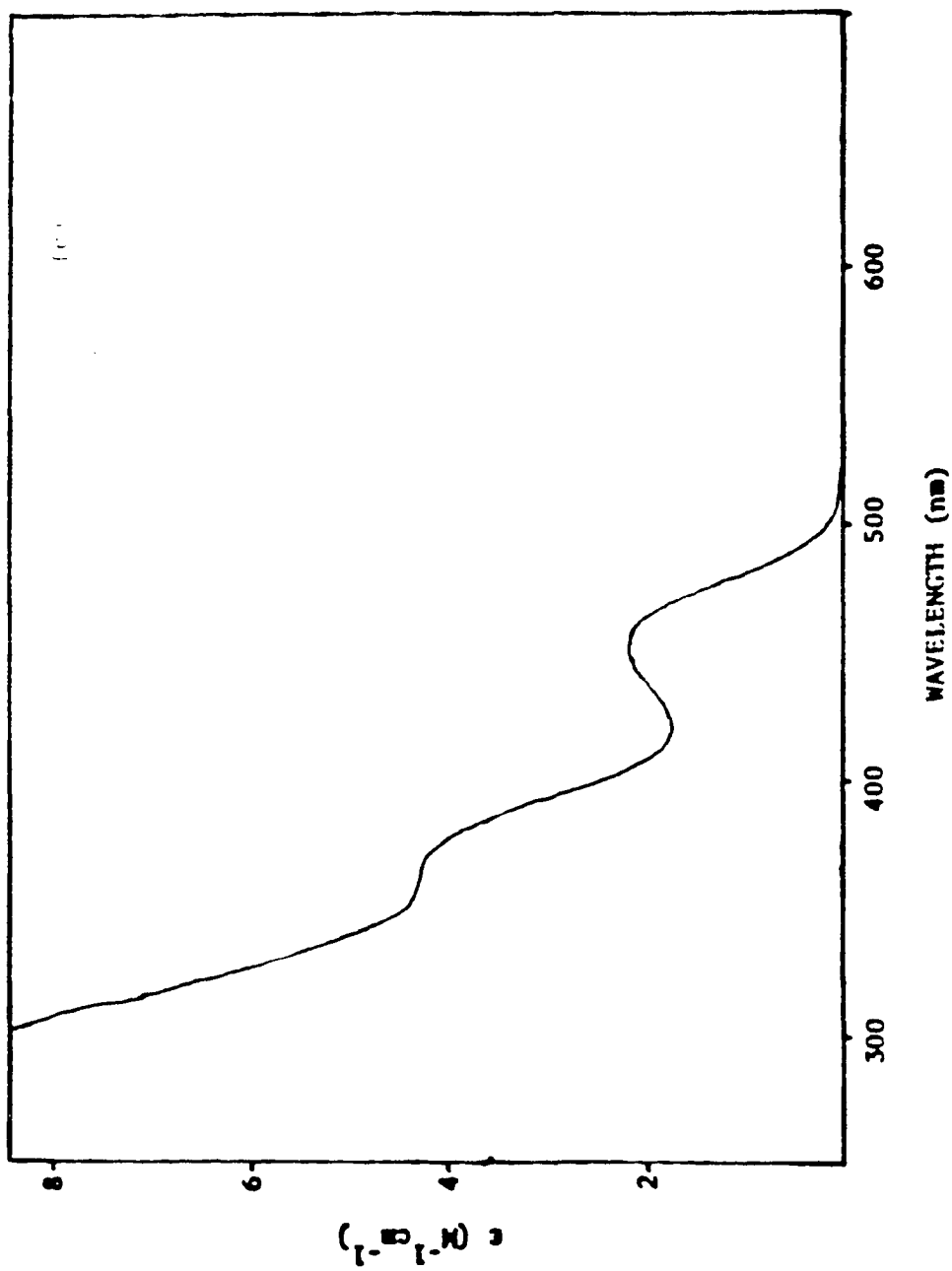
8
6
4
2
300
400
500
600
WAVELENGTH (nm)

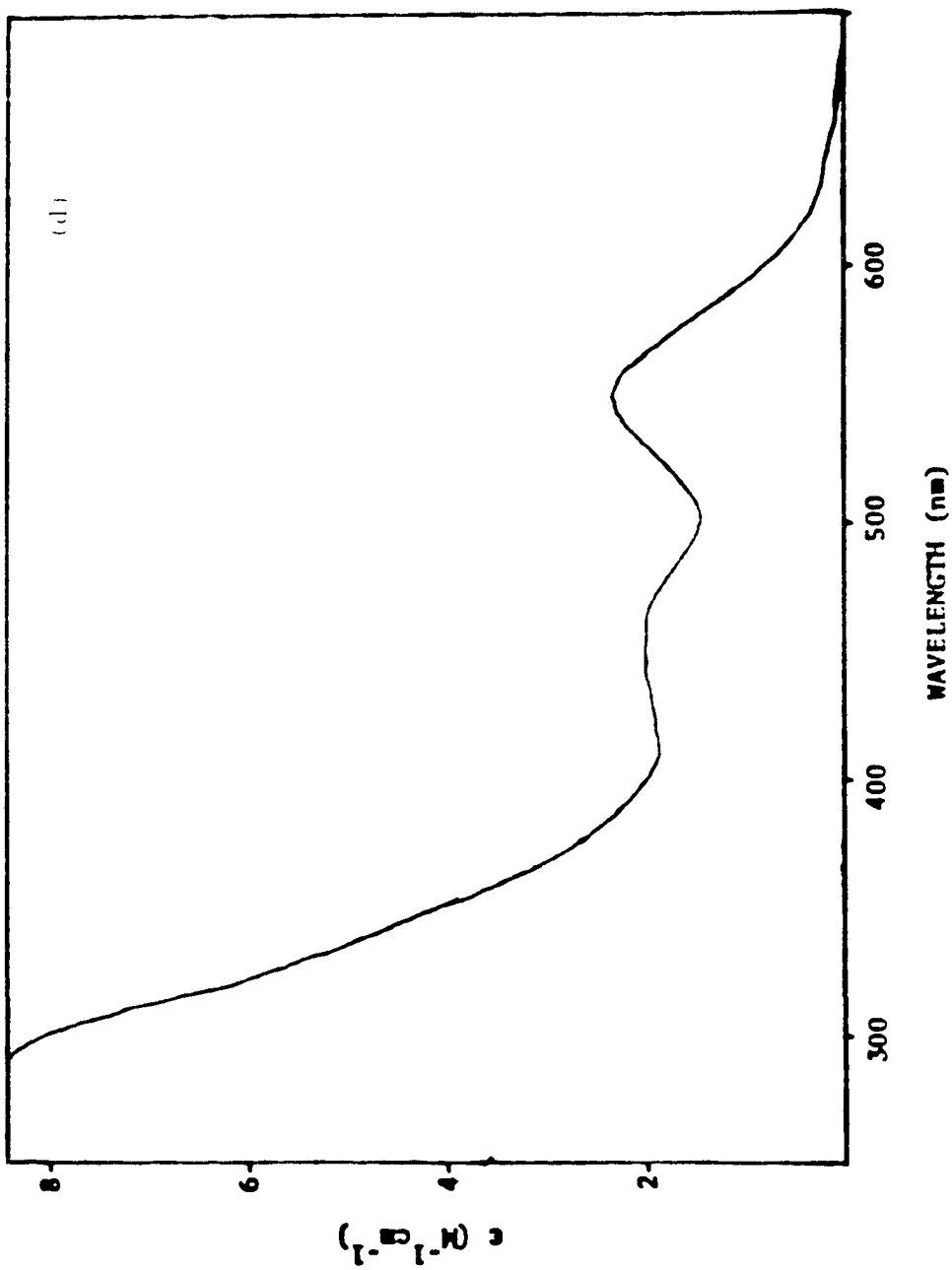
8
6
4
2
300
400
500
600
WAVELENGTH (nm)

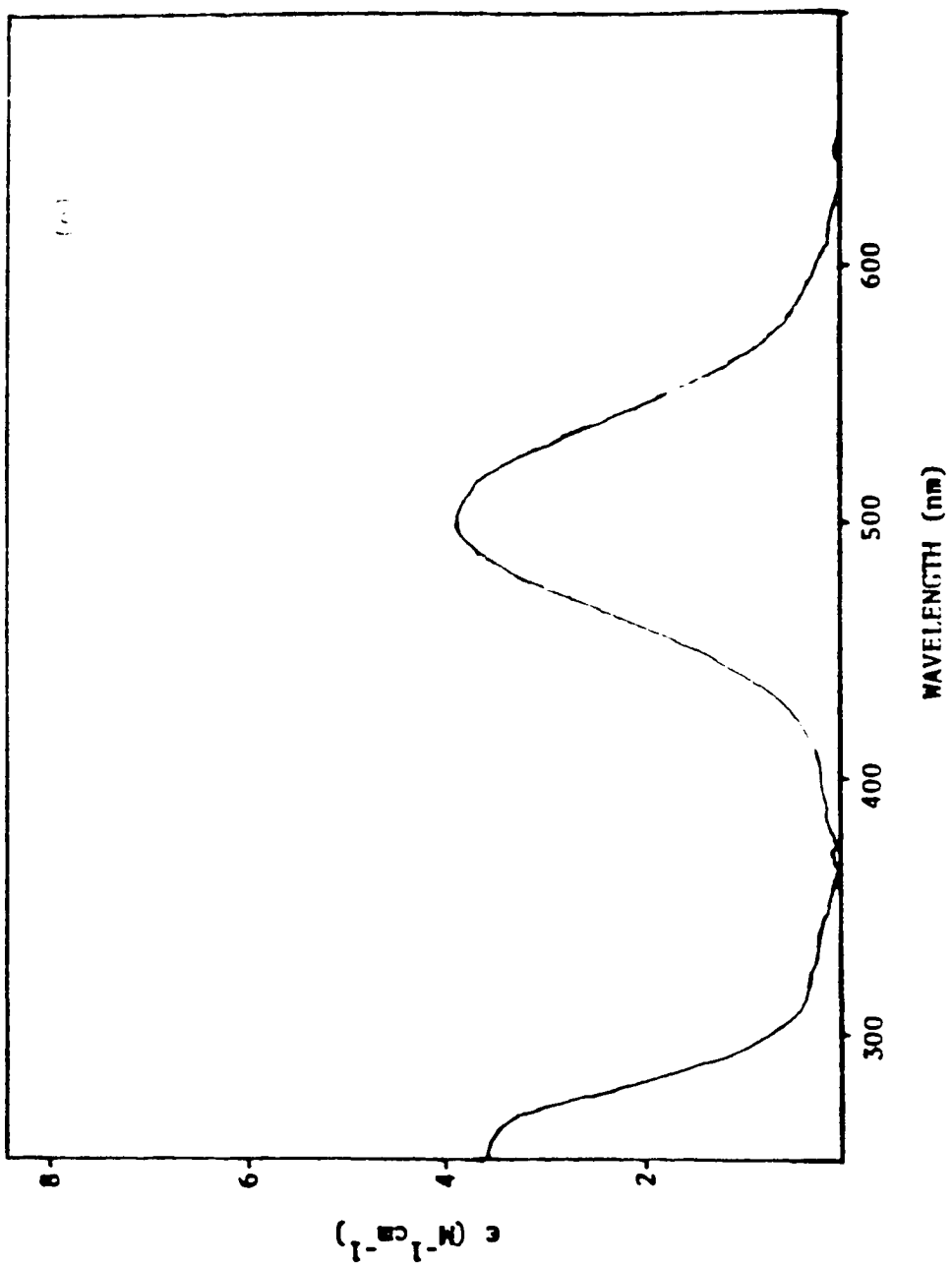
8
6
4
2
ε (M⁻¹cm⁻¹)
300
400
500
600
WAVELENGTH (nm)

to a ligand- to-metal charge transfer transition from a halide ligand to a delocalized tungsten (III) in the metal core. The absorption spectra of other monoanions were also recorded in order to probe the properties of the transition indirectly. The spectra of (a) (TBA)W_6Cl_{14} [TBA^+=(n-C_4H_9)$_4N^+$], (b) (TBA)$W_6Cl_8Br_6$, (c) (TBA)$W_6Br_8Cl_6$, (e) (TBA)$W_6I_8Br_6$ are also displayed in Figure 2 (All three clusters with terminal iodide terminal ligands were unstable to oxidation by $NOPF_6$, as was the $W_6I_8Cl_6^{2-}$ anion) and all of the solution spectroscopic data are summarized in Table 4.

Examining the data on the first four complexes in Table 4, the role of the terminal ligands and the bridging ligands in the lowest energy allowed transition can be discussed. By changing the terminal halide from chloride to bromide, the band red shifts by 5700 cm^{-1} (W_6Cl_8 core) and 3800 cm^{-1} (W_6Br_8 core), with very little change in the extinction coefficient. Changing the bridging halides while keeping the same terminal ligand results in a much smaller shift in $\overline{\nu}_{max}$ for the lowest energy transition, 2970 cm^{-1} ($W_6Cl_{14}^-$ to $W_6Br_8Cl_6^-$) and 1150 cm^{-1} ($W_6Cl_8Br_6^-$ to $W_6Br_{14}^-$) with the extinction coefficients of the transitions of the W_6Br_8 core about 25% lower than the corresponding ϵ for the W_6Cl_8 core. These results indicate that the charge transfer is from a terminal ligand since the energy of the transition decreases significantly upon exchange of the terminal chlorides for bromides. The lower extinction coefficients for the transitions in the W_6Br_8 core with respect to the W_6Cl_8 core may be due to a decreased overlap of the tungsten and terminal halide orbitals due to steric bulk around the metals imposed by

Table 4.

Electronic Absorption Spectral Data

Complex	λ_{max}(nm)	$\bar{\nu}_{max}$(cm^{-1})	ϵ ($M^{-1}cm^{-1}$)
$(TBA)W_6Cl_{14}$	400	25000	3010
	352	28400	3870
$(TBA)W_6Cl_8Br_6$	518	19300	3200
	450	22200	2880
$(TBA)W_6Br_8Cl_6$	454	22030	2340
	368	27170	4490
$(PPN)W_6Br_{14}$	551	18150	2560
	460	21740	2220
	441	22680	2200
	295	33900	9020
$(TBA)W_6I_8Br_6$	501	19960	4270
	255	39220	3880

All spectra recorded in methylene chloride solution.

the larger halides. This is supported by the structural study done on the dianions[3]. As usual in these tungsten clusters, the iodide-bridging ligand is unique[4]. The lowest energy transition of the $W_6I_8Br_6^-$ ion is at *higher* energy than the lowest energy transition in either the $W_6Cl_8Br_6^-$ or the $W_6Br_{14}^-$ ions. Also, there are no intense bands in the absorption spectrum of the $W_6I_8Br_6^-$ ion between 300 and 400 nm. Beyond noting these descrepancies, no interpretation can be made at this time.

The EPR spectrum of $(PPN)W_6Br_{14}$ in frozen methylene chloride solution at 9 K is shown in Figure 3. Raising the temperature of the sample causes the EPR spectrum to broaden and finally be indistinguishable from the baseline at 25 K. While this process is not understood, the washing out of the EPR signal may involve the interchange of axes of distortion. The EPR spectrum at 9 K is clearly anisotropic, which is in line with the EPR spectra taken of analogous $Mo_6X_{14}^-$ clusters[1], although, in this case, the $g_{\|}$ tensor cannot be easily determined. Variable temperature magnetic data are plotted in Figure 4. There appears to be a transition point in the data at very low temperatures where μ_{eff} becomes significantly greater than the spin-only value (1.73 B.M.). This kind of behavior is consistent with a ^2E ground state[5].

DISCUSSION

Due to the complexity of the spectroscopic problem, calculational models have been used to interpret the properties of the $Mo_6X_{14}^{2-}$ and $W_6X_{14}^{2-}$ clusters[6]. The model which best fits the $Mo_6Cl_{14}^-$ EPR data and the $Mo_6X_{14}^{2-}$

Figure 3. EPR spectrum of (PPN)W_6Br_{14} in frozen methylene chloride solution at 9 K (9.182 GHz).

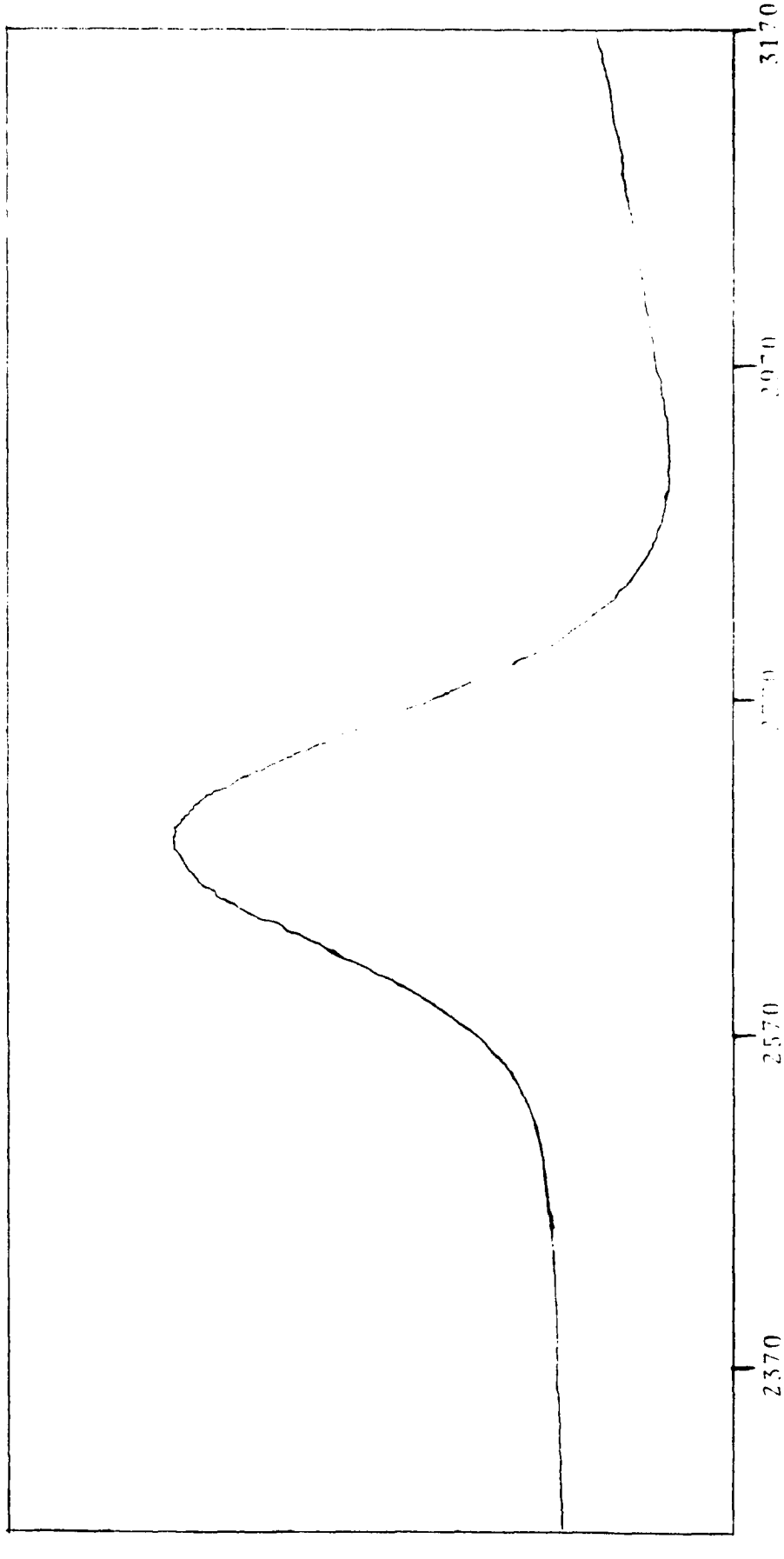
3170
2570
2370
H (GAUSS)

Figure 4. Variable temperature magnetic susceptibility data for powdered $(PPN)W_6Br_{14}$.

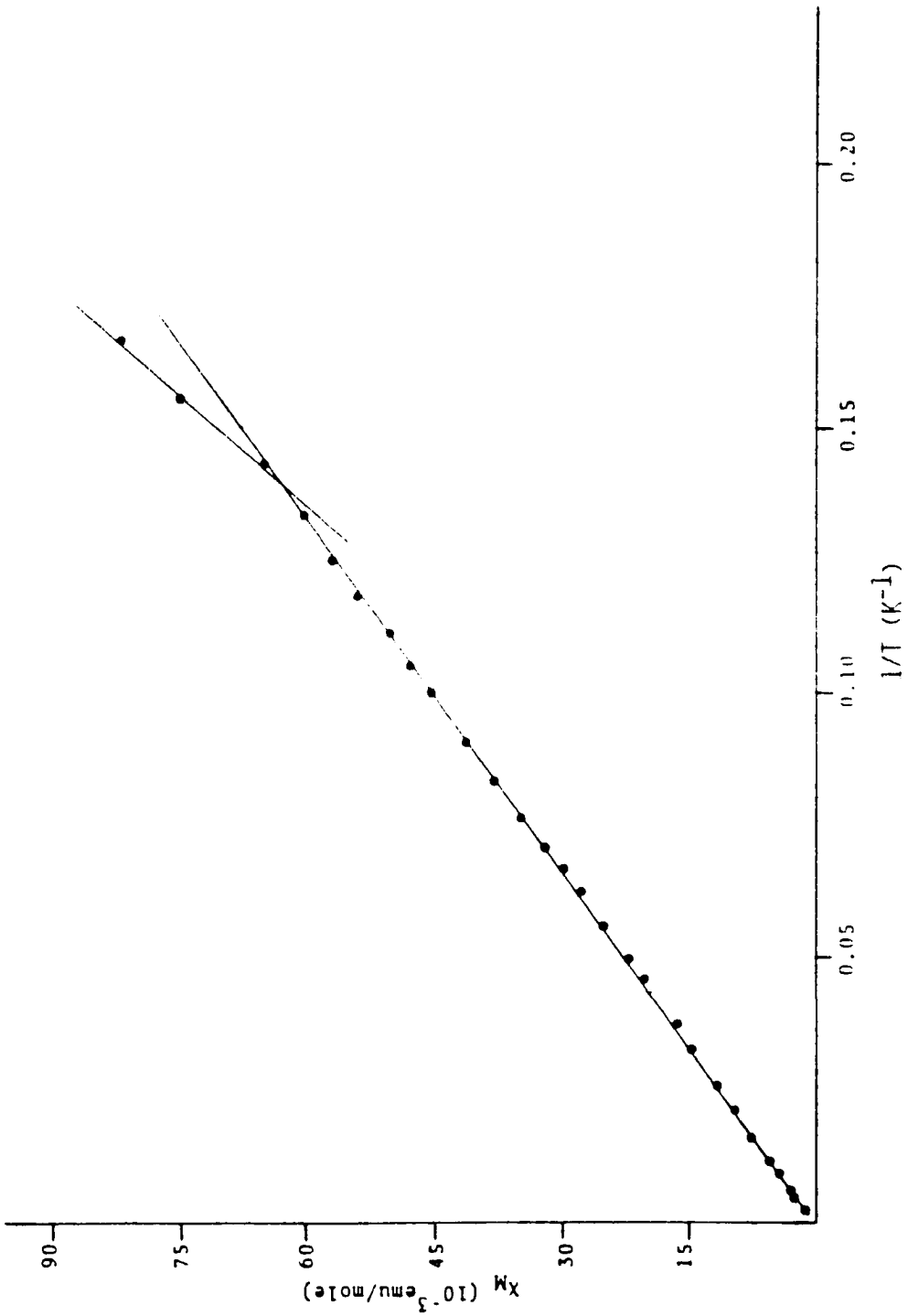
90
75
60
45
30
15
χM (10⁻³emu/mole)
0.05
0.10
0.15
0.20
1/T (K⁻¹)

emission data is derived from an extended Hückel molecular orbital calculation by Hoffman and Eubanks[7]. The feature of that model relevant to this work is that the highest occupied MO is a filled e_g orbital. The anisotropic EPR spectra of all the $M_6X_{14}^-$ ions studied bear this out, and an analysis of the $Mo_6Cl_{14}^-$ spectrum implies that the distortion is an axial compression[1]. Unfortunately, the crystal structure of $(PPN)W_6Br_{14}$ has failed to confirm this since the structure shows no preferred orientation axis. The lack of unusually large thermal ellipsoids implies that the distortion, if there is one, is not large enough to be "frozen" in a low temperature study.

A comparison of the $W_6Br_{14}^{2-}$ and $W_6Br_{14}^-$ bond lengths does lead to certain conclusions, however (Table 5)[3]. The monoanion has a slightly enlarged octahedron compared to the dianion, an indication perhaps that the electron removed in the oxidation is from a bonding orbital (although the increased charge on the tungsten core would be expected to expand it also). The W-Br(axial) bond is significantly shorter in the monoanion, presumably due to the electrostatic attraction of the negatively charged halide to the now more positively charged W_6 unit. Surprisingly, the W-Br (facial) bonds are not significantly shorter in the monoanion despite the higher charge on the metals. Perhaps this is a manifestation of the ligand effects seen on the $W_6X_{14}^{2-}$ structures. The expected shortening of the metal-bromide(facial) bond upon oxidation of the metal core may be compensated by the decrease in the interaction of the metal orbitals with the bromide *d* orbitals[4].

Table 5.

Bond Distances in $W_6Br_{14}^{2-}$ and $W_6Br_{14}^{-}$

	Distance (Å)	
Atoms involved	$W_6Br_{14}^{2-}$	$W_6Br_{14}^{-}$
W-W(*cis*)	2.635(7)	2.652(9)
W-W(*trans*)	3.726(4)	3.750(12)
W-Br(axial)	2.587(4)	2.542(10)
W-Br(facial)	2.628(9)	2.615(10)

REFERENCES

1. a.) Maverick, A.W.; Gray, H.B. *J. Am. Chem. Soc.*, **1981**, *103*, 1298. b.) Maverick, A.W.; Nadjdzionek, J.S.; MacKenzie, D.; Nocera, D.G.; Gray, H.B. *J. Am. Chem. Soc.*, **1983**, *105*, 1878. c.) Zietlow, T.C.; Hopkins, M.D.; Gray, H.B. *J. Solid State Chem.*, in press.
2. Main, P.; Woolfson, M.M.; Lessinger, L.; Germain, G.; Delcleroq, J.-P.; Hull, S.E. MULTAN 78; University of York, York, England.
3. Zietlow, T.C.; Schaefer, W.P.; Sadeghi, B.; Hua, N.; Gray, H.B., manuscript in preparation.
4. Zietlow, T.C.; Nocera, D.G.; Gray, H.B., submitted for publication.
5. Mabbs, F.E.; Machin, D.J. *Magnetism and Transition Metal Complexes*, Chapman and Hall:London, 1973, 95.
6. a.) Seifert, G.; Finster, J; Müller, H. *Chem. Phys. Lett.*, **1980**, *75*, 373. b.) Cotton, F.A.; Stanley, G.G. *ibid.*, **1978**, *58*, 450. c.) Korol'kov, D.; Pak, V.N. *Zh. Struk. Khi.*, **1973**, *14*, 1098.
7. Hoffmann, R.; Hughbanks, T., personal communication.

CHAPTER 6

Effect of Alkyl Phosphine Ligands on the Photophysics and Reduction Potentials of Hexanuclear Molybdenum Halide Clusters

Effect of Alkyl Phosphine Ligands on the Photophysics and Reduction Potentials of Hexanuclear Molybdenum Halide Clusters

Thomas C. Zietlow and Harry B. Gray*

Contribution No. from the Arthur Amos Noyes Laboratory of Chemical Physics, California Institute of Technology, Pasadena, California, 91125.

Abstract. The effect of trialkylphosphine ligands on the photophysics and reduction potentials of the Mo_6Cl_{12} cluster has been studied. The emission spectra of the $(PR_3)_2Mo_6Cl_{12}$ (R = -Et, -Pr, -Bu) show only a slight dependence on the alkylphosphine with the energy of the emissive excited state increasing slightly with increasing basicity of the phosphine. The photophysical data imply that the nature of the transition is not affected by the phosphines since the radiative rate is the same, but the non-radiative rate for the phosphine derivatives is twice that of the $Mo_6Cl_{14}^{2-}$ cluster. The phosphine derivatives are slightly more easily reduced than the $Mo_6Cl_{14}^{2-}$ cluster; this is attributed to the charge difference.

The hexanuclear clusters have been shown to undergo photo-induced electron transfer[1] and energy transfer[2] to appropriate quenchers, but so far the goal of photochemistry involving the transfer of more than one electron has not been achieved. The problem may be the lack of suitable coordination sites on the cluster molecule for potential substrates to bind[3]. In an effort to activate the cluster molecules toward potential substrates the effect of terminal ligands other than halides has been investigated with the idea of incorporating substrate coordination sites on these ligands. The first such attempt deals with the photophysics and electrochemistry of *bis* phosphine derivatives of the Mo_6Cl_{12} cluster. These phosphines can be used as links to electron transfer quenchers in order to determine the effect of driving force on the rate of electron transfer in a unimolecular system involving potentials in the range of normal chemical and biological significance.

EXPERIMENTAL SECTION

The phosphine cluster compounds were synthesized according to the method of Hamer *et al.*[4], using $P(\text{-}CH_3)_3$, $P(\text{-}CH_2CH_3)_3$, $P(\text{-}CH_2CH_2CH_3)_3$, and $P(\text{-}CH_2CH_2CH_2CH_3)_3$; the Mo_6Cl_{12} starting material was purchased from the Cerac Company and purified as described earlier[5]. The methylene chloride and 2-methyltetrahydrofuran solvents used in the photophysical measurements were reagent grade and were dried and vacuum distilled before use.

Physical Measurements. Emission lifetime experiments were performed using the second harmonic (532 nm) of a Nd:YAG laser (fwhm = 8 ns).

Emission spectra were run on an instrument made at Caltech and described elsewhere[6]. Cyclic voltammetry was done on PAR Models 175, 173, and 179 electronics. Working and counter electrodes were platinum.

RESULTS AND DISCUSSION

The synthetic method used results in a mixture of the *cis* and *trans* isomers of the disubstituted cluster (Figure 1). Statistically, a 4:1,*cis*:*trans* ratio is expected, but steric effects in the larger phosphine alkyl groups may shift the equilibrium ratio more towards the *trans* isomer. Phosphorous NMR spectroscopy reveals that the two isomers are about 1:1 in the *bis* (tri-n-propylphosphine) derivative of the Mo_6Cl_{12} cluster. No attempt was made to separate the two isomers. All emission lifetime showed monophasic decay and the emission spectra were not unusually broad, indicating the emissive state is not affected by the configuration of the phosphines, as expected from earlier work done on the sensitivity of the molybdenum cluster's emissive excited state to the halide ligands[7].

A sample emission spectrum of the $(PPr_3)_2Mo_6Cl_{12}$ complex in 2-methyltetrahydrofuran solution is displayed in Figure 2. A spectrum taken at 77 K is in Figure 3. The spectral features of three phosphine derivatives (the PMe_3 derivative was totally insoluble in common solvents) are given in Table 1, along with $(TBA)_2Mo_6Cl_{14}$ as a reference. There is very little difference in the spectra indicating the energy of the emitting excited state is not perturbed greatly by the addition of the phosphine ligands. This is in accord with the earlier findings that the energy of the emissive excited state

Figure 1. The *cis* and *trans* isomers of $[(CH_3CH_2)_3P]_2Mo_6Cl_{12}$.

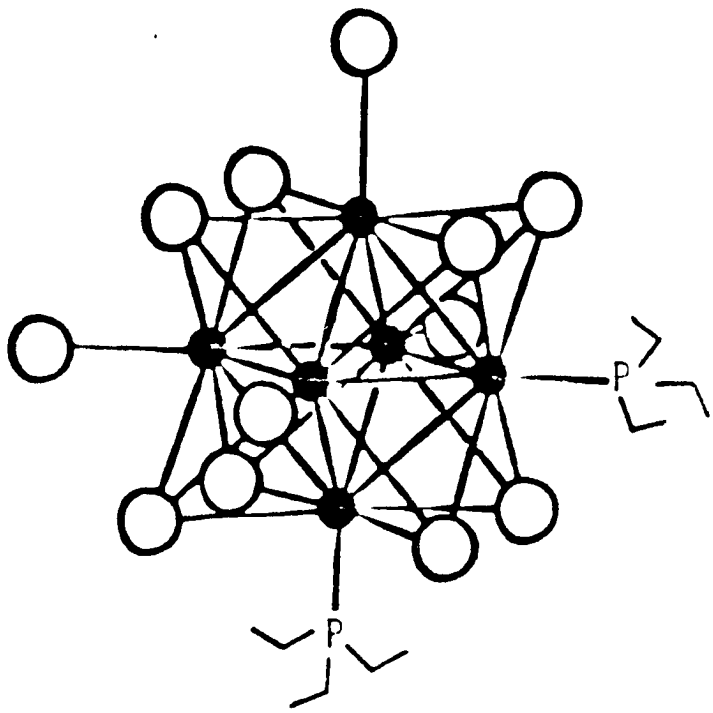
P
P

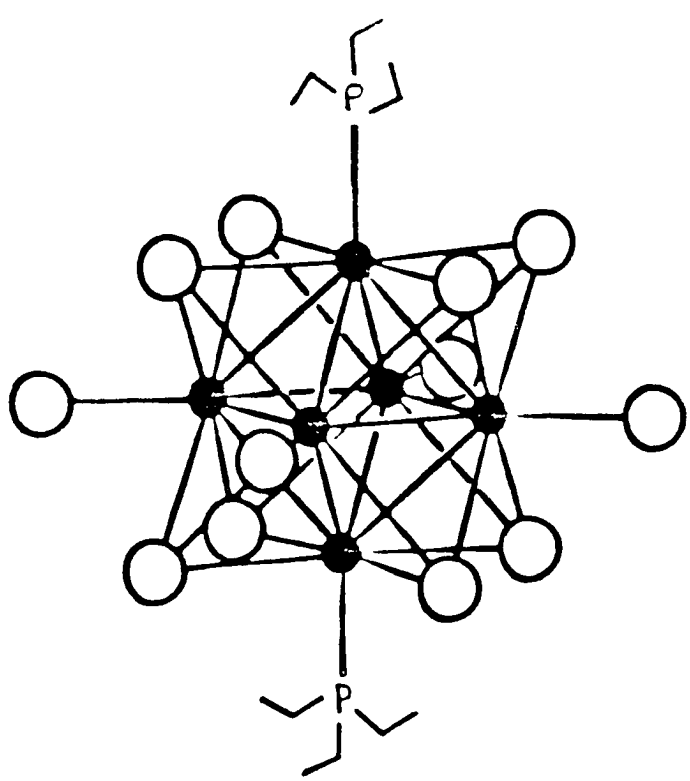
P
P

Figure 2. Uncorrected emission spectrum of $(PPr_3)_2Mo_6Cl_{12}$ in 2-methyltetrahydrofuran solution at 295 K, 366 nm excitation.

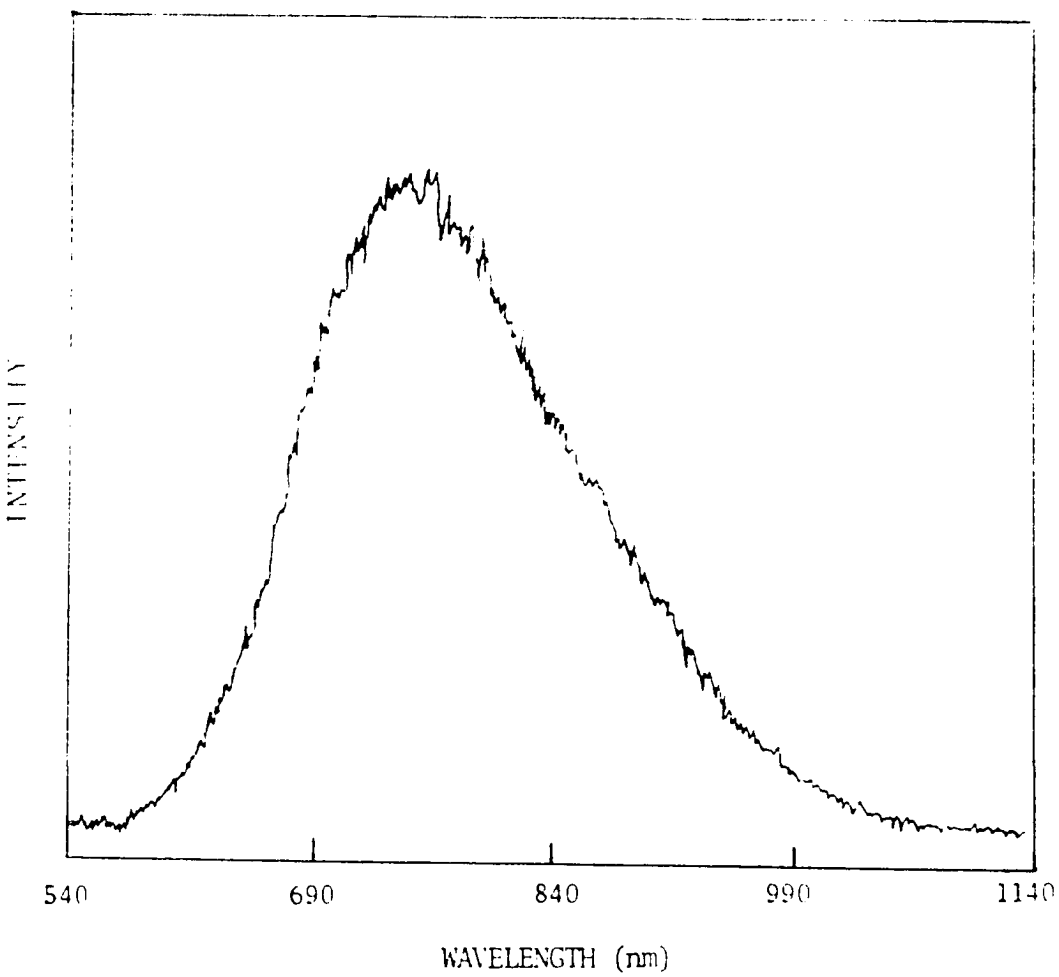
INTENSITY
540
690
840
990
1140
WAVELENGTH (nm)

Figure 3. Uncorrected emission spectrum of $(PPr_3)_2Mo_6Cl_{12}$ in a 2-methyltetrahydrofuran glass at 77 K, 366 nm excitation.

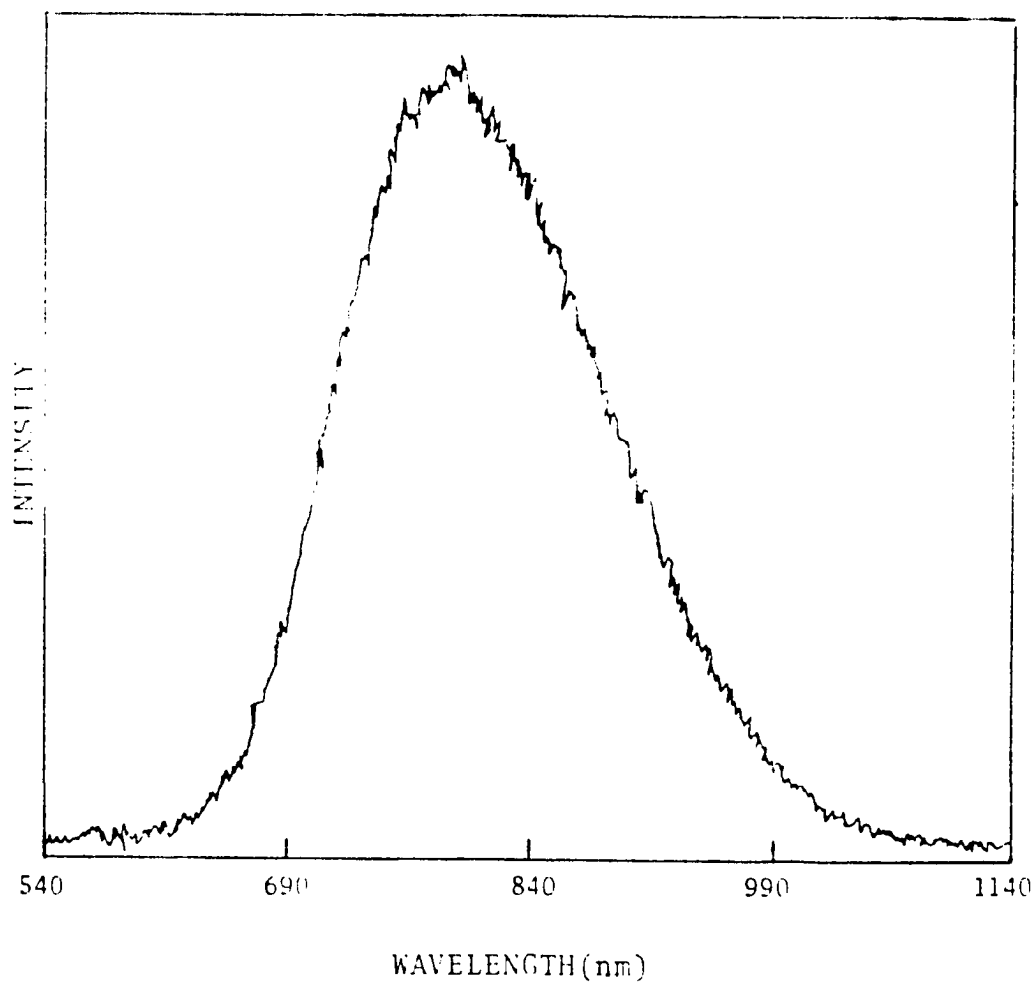
INTENSITY
540
690
840
990
1140
WAVELENGTH(nm)

Table 1.

Emission Spectral Data for $(PR_3)_2Mo_6Cl_{12}$

Complex	λ_{max} (nm)	$\bar{\nu}_{max}$ (cm^{-1})	fwhm (cm^{-1})
$(Et_3P)_2Mo_6Cl_{12}$	756	13230	3630
$(n\text{-}Pr_3P)_2Mo_6Cl_{12}$	750	13330	4160
$(n\text{-}Bu_3P)_2Mo_6Cl_{12}$	744	1344[illegible]	354[illegible]
$(TBA)_2Mo_6Cl_{14}$	747	133[illegible]	373[illegible]

All data recorded in methylene chloride solution at 22±2°C.

is independent of the halide ligands[7].

The emission lifetimes and emission quantum yields for the phosphine derivatives at room temperature in methylene chloride solution are displayed in Table 2. The calculated radiative and non-radiative rates are also shown in Table 2. The important point to note is the difference in the emission lifetimes between the $Mo_6Cl_{14}^{2-}$ and the $(PR_3)_2Mo_6Cl_{12}$ clusters at room temperature; this difference is due to the increase in the non-radiative rate by a factor of two in the phosphine derivative relative to the all-halide cluster. The radiative rate out of the emissive excited state is independent of the ligands, implying that the picture of a metal-centered excited state appears to be correct for these Mo_6 clusters.

A temperature dependence study was performed on the $(PPr_3)_2Mo_6Cl_{12}$ complex in 2-MeTHF solution. The solvent was chosen due to its ability to form a glass at low temperatures. However, the performance of a variable temperature quantum yield experiment becomes difficult when the absorption of the sample at a particular wavelength is temperature dependent. For this experiment, the excitation line was 366 nm where the absorption of the sample was greater than 2, which means that greater than 90% of the photons hitting the sample were absorbed. At lower temperature, this absorption increases, but does not change the number of photons absorbed by the sample a great deal. Of course, a front surface collection geometry was required due to the very high absorbance of the sample. The ϕ_{em} (T) data are shown in Table 3. This temperature

Table 2.

Photophysical Data for $(PR_3)_2Mo_6Cl_{12}$ Complexes

Complex	ϕ_{em}	τ (μsec)	k_r (s^{-1})	k_{nr} (s^{-1})
$(Et_3P)_2Mo_6Cl_{12}$	1.5	85	180	$1.2x10^4$
$(n\text{-}Pr_3P)_2Mo_6Cl_{12}$	1.3	84	160	$1.2x10^4$
$(n\text{-}Bu_3P)_2Mo_6Cl_{12}$	1.9	82	230	$1.2x10^4$
$(TBA)_2Mo_6Cl_{14}$	3.0	148	220	$6.5x10^3$

All data recorded in methylene chloride solution at 22±2°C.

Table 3.

Temperature Dependence of ϕ_{em} for $(n\text{-}Pr_3P)_2Mo_6Cl_{12}$

T(K)	Relative ϕ_{em}
292	1.00
222	1.32
185	1.47
155	1.65

Data taken in 2-methyltetrahydrofuran solution/glass. Excitation lin-
366 nm.

dependence of the lifetime implies that the radiative rate is not changing, but there is a non-radiative pathway which is temperature dependent in the phosphine derivatized clusters[8].

Another reason for the investigation of the properties of these phosphine derivatives of the clusters was the likelyhood that the phosphine complexes would be fairly easy to reduce, due to the molecule's now being neutral instead of a dianion, and the ability of phosphine ligands to stabilize low-valent molybdenum. The reduction potentials for the phospine derivatives are shown in Table 4. The first thing to recognize is that, indeed, the phosphine derivatives are considerably easier to reduce relative to the $Mo_6Cl_{14}^{2-}$ anion, without a great dependence on the alkyl chain length. Unfortunately, the cyclic voltammograms do not indicate that the reduction is fully reversible. The best cyclic voltammogram (most reversible) is that of $(PPr_3)_2Mo_6Cl_{12}$ in THF solution; this is displayed in Figure 4. The $E_{\frac{1}{2}}$ values for all the clusters were determined by averaging the anodic and cathodic peak potentials, but the ratios of the peak currents were not equal to one, and the peak-to-peak separations were typically over 100 mV.

Excited State Intramolecular Electron Transfer Reactions.

The conclusion which is reached from the work described above is that the fundamental properties of the emissive excited state of the $Mo_6Cl_{14}^{2-}$ systems are not greatly perturbed by the replacement of two axial chlorides with two tertiary alkyl phosphines. This finding can probably be generalized to the analogous tungsten clusters, $W_6X_{14}^{2-}$ (X = Cl, Br, I). Assuming the

Table 4.

Reduction Potentials of $(PR_3)_2Mo_6Cl_{12}$ Clusters

Complex	Solvent	$E_{\frac{1}{2}}$(red)*
$(Et_3P)_2Mo_6Cl_{12}$	CH_2Cl_2	-1.15 V
$(n\text{-}Pr_3P)_2Mo_6Cl_{12}$	CH_2Cl_2	-1.16 V
	THF	-1.10 V
$(n\text{-}Bu_3P)_2Mo_6Cl_{12}$	THF	-1.25 V

*Potentials are versus SCE at 22±2°C. Pt bead working and Pt wire auxillary electrodes.

Figure 4. Cyclic voltammogram of $(PPr_3)_2Mo_6Cl_{12}$ in tetrahydrofuran (0.1 M $TBAPF_6$, 22°C).

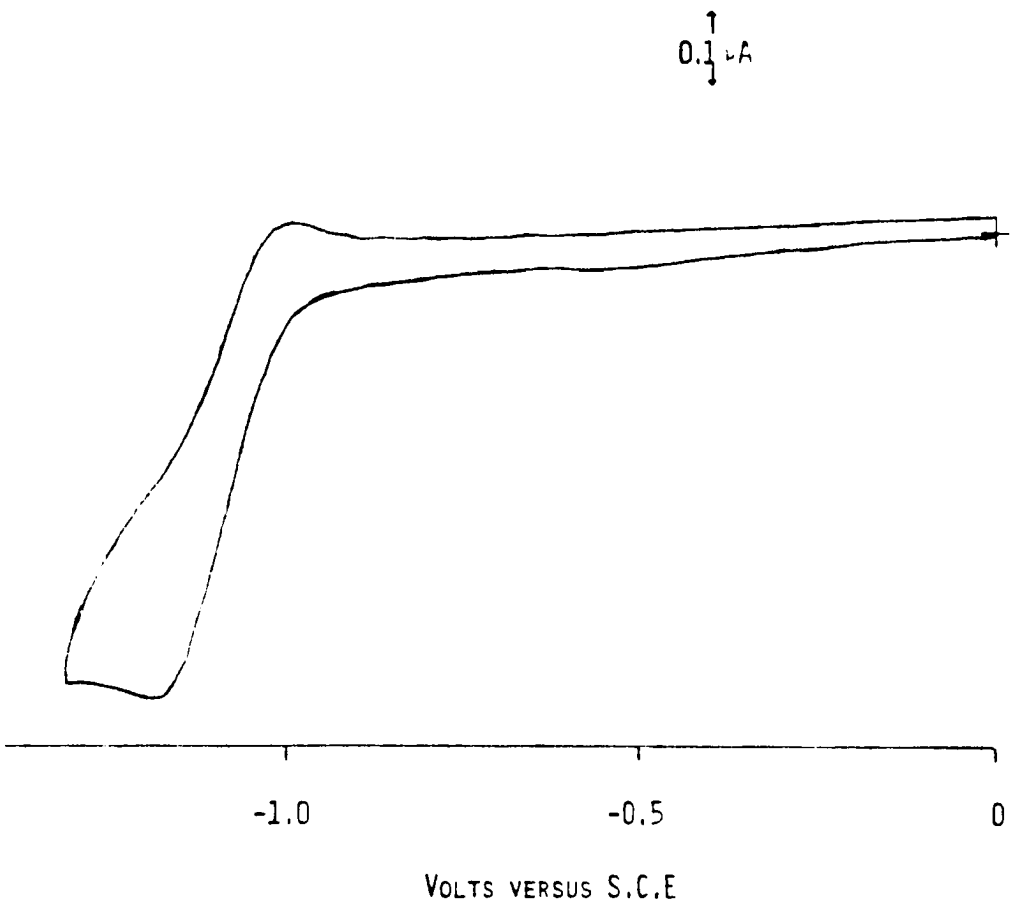
0.1 μA
-1.0
-0.5
0
VOLTS VERSUS S.C.E

bis phosphine substitutents affect the tungsten cluster redox potentials to the same extent as the molybdenum clusters, these functionalized clusters have a large range of redox potentials to use in the study of electron transfer processes. If an electron acceptor (or donor) molecule can be attached to the phosphine through a suitable hydrocarbon spacer, and the phosphine attached to a hexanuclear cluster, the dependence of the electron transfer rate on the driving force of the reaction can be conveniently studied.

In this laboratory, a large number of experiments have been done to determine the driving force, distance, and orientation dependencies on the rate of electron transfer[9]. The driving force dependence work has been primarily bimolecular-quenching studies where the overall driving force of the excited state redox reaction is known, but the intramolecular distance is not fixed.[10] By attaching the quencher to the chromophore, the distance is determined from high-driving force to low-driving force and effects such as the temperature dependence of the electron transfer rate can be conveniently studied over a wide range.

The planned excited state intramolecular electron transfer studies will proceed using pyridinium ion derivatives used in previous bimolecular-quenching studies attached covalently to a phosphine ligand on the cluster (Figure 5). The intramolecular electron transfer rate will be determined by emission quantum yield measurements and transient kinetics. A reaction scheme for this series is shown below for an electron accepting quencher (i.e., a pyridinium ion):

Figure 5. Model for chromophore/quencher complex to be used in electron transfer studies.

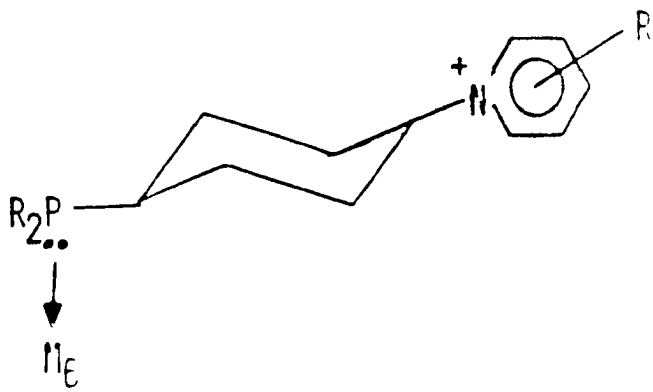
R
+
N
R2P
E

$$M\sim\sim A^{+} \rightarrow M^{*}\sim\sim A^{+} \quad (1)$$

$$M^{*}\sim\sim A^{+} \rightarrow M^{+}\sim\sim A^{\cdot} \quad (2)$$

$$M^{+}\sim\sim A^{\cdot} \rightarrow M\sim\sim A^{+} \quad (3).$$

Reaction (2) can be monitored by emission quantum yield difference and reaction (3) by transient spectroscopy. The rate constants for the intramolecular electron transfer can be compared to the bimoleuclar quenching done on the same system with the same driving force.

Work on the phosphine chemistry required to attach the quenchers to the clusters has been fruitful. DuBois has synthesized and characterized:[11]

(a) $Ph_2PCH_2CH_2(C_5H_5N)$

(b) $Et_2PCH_2CH_2(C_5H_5N)$

(c) $Pr_2PCH_2CH_2(C_5H_5N)$

(d) $Ph_2POCH_2CH_2Br$.

Preliminary reactions of (a) and (b) with Mo_6Cl_{12} in tetrahydrofuran and ethanol solutions resulted in immediate formation of a precipitate. Subsequent ^{31}P NMR spectra indicated that the ligand was bound to the metal cluster through both the phosphine and the pyridine nitrogen. After 14 days, no change was observed in the ratio of P-bound to N-bound ligands, and the method was discarded[11]. The reaction of $Ph_2POCH_2CH_2Br$ with

Mo_6Cl_{12} is very promising in that the phosphine can only bond through the phosphorous. The pyridine with various substituents can be added to form

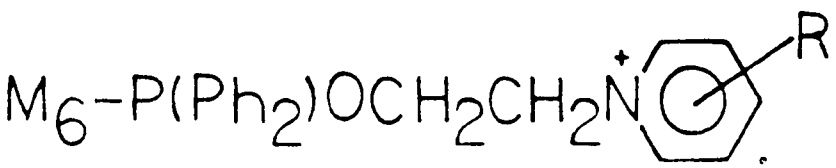

Work on this reaction sequence is continuing.

REFERENCES AND NOTES

1. Maverick, A.W.; Gray, H.B. *J. Am. Chem. Soc.*, **1981**, *103*, 1298.
2. Zietlow, T.C.; Hopkins, M.D.; Gray, H.B. *J. Solid State Chem.*, in press.
3. Vaughn, P.A. *Proc. Nat. Acad. Sci.*, **1950**, *36*, 461.
4. Hamer, A.D.; Smith, T.J.; Walton, R.A. *Inorg. Chem.*, **1976**, *15*, 1014.
5. Maverick, A.W. Ph.D. Dissertation, California Institute of Technology. 1982.
6. Rice, S.F. Ph.D. Dissertation, California Institute of Technology. 1982.
7. Maverick, A.W.; Nadjdzionek, J.S.; MacKenzie, D.; Nocera, D.G.; Gray, H.B. *J. Am. Chem. Soc.*, **1983**, *105*, 1878.
8. Using the relations

$$\frac{\phi_{em} = k_r}{(k_r + k_{nr})}$$

and

$$\frac{1}{\tau = k_r + k_{nr}}$$

it is clear that if the emission lifetime and quantum yield both increase to the same extent as the temperature is lowered, then k_r is constant and k_{nr} is a function of the temperature.

9. Winkler, J.R.; Nocera, D.G.; Yocum, K.M.; Bordignon, E.; Gray, H.B. *J. Am. Chem. Soc.*, **1982**, *104*, 5798.
10. a.) Nocera, D.G.; Gray, H.B. *J. Am. Chem. Soc.*, **1981**, *103*, 7349. b.) Marshall, J.L.; Stobart, S.R.; Gray, H.B. *J. Am. Chem. Soc.*, **1984**, *106*, 3027.
11. Dubois, D., personal communication.

CHAPTER 7

Isolation and Characterization of Pentanuclear Molybdenum Halide Clusters

Isolation and Characterization of Pentanuclear Molybdenum Halide Clusters

Thomas C. Zietlow and Harry B. Gray*

Contribution No. from the Arthur Amos Noyes Laboratory of Chemical Physics, California Institute of Technology, Pasadena, California, 91125.

Abstract. The cyclic voltammogram of $[(n\text{-}C_4H_9)_4N]_2Mo_5Cl_{13}$ shows two quasi-nernstian redox couples: $E_{\frac{1}{2}}(ox)$ = 0.49 V, and $E_{\frac{1}{2}}(red)$ = -0.36 V *vs.* Ag/AgCl in methylene chloride solution. Both the electrochemically stable $Mo_5Cl_{13}^-$ and $Mo_5Cl_{13}^{3-}$ clusters have been isolated as their tetrabutylammonium salts. The synthesis of $[(n\text{-}C_4H_9)_4N]_2Mo_5Br_{13}$ is described along with its cyclic voltammogram, which also shows two quasi-nernstian waves at $E_{\frac{1}{2}}(ox)$ = 0.41 V and $E_{\frac{1}{2}}(red)$ = -0.33 V [$(n\text{-}C_4H_9)_4NMo_5Br_{13}$ and $((n\text{-}C_4H_9)_4N)_3Mo_5Br_{13}$ have been isolated]. The $[(n\text{-}C_4H_9)_4N]_3Mo_5X_{13}$ complexes are paramagnetic, and their temperature-dependent magnetic behavior is interpreted in terms of two thermally populated sublevels of a $^3A_2(e^2)$ ground state. Sublevel splittings of < 4 cm^{-1} in $Mo_5Cl_{13}^{3-}$ and 15(5) cm^{-1} in $Mo_5Br_{13}^{3-}$ are estimated from EPR data. The relevance of these results to the photophysical behavior of the $Mo_6X_{14}^{2-}$ parent clusters is discussed.

Our interest in the electronic structures of molybdenum(II) and tungsten(II) halide clusters began with the discovery of intense luminescence from $Mo_6Cl_{14}^{2-}$. The extremely long luminescent lifetime (180 μsec in acetonitrile solution at room temperature)[1] and rich excited state electron transfer chemistry of this and analogous $Mo_6Br_{14}^{2-}$ and $W_6Cl_{14}^{2-}$ clusters[2] have led us to investigate the chemical and photochemical properties of the pentanuclear clusters of the $Mo_5Cl_{13}^{2-}$ type. Structurally, $Mo_5Cl_{13}^{2-}$ is a square pyramid of molybdenum atoms with four triply bridging chlorides on the faces of the pyramid, four chlorides bridging the basal molybdenum atoms and five axial chlorides[3] (essentially the $Mo_6Cl_{14}^{2-}$ structure with one metal atom and its axial chloride removed). The open coordination site in these pentanuclear clusters could potentially facilitate ground and excited state multielectron transfer reactions.

Here we report the results of our studies of the spectroscopic, electrochemical, and magnetic properties of (n-Bu_4N)Mo_5X_{13}, (n-Bu_4N)$_2Mo_5X_{13}$, and (n-Bu_4N)$_3Mo_5X_{13}$ (X = Cl, Br) complexes. These measurements have allowed us to evaluate various electronic structural models[4,5] for these and related clusters.

EXPERIMENTAL SECTION

Materials. The methylene chloride (Burdick and Jackson reagent grade) used in reactions and physical characterizations was dried over CaH_2. and vacuum distilled onto 3Å molecular sieves. All other materials were of reagent grade and used without further purification.

Cluster compounds :

$-(n-Bu_4N)_2Mo_5Cl_{13}$ was prepared by the literature method[3] and recrystallized from methylene chloride/petroleum ether.

$-(n-Bu_4N)_3Mo_5Cl_{13}$ was prepared by chemical reduction of (n-$Bu_4N)_2$ Mo_5Cl_{13} by stirring over zinc metal in dry, deoxygenated methylene chloride solution. A sample reaction: (n-$Bu_4N)_2Mo_5Cl_{13}$ (100 mg) was dissolved in 30 mL of deoxygenated methylene chloride and stirred with a slight excess of n-Bu_4NCl and zinc for 24 hours. The solution was filtered and petroleum ether distilled on top of the methylene chloride to crystallize the product. Recovery of the red crystals is about 80% . The solution is air-sensitive but the crystals only slowly (days) decompose in air. Anal. for $C_{48}H_{108}N_3$ Mo_5Cl_{13}: Calcd. C, 34.56; H, 6.53; N, 2.52. Found.C, 34.57; H. 6.63; N, 2.53.

$-(n-Bu_4N)Mo_5Cl_{13}$ was synthesized by chemical oxidation of (n-$Bu_4N)_2Mo_5Cl_{13}$ (100 mg) with chlorine in methylene chloride solution. The

chlorine was removed from the reaction mixture by purging with argon and the blue solution was layered with petroleum ether to crystallize the product. Recovery of purple-blue crystals was 95% . Anal. for C_{16} $H_{36}NMo_5Cl_{13}$: Calcd. C, 16.24; H, 3.07; N, 1.18. Found. C, 17.49; H, 3.43; N, 1.23.

$-(n-Bu_4N)_2Mo_5Br_{13}$ was synthesized in an analogous manner to the chloride preparation. Aluminum bromide (6.2 g). potassium bromide (1.6 g), bismuth trichloride (1.1 g), bismuth (0.5 g), and potassium hexachloromolybdate(III) (0.5 g) were placed in a quartz tube that was evacuated and sealed off under vacuum. After 3 hours of slow heating to 300°C [CAUTION! Explosion Danger!] and 1 hour at 300°C, the tube was allowed to cool to room temperature, broken, and the contents extracted with 6 N HBr and filtered. The filtrate was treated with n-Bu_4NBr, causing a dull green precipitate to form. This was collected by vacuum filtration and dissolved in methylene chloride; this solution was dried over anhydrous $MgSO_4$, and crystallized with petroleum ether. The yield of crystalline material was 120 mg. Anal. for $C_{32}H_{72}N_2Mo_5Br_{13}$: Calcd. C, 19.16; H, 3.59; N, 1.40. Mo, 23.95; Br, 51.90. Found. C, 19.39; H, 3.67; N, 1.49; Mo, 23.75; Br, 51.99.

$-(n-Bu_4N)_3Mo_5Br_{13}$ was synthesized by reduction of (n-$Bu_4N)_2Mo_5Br_{13}$ in a completely analogous manner to that of the chloride. Both the light green solution and the crystals are air-sensitive. Anal. for $C_{48}H_{108}N_3Mo_5Br_{13}$: Calcd. C, 25.67; H, 4.66; N, 1.87. Found. C, 25.19; H, 4.66; N, 1.90.

$-(n-Bu_4N)Mo_5Br_{13}$ was also made in the same manner as the chlo-

ride, using bromine as the oxidant of the $(n\text{-}Bu_4N)_2Mo_5Br_{13}$. Crystallization of the methylene chloride solution with petroleum ether resulted in emerald green crystals.

Analytical Procedures: Carbon, hydrogen, nitrogen, molybdenum, and bromide were determined by Galbraith Microanalytical Labs, Inc.

Physical Measurements: Room temperature magnetic susceptibility measurements were made on a Faraday balance with $HgCo(SCN)_4$ as calibrant. Variable temperature susceptibility measurements were made at the University of Southern California on a SQUID-based (S.H.E. Corporation) Model 805 variable temperature susceptometer with a 2 K option. Electronic spectra were recorded on a Cary 17 spectrometer. EPR spectra were measured on a Varian E-Line Century Series spectrometer equipped with an Air-Products Heli-Tran cooling system. Cyclic voltammetry was performed on a PAR Model 174A polarographic analyzer with a Houston Instruments 2000 X-Y recorder. Controlled potential electrolyses were performed with a Model 179 PAR potentiostat.

RESULTS AND DISCUSSION

Electrochemistry. Cyclic voltammetry done on methylene chloride solutions of $(n\text{-}Bu_4N)_2Mo_5Cl_{13}$ and $(n\text{-}Bu_4N)_2Mo_5Br_{13}$ revealed one wave cor-

responding to an oxidation and one wave corresponding to a reduction for each complex (Figure 1). The oxidation couple in the $Mo_5Cl_{13}^{2-}$ system has an $E_{1/2}$ = 0.49 V.[6] The reduction couple occurs at $E_{1/2}$ = -0.36 V. The analogous couples in the $Mo_5Br_{13}^{2-}$ system occur at $E_{1/2}$ = 0.41 V and $E_{1/2}$ = -0.33 V (oxidation and reduction, respectively). All waves displayed quasi-nernstian behavior with a plot of i_p vs. $\nu^{1/2}$ linear over the scan rate range 20-500 mV s^{-1}, which indicates that the electron transfer at the electrode is not rate-limiting at these scan rates. The peak separation for the same range of scan rates was 70 ± 5 mV for both systems, increasing slightly with higher scan rate; the discrepancy from the 59 mV predicted for one electron transfer is probably due to uncompensated solution resistance. The cathodic to anodic peak current ratios (reduction) and anodic to cathodic peak current ratios (oxidation) were 1.10 ± 0.10, again indicating quasi-nernstian behavior.

Comparison of the cyclic voltammograms of the two systems shows that the bromide is more easily oxidized than the chloride, which is in accordance with our results for the Mo_6 system.[2] Somewhat surprisingly, the bromide is also more easily reduced than the chloride in the pentanuclear clusters, although by only 30 mV. In the Mo_6 systems we have observed reversible reductive electrochemistry in only the $Mo_6Cl_{14}^{2-}$ system.[7]

Bulk electrolysis of $Mo_5Cl_{13}^{2-}$ in methylene chloride solution at a potential anodic to the oxidation couple resulted in a purple-blue solution with a CV identical to that of the starting material. The product was not iso-

Figure 1. Cyclic voltammogram of (top) $(n\text{-}Bu_4N)_2Mo_5Cl_{13}$ and (bottom) $(n\text{-}Bu_4N)_2Mo_5Br_{13}$ in methylene chloride solution with 0.2 M $(n\text{-}Bu_4N)PF_6$ as supporting electrolyte. Potentials are *vs.* a Ag/AgCl reference electrode

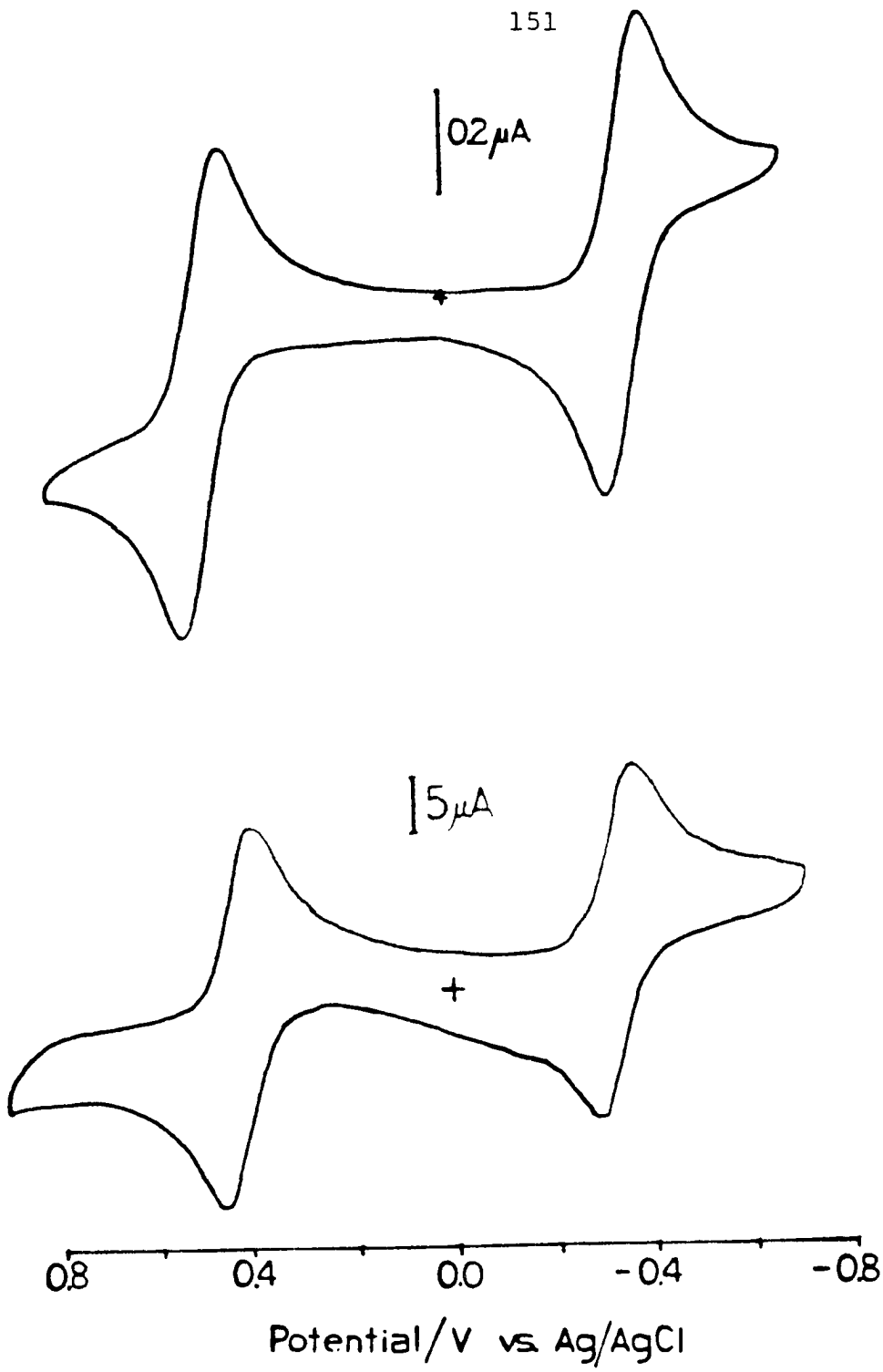
0.2μA
5μA
0.8
0.4
0.0
-0.4
-0.8
Potential/V vs. Ag/AgCl

lated since chemical oxidation resulted in the same material (identified by its optical absorption spectrum). Electrolysis at a potential cathodic to the reduction wave resulted in clean conversion to $Mo_5Cl_{13}^{3-}$ (identical CV). Again, chemical means proved more convenient to work up the product. The electrochemical behavior of the $Mo_5Br_{13}^{2-}$ cluster is similar to that of the chloride (Table 1).

Electronic Spectra. Electronic spectral data for the cluster compounds are set out in Table 2. The spectra of the $Mo_5X_{13}^{2-}$ and $Mo_5X_{13}^{-}$ clusters are clearly analogous. The small apparent difference in the spectra of the $Mo_5Cl_{13}^{2-}$ cluster upon one-electron oxidation may imply that the low energy electronic transitions terminate in a partially filled (one-electron) degenerate orbital; the same excitations into this degenerate orbital in the $Mo_5X_{13}^{-}$ cluster should be at slightly lower energy because of reduced electron-electron repulsion. If this orbital were nondegenerate, the spin pairing energy for these excitations in $Mo_5Cl_{13}^{2-}$ would be expected to lead to a much larger difference in the band positions upon oxidation. Alternatively, the excitations may be viewed as charge transfer from the apical molybdenum atom (Mo(II)) to a delocalized orbital on the partially oxidized (Mo($II\frac{1}{4}$)) basal molybdenum atoms. In this way we could rationalize the red shift in the visible bands upon cluster oxidation (2- to 1-), because of the more favorable charge transfer to the four basal Mo($II\frac{1}{2}$) atoms.

Upon exchanging bromide for chloride in both $Mo_5X_{13}^{2-}$ and

Table 1.

Electrochemical Data

Cluster ion	$E_{\frac{1}{2}}(ox)$	$E_{\frac{1}{2}}(red)$
$Mo_5Cl_{13}^{2-}$	0.49 V	-0.36 V
$Mo_5Br_{13}^{2-}$	0.41 V	-0.33 V

All cyclic voltammograms done in a 0.2 M solution of $(n\text{-}Bu_4N)PF_6$ in methylene chloride. All potentials are versus Ag/AgCl reference electrode.

Table 2.

Electronic Spectral Data

Cluster ion	1.	2.	3.	4.	5.
$Mo_5Cl_{13}^{3-}$	796[150]	580s[300]	482[1000]	350[3700]	312[5600]
$Mo_5Cl_{13}^{2-}$	723[960]	543[1300]	458[2400]	272s[13000]	
$Mo_5Cl_{13}^{-}$	742[2040]	557[1830]	489[2360]		
$Mo_5Br_{13}^{3-}$	753s	588s	473		
$Mo_5Br_{13}^{2-}$	730[370]	570[890]	473[1800]		
$Mo_5Br_{13}^{-}$	768[1660]	612[1390]	520[1510]		

All complexes are the n-Bu_4N salt in methylene chloride solution at 300 K. Spectra recorded from 1200-250 nm. Reported in nm[ϵ ($M^{-1}s^{-1}$)].

$Mo_5X_{13}^-$, the visible absorption bands red shift only a small amount, indicating that there is very little halide character in the electronic transitions. Therefore, it appears that the HOMO and the lowest-lying empty orbitals are primarily metal localized, a conclusion that accords well with an EHMO calculation that gives the HOMO 96% metal character.[5]

EPR Spectra. The X-band (9.265 GHz) EPR spectrum of $Mo_5Cl_{13}^{2-}$ in a frozen methylene chloride solution (77 K) is displayed in Figure 2. The spectrum can be accounted for by an axially symmetric doublet ground state ($g_\perp$ = 1.96 and $g_\parallel$ = 2.00). No hyperfine splitting was observed. The pentanuclear cluster anion may be thought of as an extreme case of a tetragonally distorted octahedron, which is consistent with $g_\perp < g_\parallel$ in the EPR spectrum.[8]

The EPR spectrum of (n-$Bu_4N)_2Mo_5Br_{13}$ in frozen methylene chloride solution (70 K) is shown in Figure 3. The spectrum is isotropic with g = 2.01. The other absorption expected by analogy to the $Mo_5Cl_{13}^{2-}$ spectrum might be washed out due to spin-orbit coupling effects. Again, no hyperfine splitting was observed.

The EPR spectrum of $Mo_5Cl_{13}^{3-}$ (in frozen methylene chloride solution) shows a well defined anisotropic signal with an absorption at g = 1.95 and one at g = 2.0 at 70 K (Figure 4). Hyperfine splitting of about 30 gauss was observed in the spectrum. Upon cooling the sample down to liquid helium temperature, the signal loses the clear anisotropy of the 70 K

Figure 2. X-band (9.265 GHz) EPR spectrum of $(n\text{-}Bu_4N)_2Mo_5Cl_{13}$ in frozen (77 K) methylene chloride.

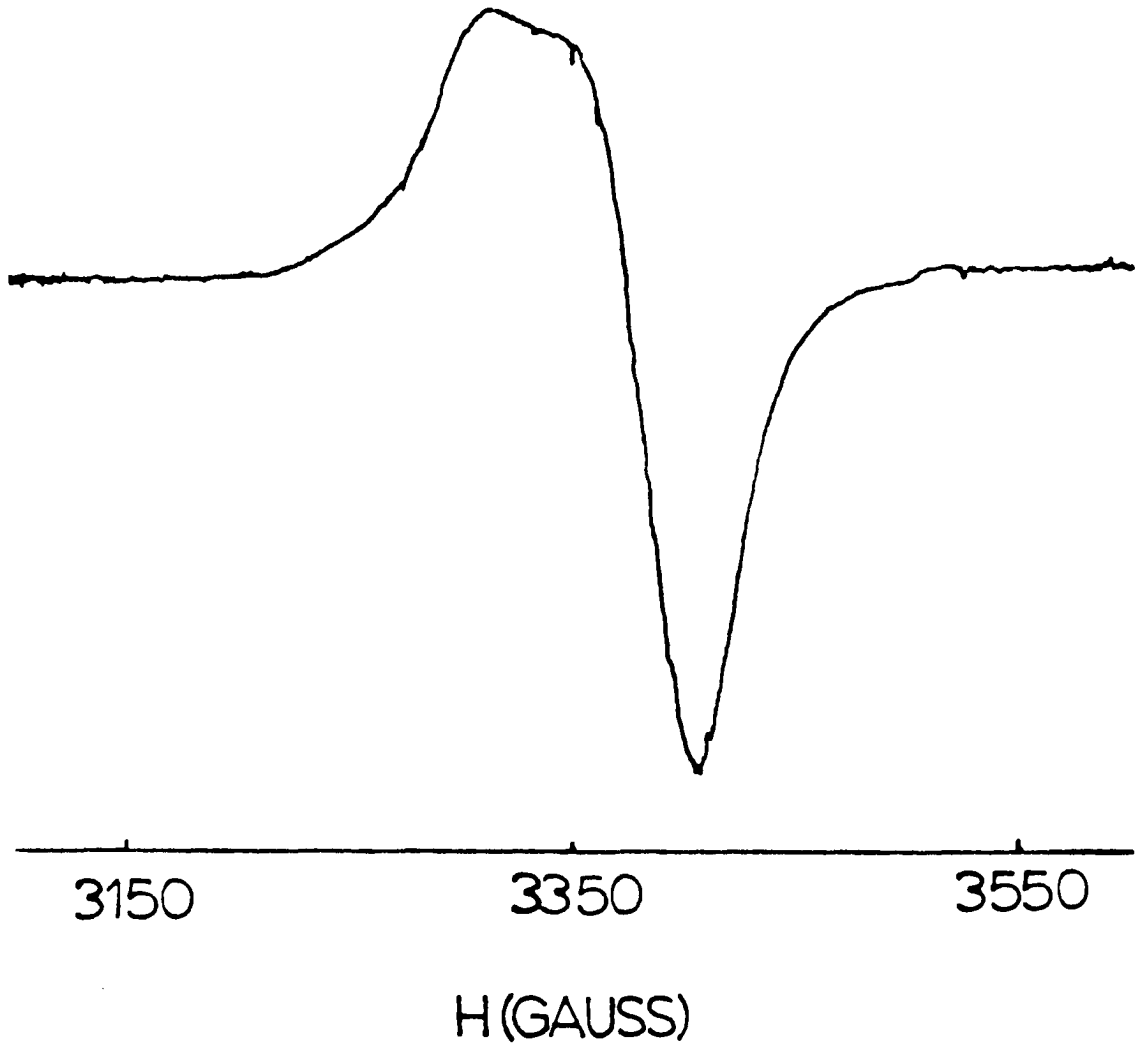
3150
3350
3550
H (GAUSS)

Figure 3. X-band (9.196 GHz) EPR spectrum of $(n\text{-}Bu_4N)_2Mo_5Br_{13}$ in frozen (70 K) methylene chloride.

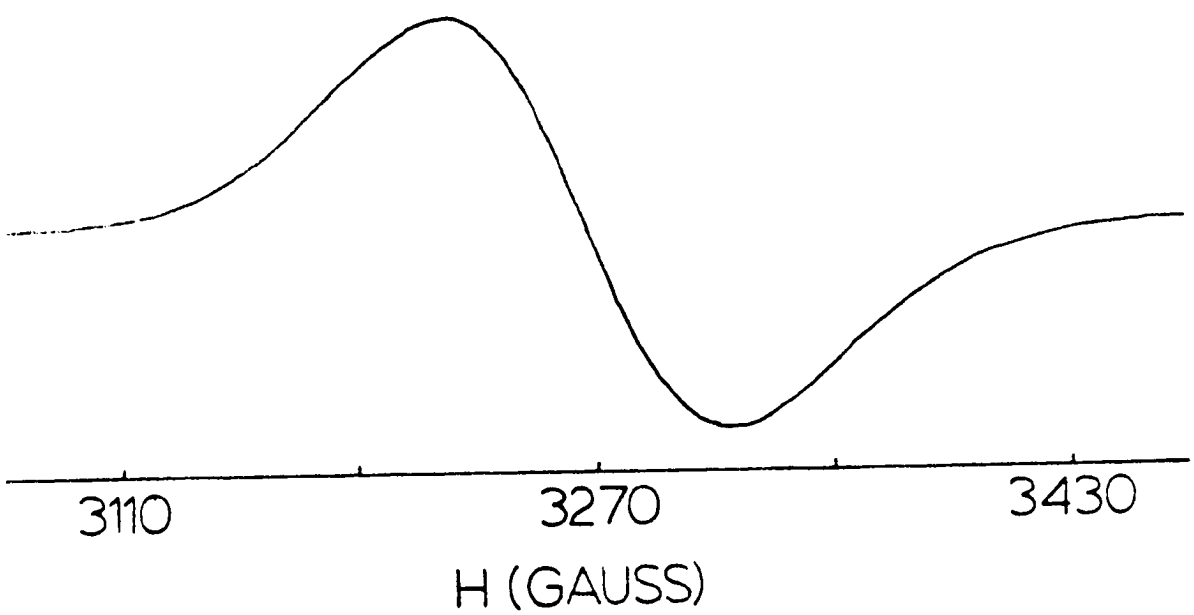
3110
3270
3430
H (GAUSS)

Figure 4. Variable temperature X-band (9.198 GHz) EPR spectra of (n-$Bu_4N)_3Mo_5Cl_{13}$ in frozen methylene chloride.

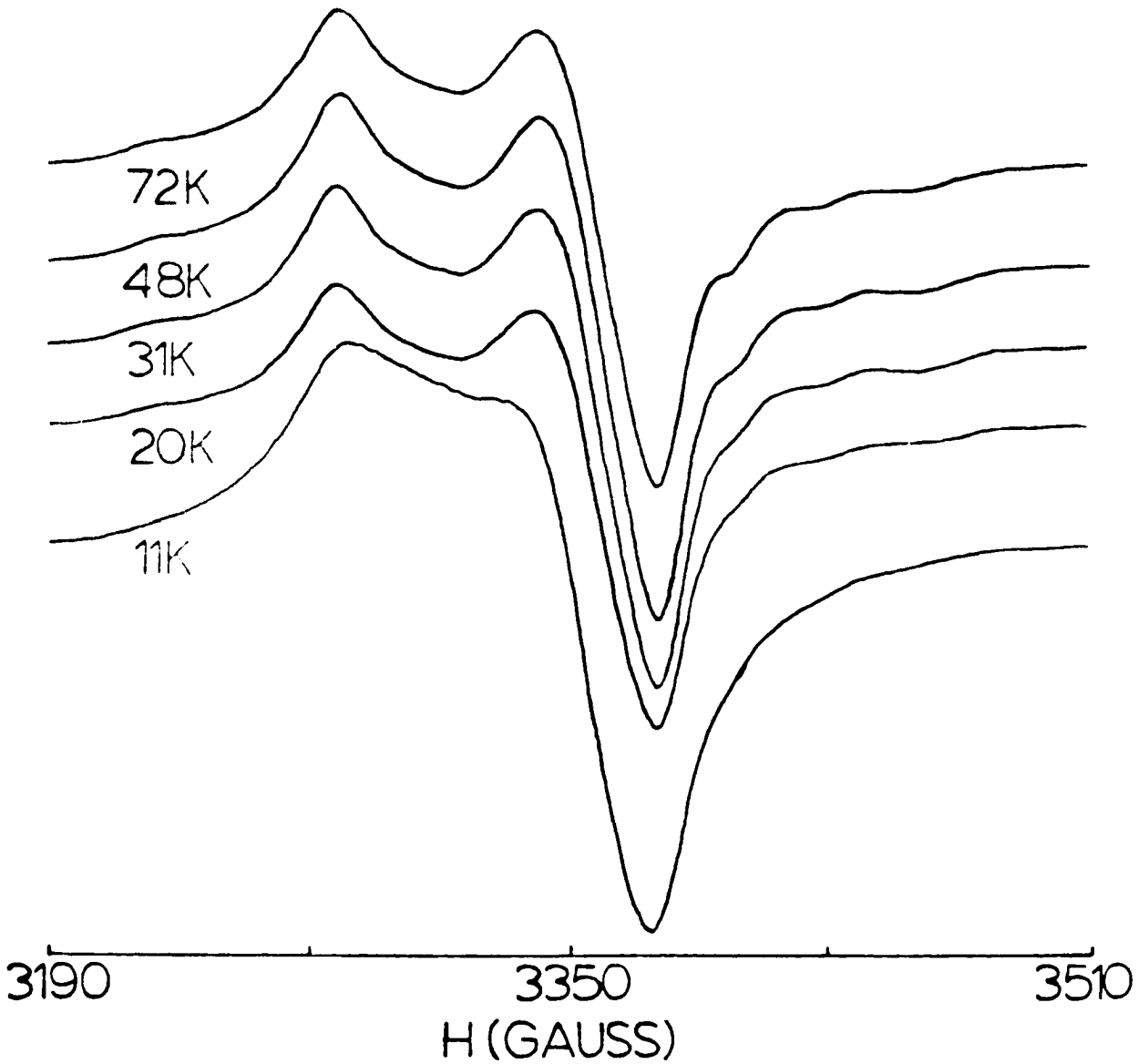
72K
48K
31K
20K
11K
3190
3350
3510
H (GAUSS)

spectrum, but does not quite become isotropic by 9 K. The hyperfine signals are lost, and no signal was observed at half-field at any of the temperatures studied. Comparing the spectra at high (70 K) and low (9 K) temperatures, the absorption at g = 1.95 diminishes as the temperature is lowered, but the signal does not quite disappear by 9 K.

The EPR spectrum of $Mo_5Br_{13}^{3-}$ displays much the same general features. The signal at 70 K shows two distinct absorptions (g = 1.97 and g = 2.01) (Figure 5). The hyperfine splitting that is resolved in the chloride is not observed in the bromide spectrum. Upon cooling, the spectrum becomes almost isotropic at 9 K. A signal at g = 4.3 can be detected at 9 K, but diminishes as the temperature as the temperature is raised to 25 K. The appearance of the spectrum at 9 K is almost that of a simple triplet state[9] with the allowed ($\Delta M_s = 1$) transition occurring at g = 2, and the forbidden ($\Delta M_s = 2$) transition at about half-field (g = 4.3).

The EPR spectra of the $Mo_5X_{13}^{3-}$ clusters may be interpreted in terms of two thermally equilibrated paramagnetic electronic states. From a simple intensity versus temperature calculation, we calculate the splitting of the two states to be <4 cm^{-1} and 15(5) cm^{-1} for X = Cl and X = Br, respectively. The loss of hyperfine coupling in the $Mo_5Cl_{13}^{3-}$ EPR spectrum (which is attributable to the Mo, with an isotope of I = 5/2) as the sample is cooled may imply that the higher energy state has significant unpaired electron density near Mo nuclei.

Figure 5. Variable temperature X-band (9.195 GHz) EPR spectra of $(n\text{-}Bu_4N)_3Mo_5Br_{13}$ in frozen methylene chloride solution.

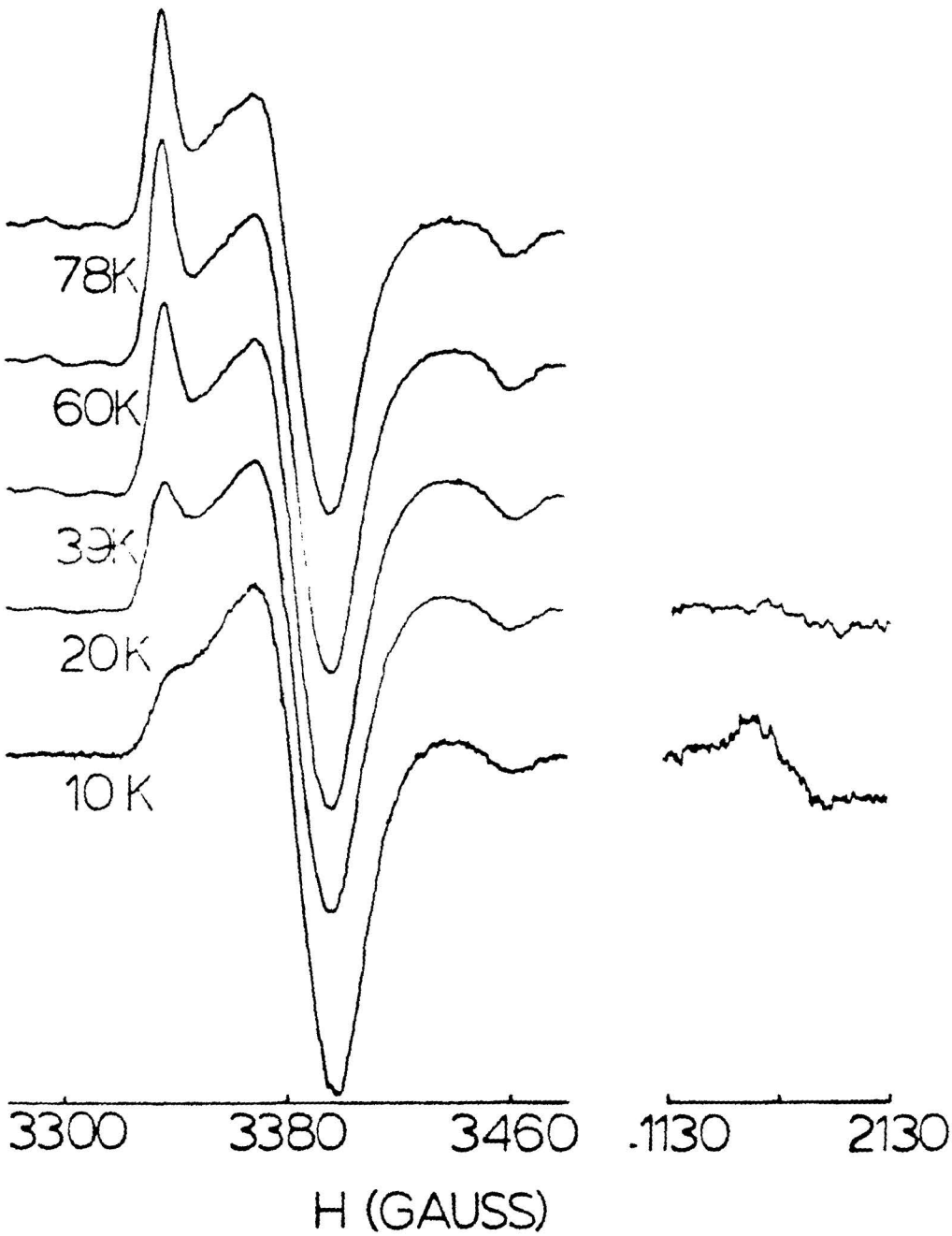
78K
60K
39K
20K
10 K
3300
3380
3460
.1130
2130
H (GAUSS)

Magnetic Susceptibility. In agreement with Beers and McCarley,[10] we found that the room temperature effective magnetic moment of (n-$Bu_4N)_2Mo_5Cl_{13}$ is 1.7 B.M. The (n-$Bu_4N)_2Mo_5Br_{13}$ cluster has μ_{eff} = 1.6 B.M. Both of these values are consistent with a simple doublet ground state. The oxidized clusters, (n-$Bu_4N)Mo_5Cl_{13}$ and (n-$Bu_4N)Mo_5Br_{13}$, were found to be diamagnetic at room temperature, whereas (n-$Bu_4N)_3Mo_5Cl_{13}$ was found to be paramagnetic at room temperature (μ_{eff} = 0.56 B.M.).

The plots of molar susceptibility versus 1/T for the two $Mo_5X_{13}^{3-}$ clusters are shown in Figures 6 and 7. The $Mo_5Cl_{13}^{3-}$ cluster appears to follow Curie-Weiss behavior over the temperature range 5-300 K. with a very slight deviation at temperatures below 5 K. These results accord very well with our EPR results, which indicate a very small (< 4 cm^{-1}) splitting of the two thermally equilibrated states. Such a small splitting implies that the magnetic data should only show deviations from Curie-Weiss behavior at very low temperatures.[11] The magnetic data for the (n-$Bu_4N)_3Mo_5Br_{13}$ powder sample show a distinct transition from the low temperature Curie-Weiss behavior. Presumably, the deviation is due to the population of the higher energy state at higher temperature.[12]

The low magnetic moments of the even electron clusters are not unprecedented for high nuclearity metal systems. The broad EPR spectra with a g tensor near 2 and low effective magnetic moments are reminiscent of conduction band electrons in bulk metals. A similar study on osmium carbonyl clusters revealed similar behavior in Os_{10} molecules.[13] Interest-

Figure 6. Magnetic susceptibility of powdered $(n\text{-}Bu_4N)_3Mo_5Cl_{13}$ as a function of reciprocal temperature. Fit is to Curie-Weiss behavior with a Curie constant of 3.9×10^{-2} emu K mol^{-1}.

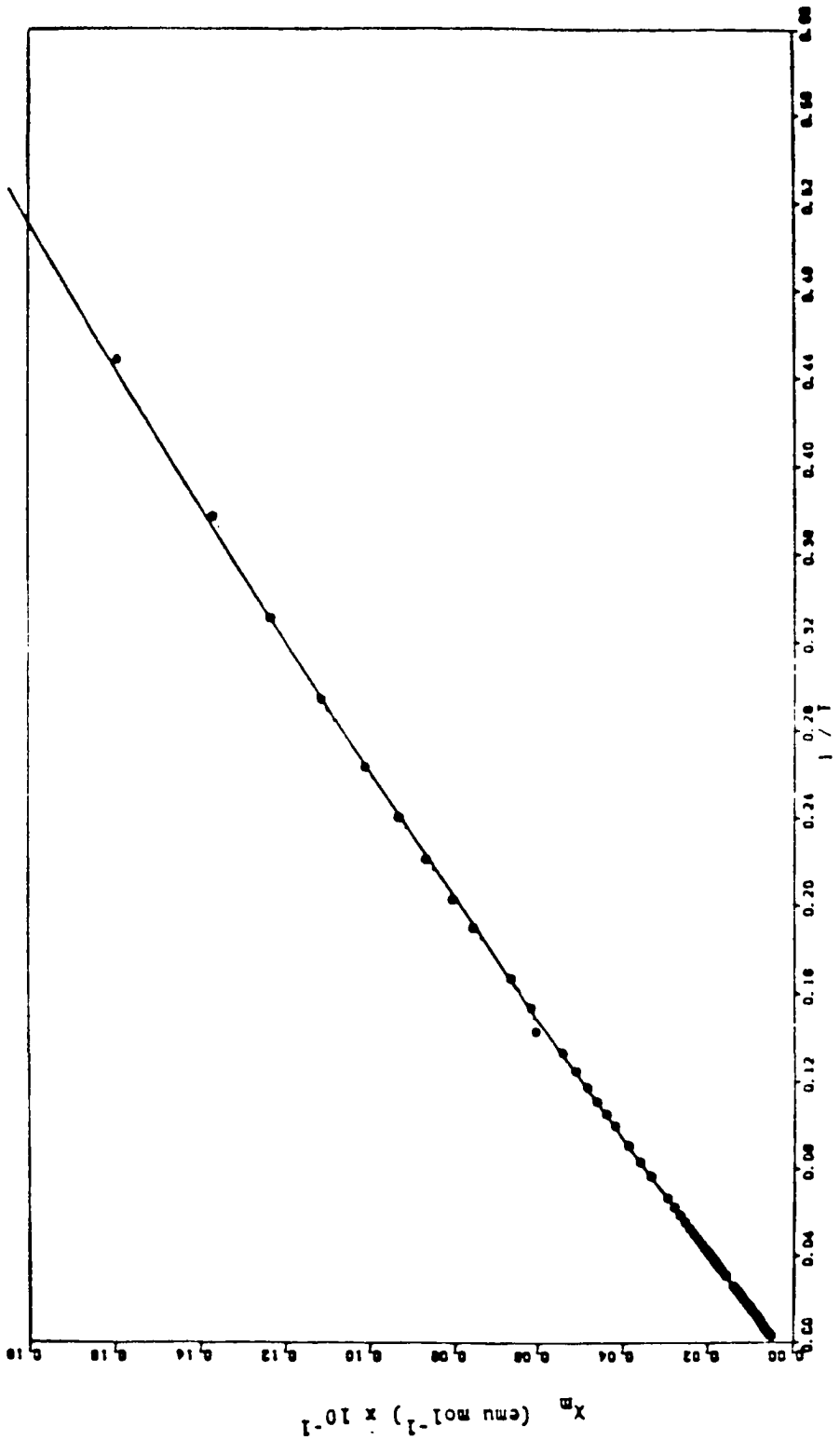
χ_m (emu mol^{-1}) x 10^{-1}
0.00
0.02
0.04
0.08
0.08
0.10
0.12
0.14
0.16
0.18
1 / T
0.00
0.04
0.08
0.12
0.16
0.20
0.24
0.28
0.32
0.36
0.40
0.44
0.48
0.52
0.56
0.60

Figure 7. Magnetic susceptibility of powdered $(n\text{-}Bu_4N)_3Mo_5Br_{13}$ as a function of reciprocal temperature.

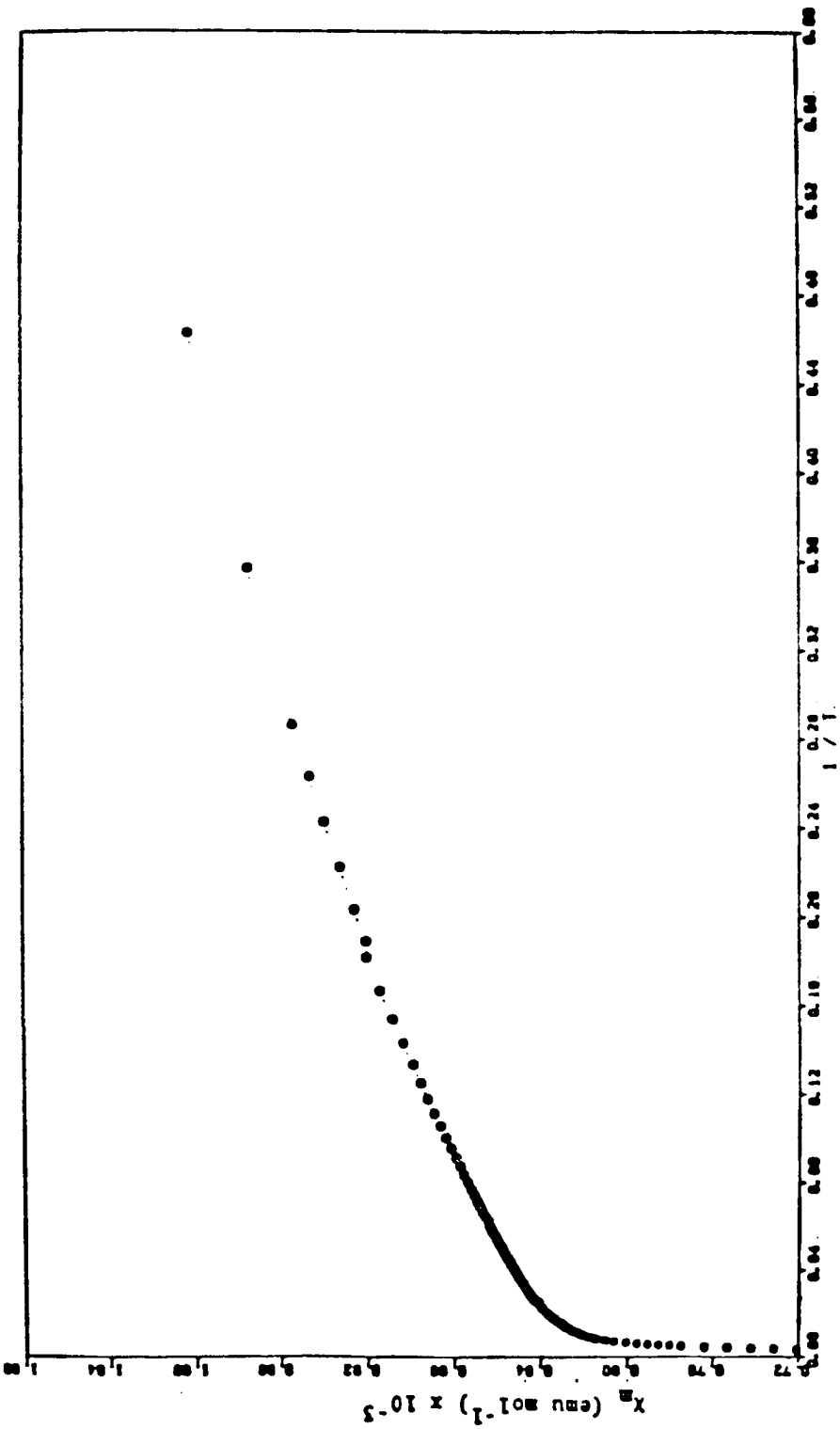
χ_m (emu mol^{-1}) x 10^{-3}
1 / T

ingly, the smaller cluster $Mo_5Cl_{13}^{3-}$ approaches bulk properties, whereas $Os_6(CO)_{18}$ appears to be "molecular." This is probably a manifestation of the stronger metal-metal interactions in these halide clusters as opposed to the importance of ligand orbitals in the carbonyl cluster bonding.

Electronic Structure. Our efforts to understand the electronic structures of the $M_6Cl_{14}^{2-}$ (M = Mo, W; X = Cl, Br, I) clusters have been aided by the EHMO calculation of Hughbanks and Hoffmann.[5] Consistent with our results, the MO diagram predicts that the lowest electronic excitation is largely metal-centered.[2] The model also predicts a tetragonal distortion upon oxidation of the metal core in M_6 clusters. The crystal structure of the $W_6Br_{14}^{-}$ anion has been recently solved, but there appears to be no preferred axis for this distortion in the crystal, so average bond lengths were all that were determined.[14]

The EHMO calculation of Meissner and Korol'kov predicts a $^3A_{2u}(e^2)$ ground state for $Mo_5Cl_{13}^{3-}$ clusters.[4] Our results indicate that the $Mo_5X_{13}^{3-}$ ground state is paramagnetic, and at least for $Mo_5Br_{13}^{3-}$ the EPR spectrum is characteristic of a triplet state at low (10 K) temperatures.[15] At higher temperatures, the two lowest electronic states in each cluster trianion are in thermal equilibrium. Splittings in the triplet states of these types of clusters may have implications in the photophysics of the hexanuclear clusters, whose lowest electronic excited state has been shown to be a triplet spin state.[16]

The picture of the electronic ground state of $Mo_5X_{13}^{n-}$ (n = 1, 2, 3) that emerges from these physical studies is well described by the EHMO

model of Meissner and Korol'kov.[4] The calculation also predicts that the partially filled e orbital in a 2- cluster is antibonding with respect to the metal cluster framework. Attempts are being made to grow crystals suitable for x-ray crystallographic analyses of the mono- and trianions of the $Mo_5Cl_{13}^{n-}$ system to test this aspect of the MO picture.

Acknowledgements. We thank Les Butler for use of his Curie-Weiss fit program and Craig Martin for his assistance in the EPR experiments. This research was supported by National Science Foundation Grant CHE81-20419.

REFERENCES AND NOTES

1. Maverick, A.W.; Gray, H.B. *J. Am. Chem. Soc.* **1981**, *103*, 1298.
2. Maverick, A.W.; Najdzionek, J.S.; MacKenzie, D.; Nocera, D.G.; Gray, H.B. *J. Am. Chem. Soc.* **1983**, *105*, 1878.
3. Jödden, K.; Schnering, H.G.v.; Schäfer, H. *Angew. Chem., inter. ed.*, **1975**, *14*, 570. Jödden, K.; Schäfer, H. *Z. Anorg. Allg. Chem.*, **1977**, *430*, 5.
4. Meissner, H.; Korol'kov, D.V. *Z. Anorg. Allg. Chem.*, **1983**, *496*, 175.
5. Hughbanks, T.; Hoffmann, R., personal communication.
6. All potentials are versus Ag/AgCl reference electrode with 0.2 M tetrabutylammonium hexafluorophosphate in methylene chloride as electrolyte.
7. Nocera, D.G.; Gray, H.B. *J. Am. Chem. Soc.*, **1984**, *106*, 824. We do see cathodic current for the reduction of $Mo_6Br_{14}^{2-}$ in acetonitrile, but the process appears to be irreversible at scan rates up to 500 mV/s.
8. Ballhausen, C.J. *Introduction to Ligand Field Theory*. McGraw-Hill: New York, 1962, 134.
9. Wertz, J.E.; Bolton, J.R. *Electron Spin Resonance, Elementary Theory and Practical Applications*, McGraw-Hill: New York, 1972, 238.
10. Beers, W.W.; McCarley, R.E. "Abstracts of Papers," *184th American Chemical Society National Meeting*, Kansas City, Missouri, **1982**, INOR 199.
11. Where kT is much greater than the splitting, an average magnetic sus-

ceptibility should follow Curie behavior.

12. Deviation from Curie behavior would be expected to occur only if the two equilibrated states have different magnetic moments associated with them.
13. Benfield, R.E.; Edwards, P.P.; Stacy, A.M. *J. Chem. Soc., Chem. Commun.*, **1982**, 525.
14. Zietlow, T.C.; Sadeghi. B.: Schaefer, W.P.; Gray. H.B., submitted for publication.
15. McCarley and co-workers have determined the crystal structure of $(PhEt_3N)_2Mo_5Cl_{13}$ (McCarley, R.E., personal communication). They find that the cluster is distorted rhombically from C_{4v} symmetry, which would split the e orbital. This splitting would not change our interpretation of the physical measurements made on the 2- cluster. Upon reduction to the 3- cluster, two things can occur: (1) the complex can return to C_{4v} symmetry, thereby resulting in a triplet ground state; or, (2) the complex can distort to the extreme of allowing for spin pairing. Our results clearly show a paramagnetic ground state for $Mo_5Cl_{13}^{3-}$.
16. Zietlow, T.C.; Hopkins, M.D.; Gray, H.B. *J. Solid State Chem.*, in press.

CHAPTER 8

Electrochemistry of Quadruply Bonded Molybdenum Dimers. Evidence for Iodide Backbonding

Electrochemistry of Quadruply Bonded Molybdenum Dimers. Evidence for Iodide Backbonding

Thomas C. Zietlow, Michael D. Hopkins, and Harry B. Gray*

Contribution No. from the Arthur Amos Noyes Laboratory of Chemical Physics, California Institute of Technology, Pasadena, California, 91125.

Abstract. The cyclic voltammograms of a series of quadruply bonded $Mo_2X_4(PR_3)_4$ dimers have been measured. Variation in the trialkylphosphine in the $Mo_2Cl_4(PR_3)_4$ (R = -Me, -Et, -Pr, -Bu) showed trends consistent with the electron donating abilities of the alkylphosphines. Variation of the halide in the $Mo_2X_4(PMe_3)_4$ (X = Cl, Br, I) series displays the opposite ordering of the redox potentials from that expected based on the electron donation properties of the halides. Several literature reports are also shown to display this "inverse halide order." The ordering is described as arising from greater metal-ligand backbonding to the iodide ligands relative to the chloride ligand..

A great deal of effort in this laboratory has been invested in the understanding of the electronic structure of quadruply bonded metal dimers, with the goal of developing these molecules as photocatalysts[1]. The study of the photochemical and photophysical properties of these species has developed a clear picture of the bonding in the ground and emitting excited states[2]. The $Mo_2X_4(PR_3)_4$ series (X = Cl, Br, I; R = $-CH_3$, $-CH_2CH_3$, $-CH_2CH_2CH_3$, $-CH_2CH_2CH_2CH_3$) is a particularly interesting example of this class of molecules, in that the dimers are stable, redox-active and possess long-lived excited states[3] which can potentially be exploited in photochemical reactions. The ground state redox properties of a complete set of these dimers have been studied in order to assess such interesting areas as the importance of one-electron potentials in multi-electron chemistry, since these molecules can undergo one-photon, two-electron chemistry[4,5]. This work has confirmed and expanded on some previous work on the oxidation electrochemistry of quadruply bonded dimers[6] and developed the reductive electrochemistry[7] of the $Mo_2X_4(PR_3)_4$ dimer systems. These dimers are ideal systems to observe electrogenerated chemiluminescence reactions; this technique can be used to study the effect of driving force, excited state energy, and excited state distortion on redox reactions (Chapter 9).

The cyclic voltammograms of a series of quadruply bonded dimers in tetrahydrofuran solution have been measured. The dimers $Mo_2Cl_4(PR_3)_4$ (R = -Me, -Et, -Pr, -Bu) have been examined to study the effect of the alkyl phosphine on redox potentials in a systematic manner, and the dimers

$Mo_2X_4(PMe_3)_4$ (X = Cl, Br, I) had their cyclic voltammograms recorded to observe the halide dependence of the redox potentials (Figure 1). The half-wave potentials versus the saturated calomel electrode (SCE) are listed in Table 1. All of the redox couples are reversible in the scan rate range 20-500 mV s^{-1}.

As the phosphine alkyl group is changed from methyl to ethyl in the $Mo_2Cl_4(PR_3)_4$ dimer, the oxidation potential in THF solution becomes less positive, as would be expected from the greater electron-donating ability of the triethyl phosphine[8]. Also, the triethyl phosphine derivative is also more soluble in THF as is the one-electron oxidized product. This factor would also tend to make the oxidation potential less positive for $Mo_2Cl_4(PEt_3)_4$ than for $Mo_2Cl_4(PMe_3)_4$. Upon further lengthening of the alkyl group on the phosphine further, there is no substantial effect on the oxidation potential: both the electron donation and solvation effects are apparently too small to notice.

The reduction potentials become more negative as the alkyl chain on the phosphine ligand is lengthened. The potential is more negative by about 100 mV for each methylene unit added to the alkyl chain. The reduction potentials being increasingly negative in this series can be rationalized by the same electron-donation arguments, but then it is puzzling as to why the reduction potentials and not the oxidation potentials are affected in the variation of the alkyl group from ethyl to propyl to butyl.

Variation of the halide, while keeping the phosphine constant, results in

Figure 1. A cyclic voltammogram of $Mo_2I_4(PMe_3)_4$ taken in tetrahydrofuran solution with 0.1 M $TBAPF_6$ as electrolyte. Platinum wires were used as working and auxiliary electrodes. The cyclic voltammogram was recorded at 200 mV s^{-1}.

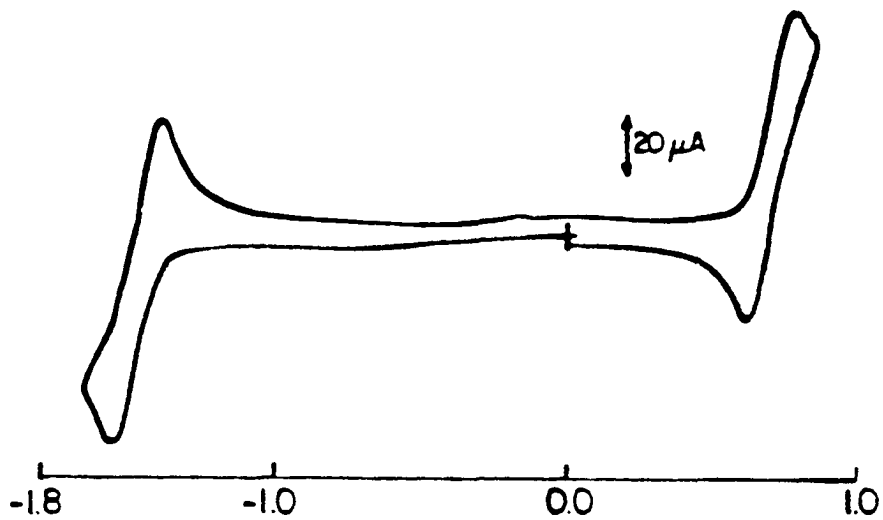
20 μA
-1.8
-1.0
0.0
1.0
Volts vs Ag/Ag+

Table 1.

Redox Potentials of $Mo_2X_4(PR_3)_4$ Dimers

Complex	$E_{\frac{1}{2}}$(ox)	$E_{\frac{1}{2}}$ (red)
$Mo_2Cl_4(PMe_3)_4$	+0.74 V	-1.70 V
$Mo_2Cl_4(PEt_3)_4$	+0.67 V	-1.81 V
$Mo_2Cl_4(PPr_3)_4$	+0.65 V	-1.89 V
$Mo_2Cl_4(PBu_3)_4$	+0.65 V	-2.00 V
$Mo_2Br_4(PMe_3)_4$	+0.87 V	-1.48 V
$Mo_2I_4(PMe_3)_4$	+0.88 V	-1.28 V

All potentials are half-wave potentials versus the saturated calomel electrode (SCE) in 0.1 M $TBAPF_6$ in tetrahydrofuran.

an unexpected ordering of the oxidation and reduction potentials. As can be seen from the data in Table 1, the dimer becomes more difficult to oxidize as X^- goes from chloride to bromide to iodide. The dimers are more easily reduced in the same order. This is the inverse order one would expect from simple electron donation arguments since Cl^- is more electron-withdrawing than Br^- and I^-.

The literature has a surprising number of examples of this "inverse halide order" for redox potentials of low valent metal complexes, but no one has provided a real explaination. Simple solvation differences do not seem to account for the order because the effect appears to be too large, and if the softer iodide ligands allow for the 1- anion to be solvated more easily, they should help in the solvation of the 1+ cation also, which is not what is experimentally observed.

A rather radical rationalization of the "inverse halide order" is to invoke the *d* orbitals on the halide and treat the halide as a π-accepting ligand. The metal center is quite electron rich, a Mo(II) with two strongly σ-donating alkyl phosphine ligands, and the *d*-*d* "π-backbonding" should increase with the larger halides. This type of approach fits in well with several aspects of the experimental data. First of all, the "inverse halide order" is due to the greater π-accepting ability of the halide, which is more important than the π-donation from the *p* filled orbitals of the halide ligand in this highly reduced system. Also, the reduction potential (a function of the δ^* orbital energy) is more sensitive to the halide ligand than the oxidation potential

(a function of the δ orbital energy) indicating the ligand orbitals interacting with the δ and δ^* are *higher* in energy than the metal-based orbitals. Based on this model also, the splitting of the δ and δ^* orbitals should be smaller as the halide becomes larger. This last, however, is expected also from p orbital π-donation arguments. Finally, Walton and co-workers have shown that exchange of the halide for a moderate π-accepting ligand (NCS^-) made the reduction potential of the system much less negative[6]. Apparently, π-backbonding interactions are very important in describing the redox properties of these systems.

In light of this model, earlier data on similar systems can be interpreted. Walton and co-workers showed that the $Re_2X_4(dppe)_2$ [dppe = diphenylphosphinoethane] and $Re_2X_4(arphos)_2$ (X = Cl, Br, I) [electronic configuration $\sigma^2\pi^4\delta^2\delta^{*2}$] can be oxidized in two one-electron steps[9]. For the first oxidation,

$$Re_2X_4(dppe)_2 \rightarrow Re_2X_4(dppe)_2^+ + e^-,$$

the potentials are more positive X = Cl< Br < I ("inverse halide order") while for the second oxidation,

$$Re_2X_4(dppe)_2^+ \rightarrow Re_2X_4(dppe)_2^{2+} + e^-.$$

the potentials are more positive X = I < Br < Cl (the "normal order"). For the highly reduced system [Re(II)] backbonding to the halides is important, hence the "inverse halide order." However, the less reduced $Re(II\frac{1}{2})$ system does not require halide backbonding and so the ordering is normal, based

on π-donation from filled halide p orbitals. If the third oxidation wave were observable, the difference in oxidation potential for the halides should increase as π-backbonding is strongly diminished and the more familiar π-donation becomes more important. The "inverse halide order" is not as pronounced in these data as in the $Mo_2X_4(PMe_3)_4$ data due to the greater ability of the dppe ligand to act as a π-acceptor relative to the PMe_3 ligand.[10]

Data taken by Walton and coworkers on another rhenium system, this one involving quadruply bonded dimers, display the inverse halide effect as a function of the π-accepting ability of the phosphine. These data involve the $Re_2X_6(PR_3)_2$ dimers, where the oxidation potentials for X = chloride and bromide for certain phosphines with both alkyl and aryl groups[11]. The data indicate that, as the phosphine becomes a better π-accepting ligand by increasing the number of aryl groups, the smaller the magnitude of the "inverse halide order" upon exchange of the chloride ligands for bromide. In the case of triethyl phosphine, where the π-accepting ability of the phosphine is expected to be very low, the difference in the reduction potentials of the chloride and bromide dimers is 120 mV.

Complex	$E_{\frac{1}{2}}(red)$
$Re_2Cl_6(PEt_3)_2$	$-0.10V$
$Re_2Br_6(PEt_3)_2$	$+0.02V$

When the phosphine ligand is the better π-accepting ligand $PEtPh_2$, the difference in the reduction potentials is only 50 mV. Thus the greater the

ability of the phosphine to π-backbond, the less the electron density at the metal center, relieving the need for the halide to backbond; thus the electrochemical results reflect less of the "inverse halide order."

This interpretation of the electrochemical data allows for some interesting predictions to be made about the structural features of the dimers dependent upon the halide. The x-ray crystal structures for the $Mo_2Cl_4(PMe_3)_4$ [12] and the $Mo_2Br_4(PMe_3)_4$ [13] dimers have been solved. There is no difference greater than the error of the structures in the metal-metal distances, nor in the metal-phosphorous or metal-halide (correcting for ionic radii differences) distances in these two structures. If the "inverse halide order" is due to this halide π backbonding as described above, then the structure of the iodide should show differences to the chloride and bromide. Since the metal-iodide bond should have some multiple bond character, it should be significantly shorter (again correcting for ionic radii) than the metal-chloride (bromide) bond.

The optical absorption spectra of these dimers offer little help in understanding this phenomenon since the energy of the singlet $\delta - \delta^*$ state is a complex function of the orbital splitting and a large spin pairing term.[14,15] The unique feature of the δ bond is the large two-electron correlation terms imposed due to the very weak overlap of the d_{xy} orbitals forming the δ bond[16]. An experiment which should show if these redox potentials are due to the halide backbonding described above, or whether some two-electron term in the δ framework is dominant, is the investigation of the analogous

tungsten dimers $W_2X_4(PMe_3)_4$ (X = Cl, Br, I). If the ordering of the redox potentials is due to the halide backbonding to the metal, the effect should be more pronounced in the tungsten series than it was in the molybdenum dimers due to both the greater W*d*-X*d* orbital overlap, and the more electropositive nature of tungsten (II) versus molybdenum (II). However, the two-electron terms in the $W_2Cl_4(PMe_3)_4$ dimers appear to be smaller than in the $Mo_2Cl_4(PMe_3)_4$ due to the greater $d_{xy} - d_{xy}$ overlap[15]; this implies that the halide effects on the ordering of the redox potentials would tend back toward the conventional ordering based on the better π-donating ability of iodide ligands. Vibrational spectra would be difficult to interpret due to the changing masses in the problem. One technique which would be useful in determining the depths of the potential wells is photoelectron spectroscopy, which can be used to determine if the iodide dimer δ orbital is really at lower energy than the δ orbital of the chloride dimer. Work in this area is continuing.

REFERENCES

1. Trogler, W.C.; Gray, H.B. *Acc. Chem. Res.*, **1978**, *11*, 232.
2. Hopkins, M.D.; Gray, H.B. *J. Am. Chem. Soc.*, **1984**, *106*, 2468.
3. Miskowski, V.M.; Goldbeck, R.A.; Kliger, D.S.; Gray. H.B. *Inorg. Chem.*, **1979**, *18*, 86.
4. Nocera, D.G.; Gray. H.B. *Inorg. Chem.*, **1984**, *23*, 3686.
5. Hopkins, M.D.; Gray, H.B., manuscript in preparation.
6. Zietlow, T.C.; Klendworth, D.D.; Nimry, T.; Salmon, D.J.; Walton. R.A. *Inorg. Chem.*, **1981**, *20*, 947.
7. Schrock, R.R.; Sturgeoff, L.G.; Sharp. P.R. *Inorg. Chem.*, **1983**, *22*, 2801.
8. Tolman. C.A. *Chem. Rev.*, **1977**, *77*, 313.
9. Brant, P.; Glicksman, H.D.; Salmon, D.J.; Walton, R.A. *Inorg. Chem.*, **1978**, *17*, 3203.
10. Cotton, F.A.; Wilkinson, G. *Advanced Inorganic Chemistry, 4th ed.*, Wiley:New York, 1980, 88.
11. Brant, P.; Salmon. D.J.; Walton, R.A. *J. Am. Chem. Soc.*, **1978**, *100*, 4424.
12. Cotton, F.A.; Extine, M.W.; Felthouse, T.R.; Kolthammer, B.W.S.; Lay, D.G. *J. Am. Chem. Soc.*, **1981**, *103*, 4040.
13. Hopkins, M.D.; Schaefer, W.P.; Gray, H.B., manuscript in preparation.
14. Hopkins, M.D.; Zietlow, T.C.; Miskowski, V.M.; Gray, H.B. *J. Am. Chem. Soc.*, **1985**, *107*, 510.

15. Miskowski, V.M.; Hopkins, M.D.; Gray, H.B., submitted for publication.

16. Zietlow, T.C.; Hopkins, M.D.; Gray, H.B. *J. Solid State Chem.*, in press.

CHAPTER 9

Electrochemistry and Electrogenerated Chemiluminescence of Quadruply Bonded Molybdenum Dimers

Electrochemistry and Electrogenerated Chemiluminescence of Quadruply Bonded Molybdenum Dimers

Thomas C. Zietlow, Michael D. Hopkins and Harry B. Gray*

Contribution No. from the Arthur Amos Noyes Laboratory of Chemical Physics, California Institute of Technology, Pasadena, California. 91125.

Abstract. The cyclic voltammograms of the quadruply bonded complexes $Mo_2X_4(PMe_3)_4$ (X = Cl, Br, I) each display a reversible one-electron oxidation couple and a reversible one-electron reduction couple. The three complexes are shown to fulfill the criteria for efficient electrogenerated chemiluminescence reactions. Indeed, all three dimers display efficient ecl; this is in contrast to the previously reported low efficiency for ecl of $Mo_6Cl_{14}^{2-}$. The difference in ecl efficiencies can be attributed to Franck-Condon arguments or to the excess energy available to the system in the $Mo_6Cl_{14}^{2-}$ cluster. A method for determining the effect of this excess energy is described.

For over a decade this laboratory has been studying the electronic and structural properties of inorganic complexes which have significant metal-metal interactions[1], with the goal of correlating their electronic structures with the photochemistry of the systems. Electrogenerated chemiluminescence (ecl) arises from the production of emissive excited states created by the reaction of species generated at an electrode. This technique has been applied to several polynuclear complexes and may enable conclusions about the properties of the excited states to be drawn. The general criteria for observation of ecl are: (a) electrode reaction redox products which are stable in the time frame of the experiment; (b) sufficient energy in the redox event to populate the emitting excited state; (c) reaction coordinates which favor production of the excited state over the thermodynamically favored ground state[2]. A system which possesses all of these characteristics is the $Mo_2X_4(PMe_3)_4$ [X = Cl, Br, I] quadruply bonded dimer[3]. These dimers have very well behaved electrochemistry in tetrahydrofuran solution[4]. Each has a single one-electron oxidation wave and a single one-electron reduction wave in its cyclic voltammogram. The redox half-wave potentials are shown in Table 1. Both waves are reversible at scan rates 10-500 mV s^{-1}, an indication that the redox products are stable in the time frame of the ecl reaction.

All three dimers in this study have highly emissive excited states about 2 eV above the ground state (Table 2)[3]. From the data in Table 1, a reaction of the $Mo_2X_4(PMe_3)_4^-$ (electronic configuration $\sigma^2\pi^4\delta^2\delta^{*1}$) and the

Table 1.

Redox Potentials

	$Mo_2 \overset{-e^-}{\rightleftharpoons} Mo_2^+$	$Mo_2 \overset{+e^-}{\rightleftharpoons} Mo_2^-$
$Mo_2Cl_4(PMe_3)_4$	+0.74V	-1.70V
$Mo_2Br_4(PMe_3)_4$	+0.87V	-1.48V
$Mo_2I_4(PMe_3)_4$	+0.88V	-1.28V

All potentials are versus SCE in 0.1 M $TBAPF_6$ in THF solution at 22°C.

Table 2.

Photophysical Parameters for $Mo_2X_4(PMe_3)_4$ Complexes in 2-Methylpentane Solution*

	$\bar{\nu}_{max,em}$ (cm^{-1})	ϕ_{em}	τ (nsec)
$Mo_2Cl_4(PMe_3)_4$	14,880	0.259	135
$Mo_2Br_4(PMe_3)_4$	14,900	0.162	90
$Mo_2I_4(PMe_3)_4$	14,030	0.123	29

*Zietlow, T.C.; Hopkins, M.D.; Gray, H.B. *J. Solid State Chem.*, in press.

$Mo_2X_4(PMe_3)_4^+$ ($\sigma^2\pi^4\delta^1$) generated at the electrode (stepped from an oxidizing to a reducing potential) has sufficient energy to make an excited state product.

Electron transfer is a much faster process than molecular reorganization, so the reaction of two ions will result in the energetically accessible state with the smallest geometric restructuring[5]. This is true in the best studied inorganic ecl system, $Ru(bipy)_3^{2+}$.[6] Formation of the emitting excited state from the $Ru(bipy)_3^+$ and $Ru(bipy)_3^{3+}$ annihilation requires the transfer of an electron from a ligand π^* orbital to a ligand π^* orbital on the other metal (or the transfer of an electron from the Ru $d\pi$ orbital to the hole in the $d\pi$ manifold of the oxidized Ru). The $Mo_2X_4(PMe_3)_4$ molecules are another case in which high ecl efficiencies should be expected. A simple molecular orbital scheme for d^4-d^4 quadruply bonded dimers is shown in Figure 1. The important molecular orbitals for both the emissive state and the electrochemistry are the δ and δ^* orbitals. The emissive excited state in these dimers is the $^1(\delta\delta^*)$ state which has been the subject of many investigations[3]. The triplet component of this excited state configuration has been estimated to be about 5000 cm^{-1} above ground[7] and is not involved in the emissive state. In the $^1(\delta\delta^*)$ state, the dimer has a formal bond order of three. Oxidation (removal of one δ electron) and reduction (addition of one electron to the δ^* orbital) both lower the metal-metal bond order to 3.5. The earlier work done on these dimers clearly demonstrates that, upon excitation to the emissive $^1(\delta\delta^*)$ state, very little change in the metal-metal bond length

Figure 1. Simple molecular orbital scheme for D_{2d} quadruply bonded dimers.

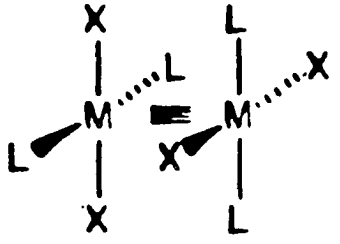

D_{2d}

M = Mo(III), W(III); d^4

X = Cl, Br, I

L = PR_3

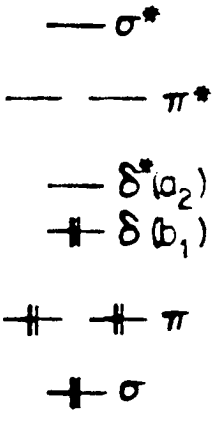

Ground state: $^1A_1 (\delta)^2$

Emissive excited state: $^1B_2 (\delta)^1(\delta^*)^1$

occurs. From a Franck-Condon analysis of the absorption and emission spectra of these complexes, the M-M bond lengthening in the $^1(\delta\delta^*)$ state is less than 0.1 $\AA$[8]. Structural work done on systems with various occupation levels of the δ and δ^* orbitals indicates very little change in the metal-metal bond upon oxidation or reduction of the $\sigma^2\pi^4\delta^2\delta^{*0}$ dimers[9]. The δ bond is not very important to the bonding in the dimers; oxidation, reduction, and excitation into the $^1(\delta\delta^*)$ state displace the respective potential energy surfaces along the M-M bonding coordinate only to a small extent, and in the same direction, thus fulfilling the third general criterion for observance of efficient ecl (Figure 2).

Upon pulsing the platinum electrode in a square-wave potential program 200 mV anodic of the oxidation wave and then stepping the potential to 200 mV cathodic of the reduction wave of the $Mo_2Cl_4(PMe_3)_4$ dimer in tetrahydrofuran solution, an intense red luminescence at the electrode was observed. A spectrum of the ecl proved to be identical to that of photoexcited $Mo_2Cl_4(PMe_3)_4$ indicating that emission was occurring from the $^1(\delta\delta^*)$ state. Both $Mo_2Br_4(PMe_3)_4$ and $Mo_2I_4(PMe_3)_4$ behaved in the same manner. A cyclic voltammogram of $Mo_2I_4(PMe_3)_4$ (Figure 3) and the ecl spectrum of $Mo_2I_4(PMe_3)_4$ (Figure 4) are typical of the series.

The lowest electronic excited state of the hexanuclear cluster $Mo_6Cl_{14}^{2-}$ has also been a focus of study in this laboratory[10]. The $Mo_6Cl_{14}^{2-}$ cluster does exhibit ecl in acetonitrile solution[11] but at a very low ($< 10^{-4}$)[12] efficiency. There are several possible explanations for the difference between the effi-

Figure 2. Potential energy surface diagram for the ground and emissive $^1(\delta\delta^*)$ excited state. The surface for the oxidized and reduced dimers would be displaced along the M-M coordinate in the same direction as the $^1(\delta\delta^*)$ state relative to the ground state.

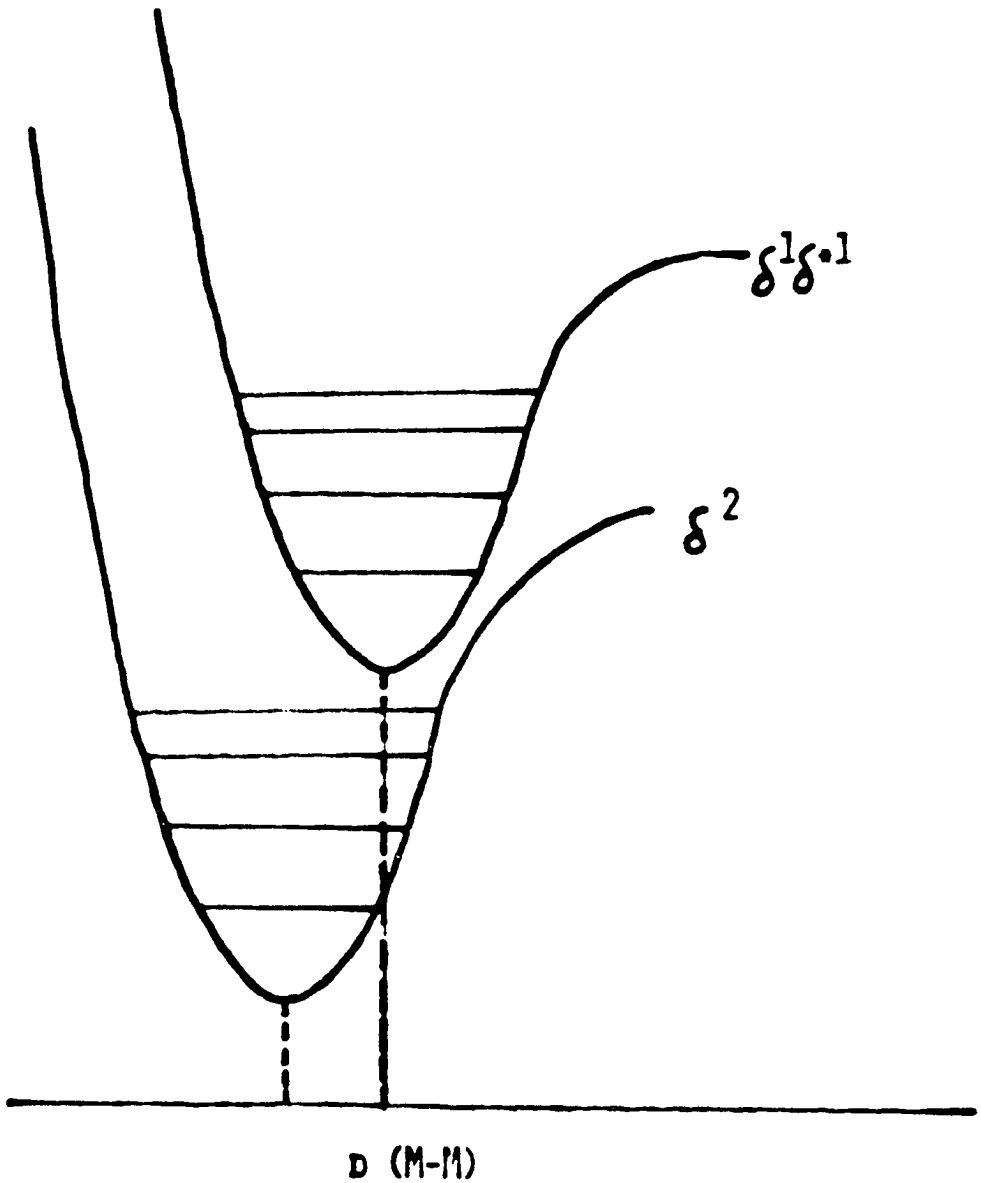
$\delta^1\delta\cdot 1$
δ^2
D (M-M)

Figure 3. Cyclic voltammogram of $Mo_2I_4(PMe_3)_4$ in tetrahydrofuran (0.1 M $TBAPF_6$, 22°C). Scan rate = 200 mV s^{-1}.

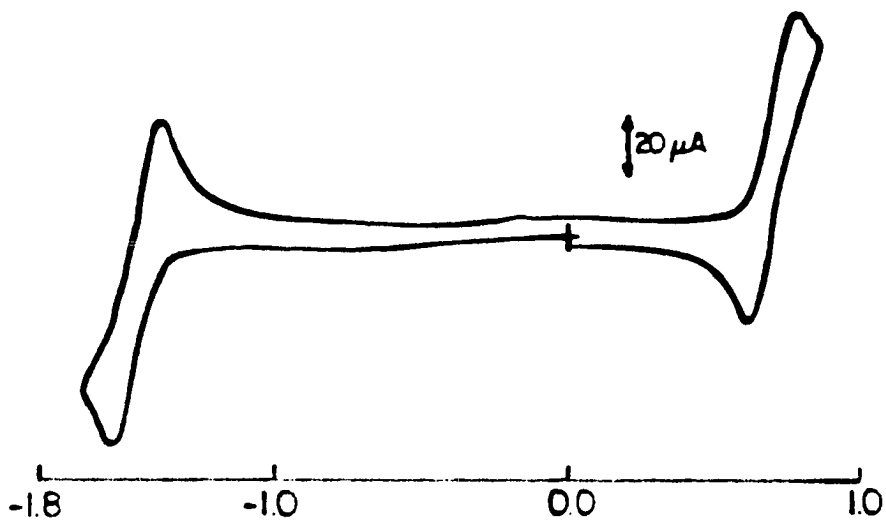
20 μA
-1.8
-1.0
0.0
1.0
Volts vs Ag/Ag+

Figure 4. Uncorrected ecl spectrum of $Mo_2I_4(PMe_3)_4$ in tetrahydrofuran solution, produced by stepping the potential at a platinum electrode between -1.5 V and +1.0 V at 100 Hz. The dots represent a photoexcited emission spectrum of the dimer in THF.

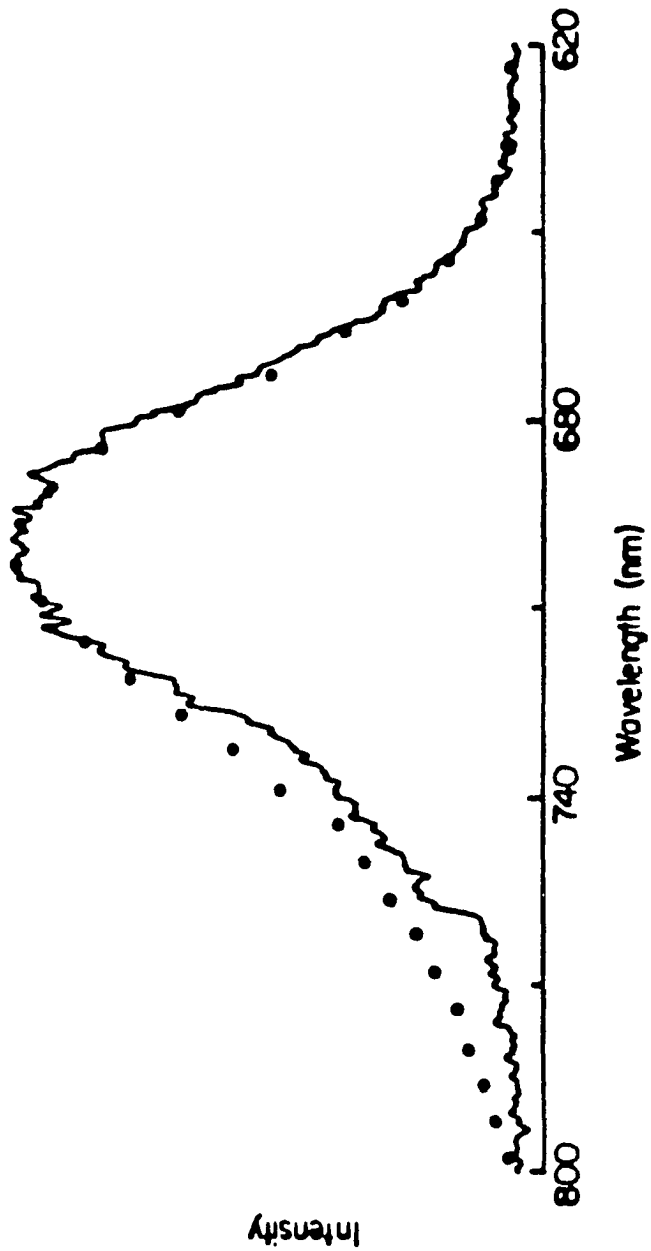
620
680
740
800
Wavelength (nm)
Intensity

cient ecl of the Mo_2 dimers and the less efficient Mo_6 clusters. The charges on the reacting pair in the dimer system are opposite (1- and 1+) while the electrode products in the cluster system are both negatively charged (3- and 1-). However, all electron transfer data on the Mo_6 system indicate that rapid electron transfer occurs between photogenerated $Mo_6Cl_{14}^{-}$ and negatively charged quenchers such as reduced chloranil[10]. This charge effect should only affect the efficiency of the ecl measured if the $Mo_6Cl_{14}^{3-}$ anion is unstable in the acetonitrile solution.

Although not as well understood as the quadruply bonded systems, the excited state of $Mo_6Cl_{14}^{2-}$ appears to be very distorted based on the large Stokes shift of the very broad emission observed[10]. Unfortunately, the excited state dynamics of the clusters are not well enough understood at this time to enable a reasonable potential well diagram to be deduced, so the reaction coordinates for the formation of the excited state versus the ground state cannot be determined.

Another important difference in the two systems involves the excess energy of the redox event over that necessary to populate the emissive excited state. For example,

$$Mo_6Cl_{14}^{3-} + Mo_6Cl_{14}^{-} \rightarrow Mo_6Cl_{14}^{2-*} + Mo_6Cl_{14}^{2-}$$

$$(E_{1/2,ox} - E_{1/2,red}) - (E_{em}) = E_{over}$$

$$3.09\ V - 1.9\ V = 1.19\ eV$$

and

$$Mo_2I_4(PMe_3)_4^- + Mo_2I_4(PMe_3)_4^+ \rightarrow Mo_2I_4(PMe_3)_4^* + Mo_2I_4(PMe_3)_4$$

$$2.16\,V \; - \; 1.95\,V \; = \; 0.21\,V.$$

The E_{over} in the dimer case is much smaller than in the hexanuclear cluster. Both of these systems display a temperature dependence on the non-radiative rate (and therefore the quantum yield of emission) out of the emissive excited state[13]. Possibly both systems are about 100% efficient, in that all of the redox events result in excited state formation, but in the cluster, the large E_{over} results in a thermally excited emissive excited state which has an activated non-radiative pathway resulting in a lower quantum yield for emission. Therefore, using the room temperature quantum yield data may not reflect the percentage of redox events resulting in the formation of an excited state.

This idea can be probed in the dimer systems by determining the ecl efficiency for a complete set of $Mo_2X_4(PR_3)_4$ dimers (Table 3). All of the quadruply bonded dimers have well-defined electrochemical behavior and similar photophysical properties. The temperature dependence of the non-radiative rate out of the emissive excited state has been determined for all of these dimers and there is a range of E_{over} to work with. If there is any thermal activation parameter involved in the ecl-generated excited state, there should be a simple relationship between the ecl efficiency and E_{over} defined by the temperature dependence of k_{nr} (and therefore, ϕ_{em})[14]. Work in this area is progressing.

Table 3.

$$E_{over} = [E_{\frac{1}{2}}(ox)\text{-}E_{\frac{1}{2}}(red)] - E_{em}$$

$Mo_2X_4(PR_3)_4$	$E_{\frac{1}{2}}(ox)$ - $E_{\frac{1}{2}}(red)$	E_{em}	E_{over}
$Mo_2Cl_4(PMe_3)_4$	2.44 V	2.12 eV	0.32 eV
$Mo_2Br_4(PMe_3)_4$	2.35 V	2.07 eV	0.28 eV
$Mo_2I_4(PMe_3)_4$	2.16 V	1.95 eV	0.21 eV
$Mo_2Cl_4(PEt_3)_4$	2.48 V	2.10 eV	0.38 eV
$Mo_2Cl_4(PPr_3)_4$	2.54 V	2.11 eV	0.43 eV
$Mo_2Cl_4(PBu_3)_4$	2.65 V	2.11 eV	0.54 eV

REFERENCES AND NOTES

1. a.) Nocera,D.G; Maverick, A.W.; Winkler, J.R.; Che, C.-M.; Gray, H.B., *ACS Symposium Series*, No. 211, **1983**, 21. b.) Caspar, J.V.; Gray, H.B. *J. Am. Chem. Soc.*, **1984**, *106*, 3029.
2. Faulkner, L.R. *Int. Revs. Science, Series Two*, **1975**, *9*, 213.
3. Hopkins, M.D.; Gray, H.B. *J. Am. Chem. Soc.*, **1984**, *106*, 2468.
4. Zietlow, T.C.; Hopkins, M.D.; Gray, H.B., submitted for publication.
5. Marcus, R.A. *J. Chem. Phys.*, **1965**, *43*, 2654.
6. a.) Tokel, N.E.; Bard, A.J. *J. Am. Chem. Soc.*, **1972**, *94*, 2862. b.) Luttmer, J.D.; Bard, A.J. *J. Phys. Chem.*, **1981**, *85*, 1155. c.) Glass, R.S.; Faulkner, L.R. *J. Phys. Chem.*, **1981**, *85*, 1160. d.) Rubinstein, I.; Bard, A.J. *J. Am. Chem. Soc.*, **1981**, *103*, 512. e.) White, H.S.; Bard, A.J. *J. Am. Chem. Soc.*, **1982**, *104*, 6891.
7. Hopkins, M.D.; Zietlow, T.C.; Gray, H.B. *J. Am. Chem. Soc.*, **1985**, *107*, 510.
8. Hopkins, M.D.; Miskowski, V.M.; Gray, H.B., unpublished results.
9. Cotton, F.A.; Dunbar, K.R.; Falvello, L.R.; Toma, M.; Walton, R.A. *J. Am. Chem. Soc.*, **1983**, *105*, 4950.
10. a.) Maverick, A.W.; Gray, H.B. *J. Am. Chem. Soc.*, **1981**, *103*, 1298. b.) Maverick, A.W.; Nadjdzionek, J.S.; MacKenzie, D.; Nocera, D.G.; Gray, H.B. *J. Am. Chem. Soc*, **1983**, *105*, 1878.
11. Nocera, D.G.; Gray, H.B. *J. Am. Chem. Soc.*, **1984**, *106*, 824.
12. Bard, A.J., personal communication.

13. Zietlow, T.C.; Hopkins, M.D.; Gray, H.B. *J. Solid State Chem.*, in press.

14. This is assuming that all of the dimers have similar reorganization energies.